THE UNIVERSITY OF CALGARY

The Stress-Dilatancy Behaviour of Sands: Pressure and Density Dependencies in both Monotonic and Cyclic Loading Regimes

by

Katrina Regier

A THESIS

SUBMITTED TO THE FACULTY OF GRADUATE STUDIES

IN PARTIAL FULFILLMENT OF THE REQUIREMENTS FOR THE

DEGREE OF MASTER OF SCIENCE

DEPARTMENT OF CIVIL ENGINEERING

CALGARY, ALBERTA

October, 1997

Abstract

The behaviour of geomaterials define the strength and volumetric behavioural tendencies of geotechnical structures in terms of their ability to carry load. The expression of these characteristics in a concise constitutive model is necessary to design and implement structures by safe and economical means. Some previous constitutive models of granular materials have attempted to define the interaction between stress and strain without the consideration of inherent properties of the material such as density and pressure dependencies. Other models incorporate pressure and density effects but become complicated when used to describe more complicated behaviour such as strain-softening. This thesis presents a recently developed model which incorporates the influences of these variables into Rowe's classical stress-dilatancy relationship through the use of a ratio of current to critical void ratio. Initially, an experimental program investigates the stress-dilatancy behaviour of a fine Ottawa Sand under conventional triaxial testing at various confining pressures and densities. The results of these are then used to calibrate a new stress-dilatancy relationship through the definition of eleven material parameters, with the model results showing good correlation to the measured responses. An additional laboratory analysis is included which provides an observational study of the pressure and density effects on the behaviour of Ottawa Sand subjected to low frequency, high amplitude cyclic loading.

Acknowledgements

Appreciation is especially offered to my supervisor, Dr. R. Wan, for his endless patience and guidance throughout the past year. This research was supported by the Natural Sciences and Engineering Research Council of Canada and their funding is sincerely acknowledged.

I must express thanks to D. McCullough and H. Pollard for their helpful guidance and advice throughout the experimental testing; to Dr. R. Wong for his discussions on triaxial testing and soil behaviour; and to P. Guo for assistance with the analytical stages of the research.

To my family and their boundless support.

Table of Contents

List of Tables

List of Figures

Chapter 1

INTRODUCTION

1.1 Background

The behaviour of granular media is governed by a number of parameters including stress path, initial void ratio, particle shape and confining stresses. One parameter in particular, initial void ratio, plays a vital role in the dependency of volume change with a variation in stress. The void ratio, e, is described as the ratio of volume of voids to volume of solids.

A loose sample, one with a high initial void ratio, will contract with the application of a deviatoric stress. In conventional triaxial compression tests, this is reflected by an increase in stress ratio, σ_1/σ_3, where σ_1 and σ_3 are the applied stresses in the respective major and minor principal directions. A typical stress-strain curve results in a reduction in the rate of stress increase with increasing strain up to a point where a small increase in stress results in substantial strain. A dense granular sample, one with a low initial void ratio, may contract initially with the application of a deviatoric stress. However, the dense configuration of the particles and their arrangement will inevitably cause the soil to expand and dilate due to a tendency for the particles to slip against and override each other. The result is a sample with a greater volume than initially measured.

The definition of dilatancy must be used with care. When describing a dilatant material, it encompasses the entire plastic volumetric behaviour of that material. Conversely, when used to describe volume changes, the term dilatancy pertains only to the volumetric expansion of a granular media.

The stress-strain curve of a dense sand shows a peak strength followed by a strain softening and a residual strength. Casagrande has found [1] that the residual strength corresponds to a void ratio approximately equal to that of the final void ratio of a loose sand. This specific void ratio is termed as the critical void ratio.

The confining pressure, σ_3, is another parameter which influences the behaviour of a granular material during shearing. As the stresses surrounding an element of soil increase, contractive tendencies cause loose soil to achieve greater densities. The critical void ratio achieved by the soil is also influenced by confining pressures as higher pressures are accompanied by lower critical void ratios.

The characterization of the dilatant behaviour of granular materials has been discussed by many authors [2], [3], [4], [5], [6]. Rowe's theory [2] is generally accepted as the most widely used stress-dilatancy relationship in soil mechanics. Developed after close scrutiny of a packing of uniform rods and balls under plain strain or conventional triaxial test conditions, it takes into account the direction in which the particles slip and the volume changes during shear. These factors are coupled with a principle of least work ratio to provide a reasonably accurate description of the volumetric behaviour of a granular material.

The ease of describing volumetric changes with stress ratio makes Rowe's expression attractive to the field of geotechnical engineering. The linear relationship is

expressed as $R = KD$ with R is defined as the above mentioned stress ratio, σ_1/σ_3, D as the dilatancy factor, $1 - d\varepsilon_v^p/d\varepsilon_1^p$, and K as a constant dependent on the friction angle φ, equal to $\tan^2(\pi/4 + \varphi/2)$. Some fundamental characteristics of the material behaviour however were omitted in the relationship. These characteristics include the influence of void ratio, in terms of whether the soil will experience hardening or softening during shear, and stress level. A recent modification of the classical stress-dilatancy equation by Wan and Guo [7] incorporates these effects, creating a much more accurate theoretical expression to follow volumetric progressions in granular materials.

1.2 Objectives of the Research

The main focus of this thesis is to examine the behaviour of granular materials subjected to conventional triaxial testing. The term conventional is used to define typical cylindrical testing, where the intermediate stress is equal to the minor stress. Further reference to triaxial testing in this thesis will imply the conventional method. The experimental results will be applied to verify a stress dilatancy model proposed by Wan and Guo [7]. Other objectives of this work include:

1. the design of a low friction interface to be used between the sample and the platens including the use of enlarged platen to permit radial expansion,

2. the determination of an acceptable method of sample preparation allowing reproducible densities (initial void ratios) and

3. the expansion of the testing to incorporate cyclic loading.

The limits of this research involve the type of materials and the methods utilized in the triaxial testing. C-109 Ottawa Sand being a standard sand common to many experimental programs is used to determine the parameters of the model. Ottawa Sand is generally composed of fairly uniform rounded grains which make it easy to work with and is an ideal material for use in triaxial testing.

Both the initial density and confining pressure are varied in an attempt to establish the validity of the proposed relationship over a wide range of conditions. The initial void ratio ranges from loose to dense to reflect all modes of strain-hardening and strain-softening. The confining pressures remain in the lower range, with a sufficient variety to capture the influence that they exhibit on granular material behaviour. Stress-strain-volumetric responses are examined for these ranges of void ratio and stress level with emphasis placed on the dilatancy behaviour of the sand.

Experimental results for the cyclic loading tests are limited to the loose and the dense sands at the highest and lowest confining pressures used in static tests. The intent of this portion of the research is to establish the evolution of material response with the number of stress cycles in an attempt to characterize any microstructure dependencies in the cyclic loading regime. The mode of failure, whether stable (shakedown) or unstable (ratcheting) is studied to determine the influence of the initial conditions required for each case. Although the model is not yet advanced to the point of being able to describe this phenomenon, the resulting data will help to achieve this goal.

1.3 Organization of the Thesis

This thesis encompasses three major topics:

1. a study into the stress-dilatancy relationship and the verification of a newly proposed model which incorporates pressure and density dependencies into granular material behaviour,

2. an experimental program involving the development of laboratory procedures used to conduct conventional monotonic triaxial testing on fine Ottawa Sand and the interpretation of test results and

3. the observation of the behaviour of fine Ottawa Sand under low frequency cyclic loading conditions including the effects of confining pressure and initial void ratio.

The above topics are described in eight chapters. This chapter gives a general description of the problem, the intentions of the thesis and a brief overview of the presentation of the thesis.

Chapter two provides a detailed literature review of the current theories in geotechnical design and the models employed to present these theories in an effective manner. A description of the stress-dilatancy interaction provides a detailed review of Rowe's theory of dilatancy as well as other methods used to explain plastic volumetric behaviour of granular materials. The chapter ends with the limitations of current theory and a brief introduction to the proposed model.

The laboratory objectives, methods and equipment utilized in the experimental portion of this research are presented in Chapter three. A detailed study of reconstituted sand sample preparation techniques and free end design are included in this section.

Chapter four contains the results of the experimental study, providing the stress-strain-volumetric responses of fine Ottawa Sand coupled with an interpretation of the behavioural characteristics exhibited by the sand. Chapter five presents the proposed model and applies the experimental results to determine the material parameters of the tested material. These parameters are then used in Chapter six to verify the model followed by a discussion of the resulting comparison between theoretical and experimental values.

Chapter seven describes the cyclic testing regime, providing modifications to the equipment and procedures, plots of the resulting responses and an observational discussion on the cyclic behaviour of Ottawa Sand.

Conclusions and recommendations for further study accompany a brief summary of the thesis research in Chapter eight.

Chapter 2

LITERATURE REVIEW

2.1 General

The evolution of the characterization of granular materials is an extensive subject with developments beginning as far back in the 1700's as limit equilibrium methods were first presented, through considerations of deformation analysis to existing non-linear elastic theory, plasticity theory and damage theory. Initial studies of particulate material interaction are credited to Coulomb [8]. The influence of individual grains limits the effectiveness of the Coulomb criterion,

$$\tau = \sigma \tan\varphi + c \tag{2.1}$$

as the relationship was developed using two intact contact surfaces. However, the criterion is still widely used today and the basis for strength behaviour of soils. This equation states that on a failure plane the shear stress, τ, is related to the normal stress, σ, by an angle of internal friction, φ. The cohesion term, c, is generally ignored for granular materials and will be omitted throughout this research as the rounded grains of Ottawa Sand do not exhibit cohesive behaviour.

Deformation theory, with respect to the shear distortion of granular material, was not considered until over a century later. The changes in volume in an element resulting from a shifting of the individual particles in that element was first introduced by Reynolds [9]. This theory better captures the essence of a granular media, unlike Coulomb's proposal which ignores micro-effects of the grains. Reynolds termed this phenomenon as dilatancy; the volumetric changes imposed by the geometry of grain packing of a material when subjected to shear.

Dilatant materials, such as soils, exhibit irrecoverable volumetric strains when sheared. The movement of the particles is dependent on the contact forces between them. Plastic shear displacements occur as the frictional resistance between two grains in an element of soil is overcome by the contact forces on the grains caused by shear stresses on the element. An element of dense material originally has some room between particles, and will initially contract as these voids are filled. The material will then expand with shear as the particles tend to slip over one another. The weaker grain contacts will slip first, causing more stresses to build up at the stronger contacts until these too become greater than the frictional resistance forces. Conversely, an initially loose configuration has a greater void space between particles, allowing the compression of the element as a whole. The contact forces tend to disperse more equally between the grains resulting in less redistribution of forces as shearing occurs.

The interaction between strength and dilatancy becomes significant when considering the behaviour of granular media. Figure 2.1 shows a common response of both dense and loose sand. The stress and volume curves have unique corresponding characteristics. For example, the peak of the dense stress-strain curve nearly coin-

cides with the maximum slope of the volume change curve. Also, both dense and loose materials exhibit horizontal stress-strain and volumetric strain curves at high axial strains. Casagrande [1] is the first to describe this condition where the material's volume changes cease and constant stress conditions occur as the critical state. Further studies noted that the critical state stress level and density of a given granular material were independent of the initial packing of the sample at normal stress levels. It is interesting to note that this may not apply at very low to extremely low stress levels where dilatancy effects are marginalized due to predominance of fabric changes [63]. In fact, the critical values of void ratio and stress level were essentially identical for a soil, regardless of the initial conditions allowing these factors to be labeled material parameters [10].

Observation of corresponding states of stress and volumetric behaviour such as peak stress with maximum expansion and critical conditions showed reoccurring results for all granular materials. This gave rise to the concept of a stress-dilatancy interaction and the possibility of being able to determine one from the other.

The ability to characterize plastic volume change behaviour with stress level lends itself to a better understanding of the reactions of granular materials to various loading conditions. Particulate deformation and arrangement influence the strength of soils. For example, a densely packed configuration of grains will exhibit a strength gain as the initial contraction and expansion phase occurs. Later, volume change rates become a maximum and peak stress is achieved as the energy required for maximum dilation is expended (Rowe *et al.* [11]). Finally, as the volume change ends, constant volume conditions occur and additional energy input to shear the

sample is no longer required.

A knowledge of the integrated stress-deformation theories and the access to constitutive models capable of describing this mode of granular material behaviour are valuable in the design and analysis of geotechnical structures. The determination of the required parameters allows the development of a precise, comprehensive description of the material response throughout the loading regime. All potential yielding and failure modes can be predicted and effectively prevented.

Existing geotechnical theories including limit equilibrium and deformation analysis will be discussed in this chapter. Some available constitutive models and dilatancy theories will then be presented. The chapter will conclude with a brief introduction and framework of the proposed research.

2.2 Existing Theories in Geotechnical Design

Current practice in the geotechnical field tends to simplify design and analysis as much as possible as economic viability plays an extensive role in the industry today. The ease of design and analysis is accomplished by utilizing basic principles to characterize upper and lower bound, or limit equilibrium solutions. Very few easily determinable material parameters can be implemented in common equations of equilibrium and/or compatibility to discern whether a given load will cause failure. The simplifications and inaccuracies of these equations are compensated by large 'safety factors', which result in a solution that does nothing to interpret the true behaviour of the material.

2.2.1 Bound Methods

The bound methods in plasticity theory are powerful design tools. Problems such as slope stability and bearing capacity generally require only a solution as to whether or not the soil will fail under certain loading conditions. Simple laboratory testing of soil samples will provide the cohesion and friction angle parameters which are used in the classical failure theory developed by Coulomb and shown in the form of a Mohr's circle diagram, see Figure 2.2. These failure criteria define the condition of ultimate collapse, and must be satisfied for bound solutions.

In basic strength analyses, extremum theories are used to approximate the solution to continuum mechanics problems. Lower and upper bound values determine failure loads which are respectively smaller and larger than the collapse loads. Precise solutions to problems of continuum mechanics involve:

1. satisfying equations of equilibrium,

2. satisfying compatibility of strains, and

3. incorporating material properties.

To simplify this process, upper and lower limits of collapse loads may be found using a bound method. This involves a simplification of the above requirements by eliminating either the equilibrium or the compatibility requirements. The material must be treated as perfectly plastic meaning that at failure it must be at critical state and the incremental plastic strain vector must be normal to the yield surface.

A lower bound solution maintains equilibrium conditions, but ignores the compatibility of strains. The lower bound solution must also correspond to a stress field

that does not violate any yield criterion. As the name suggests, this type of analysis with result in an 'unconservative' solution, underestimating the failure loads.

An upper bound solution achieves the opposite result. A 'safe' value of failure load is determined as the work done from external loading is equated to a kinematically admissible displacement field corresponding to a failure mechanism. To be kinematically admissible, the compatibility of strains must be met although equilibrium conditions do not have to be satisfied. If the upper and lower bound solutions are identical, the value is unique and represents the exact failure load.

2.2.2 Limit Equilibrium Analysis

The limit equilibrium method is a common stability analysis to find the limit equilibrium load which the geotechnical structure can sustain. The steps used in the limit equilibrium method [12] are:

1. define an arbitrary collapse mechanism of slip surfaces,
2. calculate the static equilibrium of the components of the mechanism by resolution of forces to find the strength mobilized in the soil or the external forces and
3. examine other mechanisms to find the limit equilibrium load.

The strength of the soil is usually given by the Mohr-Coulomb failure criterion. Upper and lower bound methods are combined to describe the conditions of the limit loads as the geometry of the slip surfaces must allow failure to occur but compatibility is not necessarily satisfied because the surface can take on any shape. Likewise,

overall equilibrium conditions are met but stresses within the mechanism blocks are unimportant. Wedges and slip circles are used in common analyses, although in drained loading conditions, the slip surface method meets with a statically indeterminate summation of forces. In this case, the method of slices is used to divide the block into relatively equal sized vertical slices, which are analyzed separately using simplifying assumptions to eliminate the indeterminacy and then added together to find the solution as a whole. Many different assumptions have been suggested including (a) equating the resultant of the interslice forces to zero [13], (b) making the direction of the resultant of the interslice forces horizontal [14] , as well as more complicated methods such as those suggested by Janbu [15] and by Morgenstern and Price [16].

2.2.3 Deformation Analysis

Recent developments in analytical methods such as the finite element analysis, constitutive modeling and computational capabilities are beginning to allow engineers the option to design and analyze accurately without sacrificing safety considerations. The continuum mechanics approach which was described earlier in the previous section has become attractive given the availability of today's computational power. Basically, the analysis is rigorous in that one searches for the stress and strain fields which satisfy mechanical equilibrium, strain compatibility and strength/yield criteria for a structure which is subjected to external loads. The whole analysis hinges on the proper characterization of the stress-strain behaviour of the material for an accurate calculation of deformation and stresses. The next sections will focus on this

aspect.

2.3 Some Existing Constitutive Models in Geotechnical Design

In certain desired designs, such as those requiring foundation settlements and slope deformations, the determination of stress and strain fields hold more significance than the soil strength. Typically, these strains are considered to be small enough so that they are recoverable under design working loads to justify the use of linear elastic theory.

Linear isotropic elastic behaviour incorporates Hooke's law, employing only two parameters, Young's modulus E and Poisson's ratio ν, to describe the stress-strain relationship. Due to Poisson's effect, the axial strain (principal strain), ε_1 gives rise to two lateral strains ε_2, ε_3 which are the intermediate and minor principal strains respectively. In conventional triaxial conditions, volumetric strains ε_v are determined by assuming that the minor and intermediate strains are equal, giving the equation $\varepsilon_v = \varepsilon_1 + 2\varepsilon_3$.

The use of linear elasticity, although useful for steel and rock analyses, is extremely limited in the soil mechanics field. Observation of the stress-strain curves of soils show that even the initial slope of the curve is non-linear. At large strains, the plastic deformations dominate the soil behaviour, preventing the ability of elasticity theory alone to provide useful information. However, the elastic component of

volumetric changes must be considered in the interpretation of material behaviour.

Non-linear elasticity provides a correction to the elastic theory by prescribing a dependency of elastic moduli on mean pressure and/or void ratio. It represents a more accurate depiction of soil behaviour, as it can characterize, to a certain extent, the reduction in stiffness as strain increases.

Although elastic strains govern the volume changes in the initial segment of the stress-strain curve, plastic deformations quickly begin to dominate with the development of irrecoverable strains. Mroz [17] suggests that there is no distinct separation between the onset of plastic strains, termed the yield surface, and pure elastic behaviour. This causes the size of the elastic region to become negligible and makes it difficult to define the elastic parameters. Any model using elasticity theory will be inadequate to describe the material behaviour. The integration of elastic and plastic deformation requires a more sophisticated means to represent stress-strain-volumetric behaviour. Mroz [17] provides a list of constitutive model types capable of this task. Depending of the desired accuracy and response, as well as the testing conditions, time independent model classes include:

1. non-linear elasticity and hypoelasticity,
2. perfectly plastic models with associated and non-associated flow rules,
3. isotropic hardening models with density dependency,
4. anisotropic hardening models with multiple loading surfaces,
5. endochronic or incrementally non-linear formulations avoiding loading/unloading conditions and

6. combined elasto-plastic sand damage models accounting for elastic stiffness degradation.

Once a constitutive model is defined, the solution of the boundary value problem can be initiated. Conservation of mass and conservation of energy equations ensure that the fundamental laws of physics are satisfied. The above constitutive model defines the inherent material properties. The boundary conditions are then applied to determine the solution for a particular scenario.

The solution of boundary value problems may be found by simple closed form methods for a simple set of equations. However, more complex inputs may require an advanced numerical modeling technique such as the finite element method.

2.3.1 Hyperbolic Model

The hyperbolic model is a common non-linear elastic model which describes soil behaviour with the use of a hyperbolic curve. Kondner [18] first used the equation

$$\sigma_1 - \sigma_3 = \frac{\varepsilon}{a + b\varepsilon} = \frac{\varepsilon}{[1/E_i + \varepsilon/(\sigma_1 - \sigma_3)_{ult}]} \tag{2.2}$$

to characterize the stress-strain response of a soil tested under constant confining pressures, σ_3, in triaxial conditions. In this relationship, the constants a and b are the reciprocals of the initial tangent modulus, E_i, and the ultimate stress difference, $(\sigma_1 - \sigma_3)_{ult}$, respectively.

Duncan and Chang [19] extended the model to describe the tangent modulus, E_t, at any point on the curve such that

$$E_t = \left[1 - \frac{R_f(1-\sin\varphi)(\sigma_1-\sigma_3)}{2c\cos\varphi + 2\sigma_3\sin\varphi}\right] K\, p_a \left(\frac{\sigma_3}{p_a}\right)^n \tag{2.3}$$

with constant values of the modulus number, K; modulus exponent, n, failure ratio, R_f, and the Mohr-Coulomb failure parameters, c and φ. The term p_a represents the atmospheric pressure during testing.

The model was later advanced again to account for volume changes with either an equation which captures the tangent of the Poisson's ratio [20] or the Bulk modulus value

$$B = K_b \left(\frac{\sigma_3}{p_a}\right)^m \tag{2.4}$$

where K_b is the bulk modulus number and m the bulk modulus exponent [21]

This model is attractive in that it is easily understandable and simple to use with few parameters which can be determined through standard triaxial testing. The influence of confining pressures are brought into use to define volume change characteristics as seen from Equation 2.4. Young's modulus for unloading, E_{ur}, can also be captured with the utilization of another similar equation

$$E_{ur} = K_{ur} p_a \left(\frac{\sigma_3}{p_a}\right)^n$$

by assuming that the soil behaviour is elastic for unloading and reloading. In this expression, K_{ur} is the unloading-reloading modulus number.

Limitations of the hyperbolic model are found in its use of a generalized Hooke's law to describe isotropic behaviour. Anisotropic influences cannot be captured. The model also is incapable of defining post-peak behaviour. Volumetric expansion of dense sands and overconsolidated clays will not be reflected in calculations performed using the above equations.

2.3.2 Plasticity Theory

Plastic deformation is responsible for the strain hardening and softening behaviour of a soil (Figure 2.1). Strain hardening occurs as the movement of particles against each other causes a buildup of strength in the material until peak conditions are reached. Both loose and dense particulate materials show evidence of this phenomenon. Strain softening is demonstrated only in dense sands, particularly at low stress levels, and occurs after the peak failure strength is reached, describing the weakening of the material as the soil reaches a state that can no longer manage the applied stress.

The yield surface can be defined as the stress state required to begin producing irrecoverable strains, see Figure 2.3. Prior to reaching this state, any possible loading regime will produce only elastic strains. Once a material reaches yield conditions, it begins to deform plastically and continues to change volume in this manner until it reaches the failure surface. In this way, the yield envelope is not a stationary surface but instead constantly increases with strain hardening. If strain softening is not exhibited by the soil, the yield surface will eventually become the failure surface, a stationary envelope of which contains all possible states of loading existence. If strain-softening does occur, the yield surface will touch the failure surface and then

retract as the soil achieves residual conditions.

Yield functions which characterize yield surfaces can be obtained by several methods. For example, they can be viewed as the locus of equal plastic work done or plastic shear strain to reach a certain plastic deformation state. A simpler approach is to assume that they take the same form as the failure surface [22]. In this way, the Mohr-Coulomb equation is used as both the yield and failure criterion by equating it to zero as follows,

$$F = \frac{(\sigma_1 - \sigma_3)}{2} - \frac{(\sigma_1 + \sigma_3)}{2} \sin\varphi_m = 0 \tag{2.5}$$

The mobilized friction angle φ_m controls the yielding strength characteristics up to failure, defined by the failure friction angle φ_f, and beyond to critical conditions at the constant volume friction angle φ_{cv}. Using these three conditions, Equation 2.5 can adequately describe the soil behaviour throughout the loading regime.

The Mohr-Coulomb failure surface is a mean-stress dependent failure criterion, a condition which is desired in the modeling of frictional materials. It is well suited for the two dimensional, triaxial failure conditions as the influence of the intermediate stress is omitted. When extending the Mohr-Coulomb surface to the three dimensional stress space, the failure criteria becomes more difficult to characterize, as the shape of the surface is not smooth (Figure 2.4). Other models, such as the Drucker-Prager [23] and the Matsuoka-Nakai [24] criterion, also shown in Figure 2.4, attempt to correct for this inconvenience by utilizing a continuous surface. The Drucker-Prager model is in a circular form in the spatially mobilized plane and

adequately defines the behaviour of granular materials in compression planes, but grossly overestimates triaxial extension failure. The Matsuoka-Nakai form more accurately encompasses the differences in extension and compression behaviour with a failure surface much closer to that described by the classical Mohr-Coulomb theory.

Flow theory of plasticity

Flow rules are used in plasticity theory to estimate the incremental plastic strain vector $d\boldsymbol{\varepsilon}^p$ during yielding. The incremental form of the flow rule

$$d\boldsymbol{\varepsilon}^p = d\lambda \frac{\partial G}{\partial \boldsymbol{\sigma}} \tag{2.6}$$

contains two terms typical to vector mechanics; $d\lambda$, the plastic multiplier describing magnitude of plastic strains and $\partial G/\partial \boldsymbol{\sigma}$ describing the direction of the plastic strain vector which is the normal to some plastic potential function G.

The plastic potential, G, can be determined in various ways, among others, it can be calculated by integrating the plastic strain increments measured in a test. However, it is customary to substitute the plastic potential G with the yield surface F which results in the so-called associated flow rule. Although this method lends itself well to steel materials as the plastic volume change of steel is generally negligible, the use of the associated flow rule does not accurately portray granular material behaviour when compared to experimental results. This discrepancy can also be demonstrated with theoretical means [22]. Energy must be dissipated during the plastic deformation of a soil to maintain a theoretically sound model. The normality

condition of associated plasticity ensures that the direction of the plastic shear strain vector is perpendicular to that of the yield surface. In this manner, the plastic strain vector is also normal to the total stress vector. The mathematical consequence of this condition, given the definition of work done as

$$W = \int_0^t \boldsymbol{\sigma} : \dot{\boldsymbol{\varepsilon}}^p \, dt \tag{2.7}$$

is that the energy dissipation vanishes. Indeed, this form of the plastic potential ($G = F$) assumes that the value of the dilatancy angle, ψ, written in terms of the ratio of plastic volumetric strain increments, $d\varepsilon_v^p$, to plastic shear increments, $d\gamma^p$, such that

$$\sin\psi = -\frac{d\varepsilon_v^p}{d\gamma^p}$$

is equal to that of the friction angle. However, in experimental data [22], [5], [25], the dilatancy angle is found to be as much as 20^0 less than the friction angle.

If the determination of the plastic potential is not achieved in the same form as the yield function, a non-associated flow rule results. Non-associated plasticity ensures that the dilatancy angle does not equal the friction angle and the plastic potential for this theory can be written as

$$G = (\sigma_1 - \sigma_3) - (\sigma_1 + \sigma_3)\sin\psi \tag{2.8}$$

for granular materials. Shortcomings of the non-associated law include the violation of the aforementioned normality rule, as the plastic strain increment is no longer positioned normal to the yield surface. This may cause an unstable solution as mechanical stability requirements are not necessarily met. However, the possible instability effects, viewed as being too restrictive, are a small sacrifice to accuracy if the use of the dilatancy angle can be considered in the flow rule.

Cam Clay Model

The Cam Clay model [26], [27] was developed at Cambridge and incorporated concepts of work-hardening and plasticity theory to describe the behaviour of clays. The basis of the model is the critical state theory [28] which defines the final void ratio and stress conditions that a soil will reach regardless of its initial void ratio. The Cam-Clay model also uses the basic energy equations to describe the work done as the yield surface moved from its initial position to failure.

Developed for use with isotropic conventional triaxial testing, the results are described in the three-dimensional $p-q-e$ space with $p = (\sigma_1+2\sigma_3)/3$ as mean stress, $q = (\sigma_1 - \sigma_3)$ as deviatoric stress and e as void ratio. A fundamental assumption of the original model involves equating the elastic volumetric strains to zero, although modified versions of the theory can include this factor. The basic relationships of the model include plastic, ε_v^p, and elastic, ε_v^e, volumetric strains such that in incremental form

$$d\varepsilon_v^p = \frac{(\lambda - \kappa)}{(1 + e_0)} \frac{dp}{p} \tag{2.9}$$

$$d\varepsilon_v^e = \frac{\kappa}{(1+e_0)}\frac{dp}{p} \tag{2.10}$$

where λ and κ are constants describing the compression and swelling behaviour in the $e - \ln p$ space. The projection of the critical state surface onto the $q - p$ and $e - \ln p$ spaces give

$$q = Mp \text{ and } e = e_c - \lambda \ln p \tag{2.11}$$

with M as the frictional constant and e_c the void ratio at a mean stress $p = 1$. The yield surface for the modified Cam-Clay theory is finally described by equating the plastic work done to the plastic dissipation which takes place at critical state. The following expression is classically obtained:

$$F(p,q) = p^2 - p_0 p + (q/M)^2 \tag{2.12}$$

where p_0 is the strain-hardening parameter defined incrementally as

$$\dot{p}_0 = \frac{1+e_0}{\lambda - \kappa} p_0 \dot{\varepsilon}_v^p \tag{2.13}$$

The Cam-Clay model can be used with ease as there are relatively few parameters which are determined simply from laboratory triaxial testing and the well established compression and swelling indices. The inability to characterize strain-softening effects is a major limitation, as is the increasing complexity of the model

when attempting to use it to describe soils other than normally consolidated clays.

2.4 The Stress-Dilatancy Theory

The discovery and application of dilatancy has been essential to constitutive modelling of geomaterials. Its ability to characterize particulate behaviour in terms of continuum mechanics creates a simple method of determining the portion of the frictional angle which is exerted on volume changes in the material. Before these volume changes were defined, granular material description was accomplished by using the limited relationships of either initial elastic behaviour or the peak stress failure behaviour.

The limitations of elastic assumptions in soil mechanics are many. If using an elastic theory, validity is found for only very small strains, and does not extend into the pre-peak, post-peak or residual regions of the stress-strain curve. Volume changes are all considered to be recoverable causing energy dissipation and any plastic behaviour to be ignored. While the linear elastic method is simple to use and provides relatively accurate results under low stress conditions, it can not be considered a useful tool for describing other stress states.

Failure theory to soil mechanics is used in soil mechanics to determine maximum allowable loads. Its weakness lies in that it cannot be used in conjunction with methods to identify corresponding displacements. Once again, this method only describes one stress state in the evolution of strength behaviour.

Dilatancy theory can effectively incorporate the above mentioned small strain

and peak soil states as well as areas within and beyond. It ultimately provides the dilation induced plastic volumetric strain component which needs to added to the elastic volumetric strains.

2.4.1 Evolution of Stress-Dilatancy Theories

The implementation of dilatancy into the field of soil mechanics began slowly in the 1930's with Casagrande's work [1] which explains the effect of friction angle on volume changes in soils. Taylor [29] first suggested the possibility using energy theories to separate the shear stress into friction and volume change components. The frictional component being the term previously used to encompass the entire shear stress behaviour, describing typical Coulomb interaction with two surfaces sliding against one another. The volume change component is a term which accounts for the action of particles sliding over and around one another.

The advantages of being able to split the required shear stress components, coupled with the use of energy considerations lead to advanced research into the area of dilatancy. Newland and Allely [3], in their frictional analysis of dilatancy, were the first to show that Taylor's division of the friction angle terms, while doing much to advance the concept of volume changes in granular materials, did not yet account all of the mechanisms responsible for the accurate description of soil strength. The friction angle was divided again to split the pure sliding friction from the friction caused by particle interaction and reorientation. The influence of neighbouring grains on the sliding action of a single grain can be explained when examining a random assembly of particles. Referring to Figure 2.5(a), the plane of sliding of the grains against

one another is seen to have a different orientation for every particle contact. An average angle of sliding can be assumed, obviously in a direction which is not parallel to the direction of application of shear as Coulomb's theory suggests. These two mechanisms represent the extent of Taylor's analysis of dilatant behaviour. However, Figure 2.5(b) shows the influence of various sized particles with random packing. If the upper and lower halves of the soil element are assumed to behave as a unit, the difference in the contact orientation becomes apparent. An average sense cannot be used, as the steepest contacts and mode of failure will control the behaviour of the volume changes.

2.4.2 Rowe's Stress-Dilatancy Theory

In 1962, Rowe [2] provided a theory that was very similar to the one presented by Newland and Allely [3] five years earlier. In fact, King and Dicken [30], in a comparison of the two theories found little difference in the calculated results. Although both used the same basic equations, an equilibrium stress equation and a volume change equation, Newland and Allely's theory has been relatively ignored while Rowe's theory has become well known and widely used. King and Dicken [30] credit this to the fact that Rowe's research was based on a rigorous analysis with convincing experimental comparisons. Newland and Allely [3] did not supply as convincing an argument and only considered the maximum friction angle in their analysis.

Rowe [2] begins with the definition of the basic angle of friction, φ_μ, and adds the interparticle sliding angle, β (Figure 2.6), to develop an expression of applied shear force

$$P = Q\tan(\varphi_\mu + \beta) \tag{2.14}$$

with P and Q representing respective shear and normal forces

This equation is applied to three different packing scenarios; two dimensional uniform rods, three dimensional face centred spheres and three dimensional spheres in a rhombic pattern. The test materials were all simple geometric forms, each representing a frictionless grain. In each case, the ratio of principal major to minor stresses was found to be

$$\frac{\sigma_1}{\sigma_3} = \tan\alpha\tan(\varphi_\mu + \beta) \tag{2.15}$$

with α representing a geometrical property of the packing as the angle between the plane of particle interlocking and the direction of minor principal stress, σ_3.

The above Equation 2.15 can be multiplied by the strain ratio $\varepsilon_1/\varepsilon_3 = 1/\tan\alpha\tan\beta$ or $\varepsilon_1/\varepsilon_3 = 2/\tan\alpha\tan\beta$ depending on whether it is a two dimensional or three dimensional case. As a result, the energy ratio of a fixed orientation of particle movement is given as

$$E = \frac{\sigma_1\varepsilon_1}{\sigma_3\varepsilon_3} = \frac{\tan(\varphi_\mu + \beta)}{\tan\beta} \tag{2.16}$$

The extension of the preceding experiments to random irregular particles is accomplished by assuming that the relocation of the grains occur in the most efficient manner. As the weak contacts slide and transfer more stress to the stronger con-

tacts, Rowe assumes that the beta values of the contacts are those corresponding to a minimal amount of work done by the soil. This is mathematically defined at the extreme when the change in energy with the change in the β value is equated to zero. Solving for this, one can see that $\beta = (\pi/4 - \varphi_\mu/2)$ and

$$\frac{\sigma_1}{\sigma_3} = \tan^2(\pi/4 + \varphi_\mu/2)\,(1 + d\varepsilon_v/d\varepsilon_1) \tag{2.17}$$

Although Rowe's work provided the first reasonable insight into the relationship between stress ratio and volume changes throughout both contractive and dilatant behaviour, it did have limitations. The use of a minimum energy principle brought on criticism because of the questionable nature of its origin, namely the difficulties in proving the extremum principle when friction is involved [31]. Despite this, Rowe [2] and others [32] provided experimental data which strongly supported his claims.

De Josselin de Jong [31] used the same 'sawtoothed' model as that proposed by Rowe to validate the stress-dilatancy relation with the laws of friction. He based the analysis on a maximum for the deviation angle, λ, between the force acting on a contact surface, and the normal to that surface. When applying the comparison of the deviation angle with the friction angle, φ_μ, to the friction laws, the following can be deduced:

(i) if $\lambda > \varphi_\mu$, the bodies cannot slide;

(ii) if $\lambda = \varphi_\mu$, the bodies can slide;

(iii) $\lambda < \varphi_\mu$ is impossible.

To satisfy the above rules, de Josselin de Jong [31] equated the maximum deviation angle with the friction angle and limited the deformation mode to the direction of λ_{max}. Using simple geometry, an equation resulted which is identical to Rowe's findings, i.e.

$$E^* = \tan^2(\pi/4 + \varphi_\mu/2) \tag{2.18}$$

with E^* defined as the work ratio of major and minor principal effective stresses. The difference between E^* in Equation 2.18 and E in Equation 2.16 is that Rowe's definition of ratio of work in to external work does not hold for cases of non-coaxiality. By specifying the ratio of principal stresses, de Josselin de Jong [31] eliminates this limitation.

Further models of the stress-dilatancy relationship considered the direction of grain movement to be in a plane tangential to the grain contacts [33], [34], [35]. Ueng and Lee [6] attempted to further characterize the deformation of sands, suggesting a concept which divided the grain contacts into slip and non-slip contacts. The insertion of a simplified fabric factor into the stress-dilatancy equation which accounts for the effect of non-slip contacts gave reasonable correlation to laboratory results for drained cyclic direct shear and triaxial tests. However, the confining pressure and initial density influence were still not adequately captured in this model.

2.4.3 Proposed Stress-Dilatancy Relationship

While current practice used to describe the inherent behaviour of granular materials is in many ways adequate for general design and analysis purposes, advanced models are required to capture the complicated responses of frictional materials. The model proposed herein addresses concerns of pressure and density dependencies by means of a void ratio term embedded in the original stress-dilatancy relationship. This term is capable of capturing strain-hardening and softening behaviour as well as constant volume behaviour in a simple elasto-plasticity model. The principal features of the model are a failure surface governed by a Mohr-Coulomb failure envelope, a yield surface in the same form as the failure criterion, a non-associated flow rule governing plastic behaviour and a vertical cut off cap which controls hydrostatic compaction. Chapter five presents the model in detail, with supporting equations and parameter determination methods.

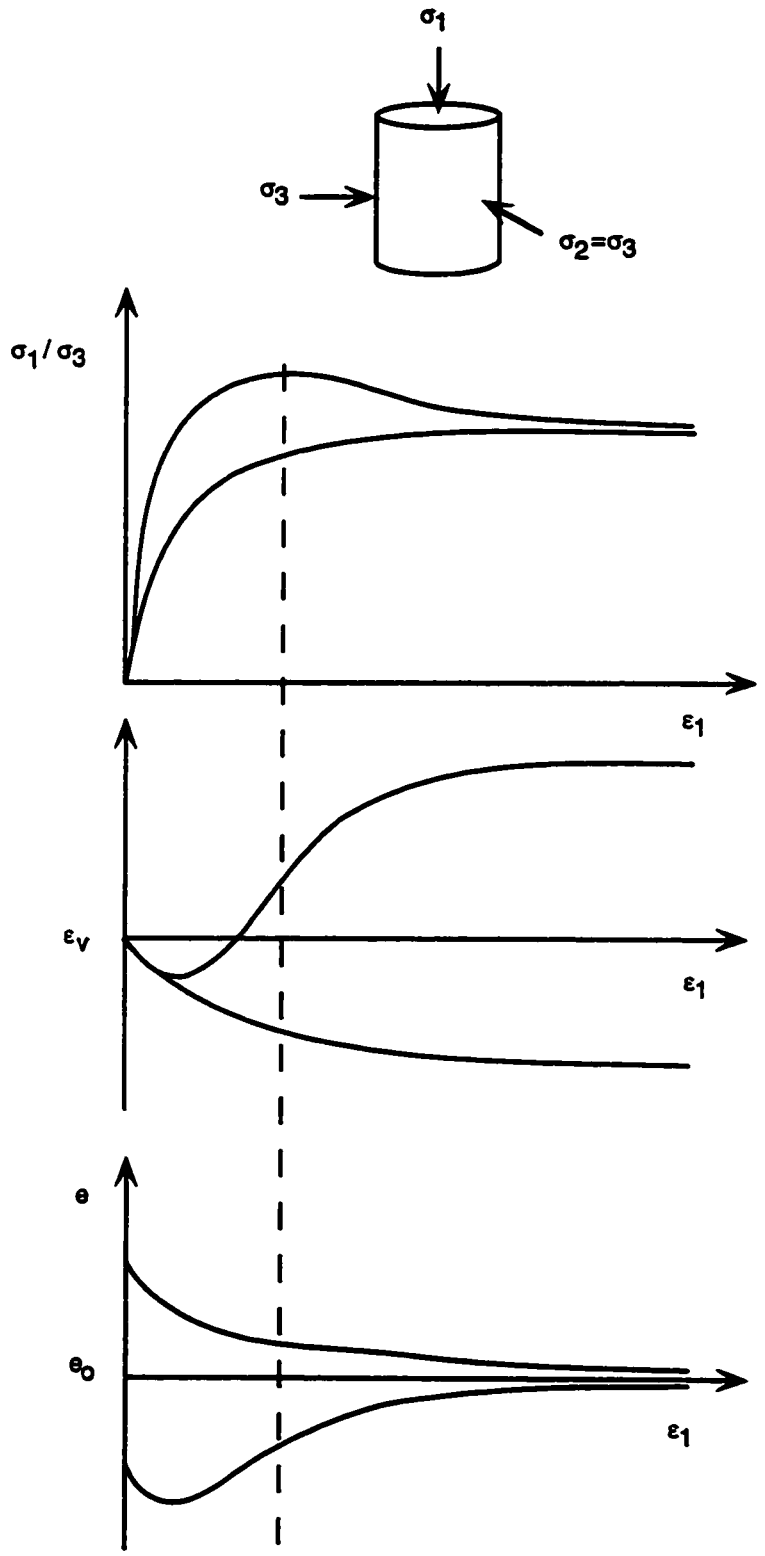

Figure 2.1 Standard Behaviour of Granular Materials under Drained Triaxial Conditions

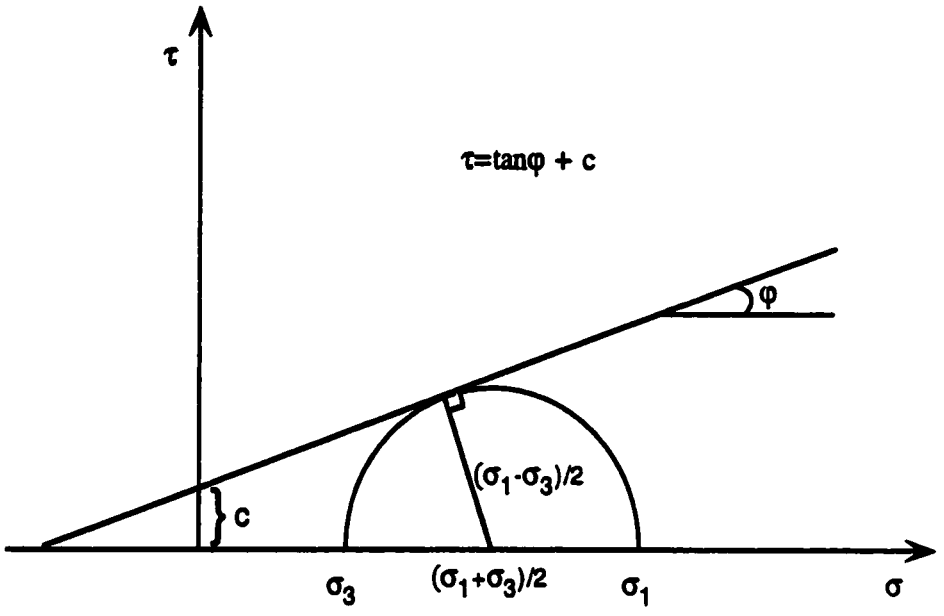

Figure 2.2 Mohr-Coulomb Failure Criterion

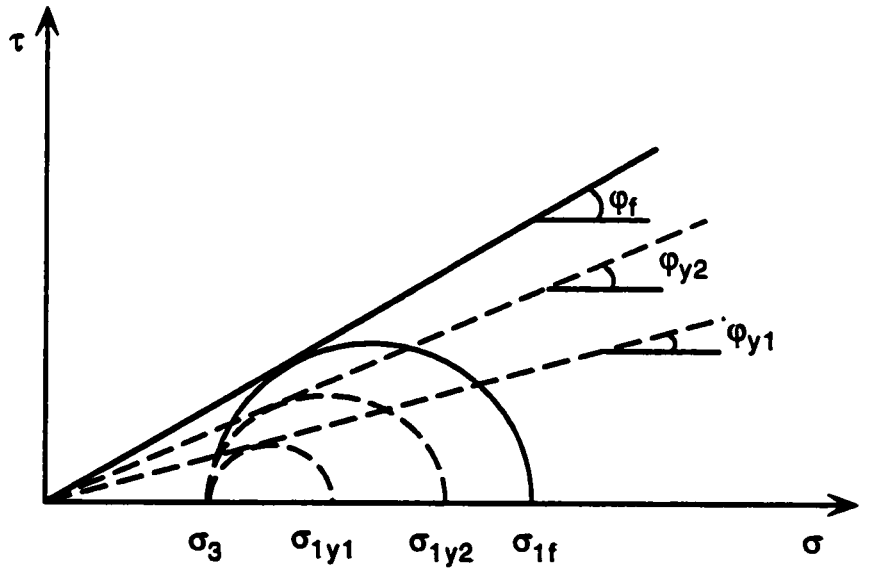

Figure 2.3 The 2-D Yield and Failure Surfaces

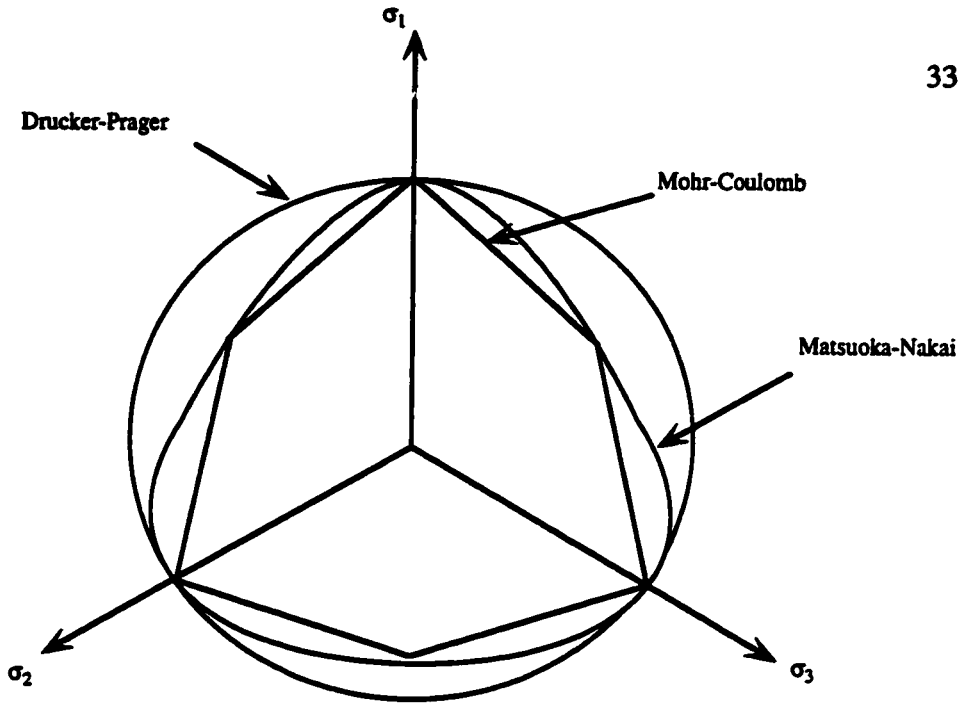

Figure 2.4 Comparison of Common 3-D Failure Surfaces

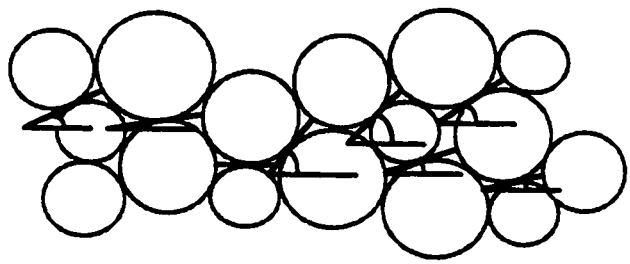

(a) Directions of grain sliding

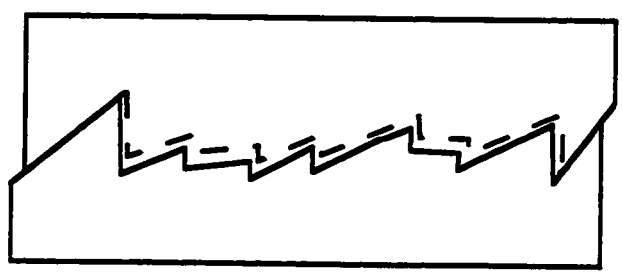

(b) Sliding along selective contacts

Figure 2.5 Microscopic View of Grain Contacts
(after Newland and Allely, 1958)

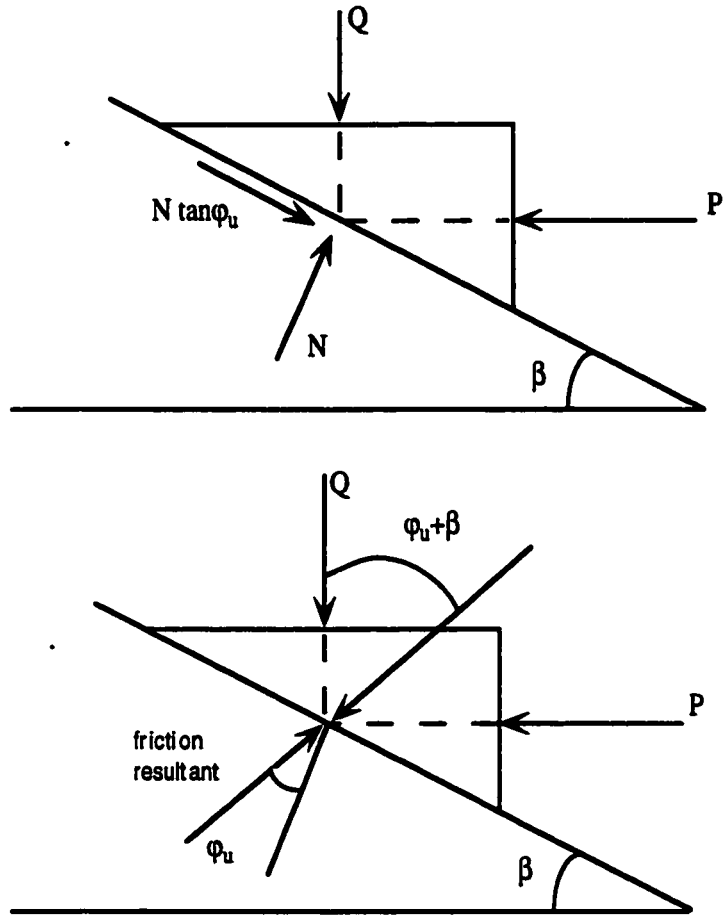

Figure 2.6 Friction of Inclined Planes
(after Rowe, 1962)

Chapter 3

EXPERIMENTAL PROGRAM

3.1 General

Triaxial testing has, in the past, been a common method used to determine the shear strength parameters of soils. At the time it was developed, engineers were primarily concerned with the ultimate failure capacities of geotechnical structures. Less concern was given to the failure mechanisms or deformation characteristics governing the material behaviour. In more recent times however, triaxial testing has evolved into a powerful tool used by researchers to determine accurate strength and deformation behaviour of soils. The development of true triaxial tests, which separate the radial stress application into two independent directions, promotes the ability to imitate cases in which the three principal stresses are unequal, $\sigma_1 \neq \sigma_2 \neq \sigma_3$. Stress path testing is another method used in triaxial testing to provide a more accurate depiction of soil behaviour, as it duplicates the stress history of the soil by varying the path of effective stresses.

Perhaps the most well known and widely used triaxial testing information, *The Measurement of Soil Properties in the Triaxial Test* by Bishop and Henkel [36] provides both a technical and theoretical evaluation of triaxial test procedures. Although published some time ago, the 'Triaxial Book' still contains much of the information

used today. Some exceptions to this are summarized in a paper by Baldi et al [37] . Baldi's re-evaluation discusses topics that are not sufficiently analyzed in the book by Bishop and Henkel [36]. It concentrates on the effects that technological advancements and increased understanding of soil mechanics have on triaxial testing.

Although the testing procedures and equipment used in this research were quite basic, it is worth mentioning that enlarged end platens were introduced to minimize strain localization in the specimen. Overall, accurate and consistent results were achieved with the testing equipment and methods described further in this chapter.

3.1.1 Testing Objectives and Specifications

The primary objective of the experimental program was to capture the stress-strain-volumetric response of Ottawa sand over varied initial densities and confining pressures. The approximate targeted void ratios of the prepared samples were chosen to be 0.53, 0.63 and 0.70 representing dense, medium dense and loose conditions, respectively. Relatively low confining pressures were utilized, capturing a wide range with 200, 500 and $800kPa$.

Nine samples were used for the monotonic loading triaxial tests to determine the parameters for a stress-dilatancy model which will be discussed further in Chapter five. The specimens prepared were all $76mm$ in diameter with a 1.2 to 1 height to diameter ratio. Each sample was formed by the moist tamping method, with the amount of material in each layer adjusted to reflect the desired initial dry density. Enlarged, lubricated end platens minimized adverse testing effects such as localized failure and barreling of the sample. The elimination of such heterogeneous behaviour

is essential in the validation of constitutive models as they are difficult to develop without the assumption of a homogeneous material.

3.1.2 Determination of Physical Material Parameters

Various preliminary tests were undertaken prior to the triaxial experiments in an attempt to characterize the Ottawa Sand (C-109). Although this material is commonly used in geotechnical research and has fairly well defined properties, it is deemed important to describe the sand in this particular investigation. The specific tests were conducted with procedures recommended by Das [38] and Liu and Evett [39] and encompassed the determination of grain size distribution, specific gravity and the maximum and minimum densities.

3.2 Testing Equipment

The testing equipment consisted of two independent vacuum sources; two independent pressure sources; a load frame; the triaxial cell; transducers to measure volume change, axial displacement, load and pressures; and tubing to connect air and water sources to the cell. Figure 3.1 offers a brief schematic of the monotonic triaxial testing setup and the placement of the above equipment.

Data was gathered using a Labtech Notebook data acquisition program [40]. The program was run on an IBM compatible PC. It logged readings of load, axial deformation, volumetric deformation, confining pressure and top and bottom pore

pressure at controlled specified time intervals. Labtech Notebook was also capable of plotting data as received, allowing an immediate, but rough, estimate of the soil behaviour.

3.2.1 Mold Design

The desire for a height to diameter ratio of 1.2 and enlarged, $89mm$, platens required the design of a specific split mold to be used in forming the samples. The aluminum mold had an interior diameter of $76mm$, with the diameter of the outer ends increased to $89mm$ to fit around the platens. Holes were cut at mid height on each side of the mold to provide a vacuum intended to hold the membrane tight against the form during the wet tamping process. Two clamps were fitted to ensure a tight seal could be maintained and the mold could be removed with ease after the sample was created. A diagram of the mold design is shown in Figure 3.2.

Initial difficulties with maintaining a seal between the two halves of the mold were avoided by placing a thin layer of Dow Corning silicon vacuum grease between them prior to clamping the mold. This proved adequate and allowed for the vacuum to hold the membrane tight against the mold during sample creation.

3.2.2 Triaxial Cell

The standard triaxial cell base was found to be acceptable for use with the intended triaxial testing with the exception of the top platen seals and the platen size. The base is shown in Figures 3.3 and 3.4. The entire cell is pictured in Figure 3.5.

A connection is provided in the cell base to attach the confining pressure line. Back pressure is controlled through one of each of the top and bottom platen inlets into the sample and measured by a pressure transducer attached to the top and bottom inlets on the opposing side. All of the four inlets into the sample can be controlled individually allowing a varied range of options when applying pressure to the sample.

Modifications to the cell involved the replacement of the standard o-ring seal used to connect the $0.125mm$ tubing from the base to the top platen. The original design created an unreliable seal with the potential to allow the cell pressure and the back pressure to influence one another. Instead, a push-to-connect fitting [41] was used at either end, capable of holding a seal up to pressures of $1500kPa$.

The cell platen size was increased from a diameter of $76mm$ to that of $89mm$. This caused a slight overlap with the new push-to-connect fittings on the base. The difficulty was overcome by cutting out a portion of the bottom half of the platen to allow room to insert the tubing into the fittings. The standard cell wall and top attachment did not require modification.

3.2.3 GDS Pressure Controller

The GDS Pressure Controller [42] was able to generate, measure and regulate liquid pressure up to $3MPa$. Its target pressure and ramping capabilities as well as the $1kPa$ accuracy and resolution made it an ideal regulator for confining pressure control.

3.2.4 Measurement Devices

The cell and back pressures were measured by pressure transducers placed in the respective pressure lines. Back pressure was measured in the lines both entering and leaving the sample to ensure no pore pressure buildup would occur during the application of confining pressure or shear stress.

Axial deformation was measured externally by means of a linear variable displacement transducer (LVDT) placed on the loading ram of the triaxial cell. An Imperial College volume change transducer was attached to the back pressure line to obtain volumetric strain values of the sample by measuring the volume of water entering or leaving the sample.

Load measurements were also taken externally by a $50kN$ capacity load cell placed on the load frame. All measurement devices were calibrated at the commencement of the test program and at regular intervals throughout testing.

3.2.5 Load Frame

The application of the axial load was provided by an ELE Digital Tritest 50 load frame [43]. The frame provides a strain-controlled loading at speeds ranging from 0.00001 to $9.99999mm$ per minute and can provide a force of up to $50kN$. Figure 3.6 shows the load frame as well as the GDS pressure controller.

3.3 Homogeneity

3.3.1 Free ends

The use of free ends in triaxial testing has been extensively discussed by many prominent authors [25], [44], [45], [46], [47], [36]. It is widely agreed that the use of lubricated ends allow for a relatively homogeneous stress distribution throughout the test specimen. This eliminates much of the tendency towards bulging of the sample, a condition where the stress interaction between the platens and the sample causes the majority of the radial strain to occur in the centre of the specimen.

The effects of bulging are witnessed by the results of the triaxial test. Increases in the initial modulus of elasticity and peak strength are a product of rough ends, as well as a less pronounced volume change. These errors, coupled with the uncertainty of interior localized stress regions give cause for the researcher to promote the use of free ends. Although practice of lubricating the area between the sample and the platen has many benefits, the use of these devices is not common to laboratory triaxial testing. The reason for this is primarily the inconvenience of preparation and additional time required during the test. Germaine and Ladd [47] provide a brief synopsis of the advantages and limitations of free versus rough ends as shown in Table 3.1.

With a knowledge of the effects of free ends on a soil sample, it is evident that different testing conditions will be instrumental on the degree of influence of these ends. An initially loose sample will not be as severely affected by barreling and other localized strain effects. The data resulting from triaxial testing on a dense sample,

Frictional Ends		**Lubricated Ends**	
Reasons For	Reasons Against	Reasons For	Reasons Against
easy set-up procedures	nonuniform stress and strain	improves uniformity at all strain levels	more difficult to assemble
simple, efficient drainage	nonuniform excess pore pressure	reduces strain rate effects	reduces small strain precision
stiff apparatus for axial strain measurement	water migration	reduces uncertainty in area correction	increases consolidation time
simple cell geometry	larger strain rate effect	essential for large strain behaviour	
	formation of rupture surfaces		

Table 3.1: Comparison of Frictional and Lubricated Ends

however, will be significantly altered as barreling is difficult to avoid without some form of lubrication on the soil-platen interface.

While the use of free ends does much to reduce the rigid zone and other localized effects, its common design can still create an interaction surface and heterogeneity. Typically in triaxial testing, a hole will be cut in the centre of the free end to allow for drainage by means of a porous stone. Although the disturbance from this hole is a relatively small rigid cone and therefore difficult to detect, Colliat-Dangus *et al.* [44] have characterized the local compactedness of the area with an x-ray scanning device. Their results show that localized failure does occur, but claim that it does not significantly effect the ability to determine the overall behaviour of the sample.

The porous stone used in the tests conducted by Colliat-Dangus and coworkers was typical of that employed in many triaxial experiments, both for design and research work. Having a much smaller diameter than the sample, the stone either sits directly against the soil or against filter paper which is placed over the soil. Even with the inclusion of free ends, the surface between the porous stone and the soil is not effectively lubricated.

An alternative method of drainage through the free ends was used by the author. The porous stones available were cut to the same size as the enlarged platens. Initially, the free ends used were typical of those used in experimental programs such as that shown in Figure 3.7, designed with a central hole with a diameter of approximately 20 *mm* to allow drainage. However, it was found that the use of a solid circular free end with four notches cut approximately 2 *mm* into the sides (Figure 3.8) could provide adequate release of water pressures using the correct placement of

filter paper. Although no numerical results were obtained to capture the influence of the free end design, the decrease in bulging effects was visibly apparent giving a more uniform cross-sectional area over the sample height.

3.3.2 Design of Free Ends

The use of free ends with the triaxial test has long ago been shown to reduce localized volume change and barreling during the procedure by providing a 'frictionless' transition between the sample and the platens [36]. More recently, studies such as those by Colliat-Dangus et al [44] limited the advantages of free ends to tests on dense sands. Looser samples exhibit little difference in behaviour when the free ends are neglected. Despite this, lubricated ends were used for all samples to avoid discrepancies in the resulting behaviour.

The free ends are formed by cutting latex membrane material and a Teflon sheet into a circle of the same diameter as the platen. These sheets are then pressed together with a layer of Dow Corning silicon vacuum grease between them. The common design of free ends includes a hole about one quarter to one third of the total diameter cut into the centre of the sheet to provide drainage [48], [44]. The entire free end is then subjected to a load of $0.5kN$ for 15 minutes, increasing to $3kN$ for the next 15 minutes and finally a $10kN$ load for 30 minutes. This ensures the absence of air pockets between the Teflon and latex, forming a consistant interface between the two surfaces. In this particular investigation, the centre hole was eliminated in an attempt to prevent the additional friction source created by the inconsistent surface. Instead, four notches were cut from the edges with filter paper wrapped around them

to allow drainage around the sides of the free ends.

3.4 Triaxial Testing

The monotonic triaxial testing procedures implemented in this research generally followed standard procedures. A great deal of time and practice were required to learn a consistent method of sample preparation and to further synchronize the shearing mechanism to achieve reproducible results. The effort proved rewarding with void ratios, back calculated from final volume measurements, measuring within 0.03 after the completion of saturation and consolidation procedures. The patterns of the stress and volume change curves were also typical of those expected from Ottawa sand.

The preparation of the sand specimen is crucial to the outcome of the investigation due to a need for reproducible results. Care must be taken through all stages prior to the actual shearing of the sample. These stages involve the placement of the sand into the mold, proper saturation of the sample, and the application of confining stresses.

The initial void ratio of the sample must be effectively controlled during testing in order to duplicate results. The difficulty in producing a consistent density throughout the sample by the method of placement has lead to a number of different techniques [49], [50], [51], [52], [53]. These methods include air pluviation; raining dry sand from a constant height into the mold, wet pluviation; pouring saturated sand into a water filled mold, vibration and tamping.

Each of the above methods can be used to prepare a saturated sand sample. However, various characteristics of the procedures suggest that the ease of preparation and the accuracy of results are dependent on the desired density and the employed method. For example, the height of drop for pluviation through air must be accurately controlled to ensure that the velocity of particles pouring into the mold remains constant throughout the fill. On the other hand, pluviation through water requires a much less accurate height of drop because most sand particles will reach terminal velocity almost instantly in water [50].

Vibration is generally used subsequent to pluviation to increase the density of the sample. Pluviation, especially through water, will create a 'loose' specimen. In order to achieve a more compact sample, a vibratory table with a constant frequency and amplitude can be used. In creating reproducible densities, care should be taken to vibrate each specimen for an equal length of time under identical conditions.

Another common method used to achieve a constant density is wet-tamping. In this process, the material is wetted to 5−10% water content. It is subsequently placed into the mold and tamped in lifts until the desired compaction is reached. Because the lower lifts tend to become more dense with the placement and tamping of layers above them, Ladd [52] suggested a method called undercompaction. The procedure involves compacting each layer to a certain percentage of the desired dry unit weight, with the first lift compacted the least and the top lift generally compacted to 100% of the desired density. The final product is a sample with a constant density throughout its length.

Advocates of the tamping procedure claim that its superiority over pluviation

results from two main disadvantages of the direct pouring of sand [51]. The first is the segregation of particles when using silts or well-graded sands. This is mostly seen in the air pluviation methods, as the velocity of a falling particle is dependent on its mass. The larger grains will reach the mold before the smaller ones, creating non-homogeneity. Pluviation through water will not show these effects as soil grains reach terminal velocity almost instantly in water. The second shortcoming of pluviation is the difficulty in preparing a sample to a specific dry unit weight, preventing the control of the initial void ratio.

3.4.1 Sample Preparation

In this particular testing program, the method of wet tamping was used. Each sample was initiated by the determination of a desired void ratio. This void ratio was based on the required density just prior to shearing, which was adjusted to account for saturation and compaction effects. Unfortunately, an exact prediction of the adjustment was impossible, causing difficulties in creating samples of exact initial densities.

The dry unit weight of sand required was determined from the void ratio. Calculations were performed based on Ladd's [52] method of undercompaction. The purpose of undercompaction is to manipulate the layer heights, compensating for the effects of additional tamping on the bottom layers, so that an even density can be maintained throughout the sample. It was found, however, that for the desired specifications of this particular research, the undercompaction adjustments were negligible. The dry sand was mixed thoroughly with water to obtain a moisture content

of 8%. The use of water in the making of remoided sand samples prevents the buildup of static electricity between the particles, thus easing the preparation procedure. The sand-water mixture was then divided into eight equal portions, placed in water tight containers and left for one hour to ensure a uniform mix.

The two porous stones used in testing were cut from a $3mm$ thick sheet of sintered steel. They were formed to completely cover the enlarged platens, with a diameter of $89mm$. To prevent gasses from entering the enclosed triaxial sample, the porous steel was boiled in deaired, distilled water for one hour just prior to placement. The porous stone, free end and filter paper were then placed on the platen of the triaxial cell base. Generally, the use of filter paper is not necessary for triaxial testing of sand specimens. Drainage is considered to be independent of time and the grains large enough to prevent the sample from washing into the porous stone. However, the Ottawa Sand in the triaxial setup did not exhibit these features. Pore pressure buildup in the sample occurred most likely as a result of insufficient drainage in the system. Tests done using various free end and filter paper configurations still showed evidence of fluctuating internal water pressures. As the Ottawa Sand is considered free draining, the pressure buildup must come from the triaxial system. It is possible that some blockage in the tubing, cell valves or volume change transducer may have been responsible for the reduction in drainage capabilities of the sample. To compensate, careful use of filter paper around the free ends was used as described previously. Filter paper was also placed over the porous stone as tests without showed evidence of sand filtering through the sintered steel and into the drainage lines. A $76mm$ diameter latex membrane was positioned around the platen and held

in place by small elastic bands. The elastic bands were used only temporarily during sample preparation to allow for a tight seal between the mold and the latex, as the o-rings did not fit under the split mold.

Vacuum grease was placed on the edges of the split mold to create an air-tight seal and the mold was secured around the bottom platen. The membrane was then stretched around the top mold opening and a vacuum was applied to hold the membrane tight against the form.

The first lift of soil was carefully poured into the mold, smoothed and then tamped in a radial pattern from the centre outwards to a height one eighth that of the entire sample. The layer was then scarified and the next lift was placed, tamped, measured and scarified.

Special care was taken during tamping of the top layer to ensure a level, homogeneous interface between the soil and the platen. The filter paper, free end, porous stone and platen were placed on this top layer with an effort made to create an even contact surface between the soil and equipment. Gentle stretching of the membrane was required to pull it off of the mold and secure it around the top platen. Two o-rings sealed the latex membrane to the top platen.

The tubing connecting the top platen and the triaxial cell base were sealed into the fittings and an internal vacuum of $10kPa$ was applied to the soil through the triaxial cell base. This vacuum held the soil in place, preventing density changes as the mold was carefully removed and the elastic bands on the bottom platen were replaced by o-rings.

To determine the actual initial density of the soil, three readings were taken of

each the specimen height and diameter. These measurements were performed with a micrometer, and were averaged and adjusted for the thickness of the membrane to find the 'exact' volume of sand.

Sealing of the triaxial chamber involved placing a light coat of silicon vacuum grease on the ends of the Plexiglas cylinder before placing it between the ends of the cell. These were tightened together and the cell chamber was entirely filled with water.

Once the cell was full, the line to the water source was detached and connected to the GDS pressure controller which brought the confining pressure to $10kPa$. The internal vacuum was simultaneously reduced, maintaining an effective stress of $10kPa$ on the sample at all times.

The triaxial cell outlets were arranged so that one pressure source could be connected to either the top or bottom of the sample, or to both. A pressure transducer was also connected to the cell, enabling readings to be taken from the top or bottom of the sample.

3.4.2 Saturation and Consolidation

Complete saturation of the specimen is required to ensure accurate results of volume change measurements in triaxial testing. The saturation procedure involves the initial flushing of the sample and subsequently an increase in back pressure. When completed, the process provides a sample that has a negligible amount of air voids. Using the assumption that neither the soil particles nor the water is compressible with load application, the volumetric strain will be entirely reflected by the amount

of water going into or coming out of the specimen. The use of CO_2 to flush the sample prior to saturation is a technique which facilitates more thorough saturation. CO_2 is more soluble in water than air, reducing the time and pressure required to adequately saturate a soil. The Ottawa Sand was flushed with CO_2 at a pressure of approximately $2kPa$ for 15 minutes before being flushed with water at $2kPa$ for 20 minutes. The low pressure used to push the gas and water through the sample ensures minimal disturbance and less chance of the creation of heterogeneity by means of particle rearrangement and or piping. It is of interest to note that the author attempted to saturate a sample of Ottawa Sand without first flushing it with CO_2. The length of time required to somewhat saturate the soil more than tripled, and the back pressure used to satisfy the B-test was significantly higher than that used in the samples which were previously flushed with the gas.

The application of back pressure will increase the compressibility and the solubility of air in water [37]. Back pressures in the Ottawa Sand were increased to between 100 and $300kPa$ depending on satisfactory results from the B-test. The B-test determines Skempton's B value [54], a parameter which measures the increase in pore pressure occurring during undrained loading due to an increase in confining pressure. To perform this test, the valves into the sample were closed, and the change in pore water pressure measured as an increase in cell pressure was applied. The test causes little disturbance to the sample as the effective stress remains virtually unchanged. If, however, the sample is not completely saturated, the effective confining pressure will increase significantly. Air voids in the sample will prevent the internal pressures from increasing at the same rate as the cell pressures, and consolidation of the soil

will take place prematurely. While the B-test reflects the degree of saturation, it does not measure this value directly. Black and Lee [55] show that for Ottawa Sand, a B value of 95% corresponds to well over 99% saturation, an amount acceptable in tests measuring volumetric strains. The triaxial specimens in this experiment held B values of at least 95% with most of them being over 97%.

The saturation of the sample can cause significant changes in the void ratio of the soil. Flushing with CO_2 and water creates a slight shifting of the soil particles, even when done at very low pressures. If not done carefully, these procedures can cause piping or large volume changes in the soil. The application of back pressure and the B-test should theoretically cause no structural breakdown as effective stresses remain constant. Realistically, uneven application of the pressures, and even a slight air content in the water or the sample can cause a rearrangement of the soil and adjust the void ratio.

Back calculations were performed in this research to determine the changes in density caused by saturation. These effects were found to be significant and therefore are incorporated into the calculations of void ratio prior to shearing.

Isotropic consolidation of the samples commenced subsequent to the completion of a satisfactory B-test. Free drainage was allowed, and the volume change transducer was implemented to measure the void ratio change as consolidation proceeded. The cell pressure was gradually raised using the ramp using the ramp function of the GDS pressure controller. Typically, the ramp was set at $2-4$ seconds per kPa to prevent pore pressure buildup. At this rate, the confining pressure was increased until the effective stress measured 200, 500 or $800kPa$, depending on the test re-

quirements. The sample was then left to consolidate until no further volume changes were witnessed.

3.4.3 Shearing of the Sample

The ELE Digital Tritest 50 load frame was used to apply an axial force to the loading piston of the triaxial cell. Prior to the onset of the initial load, the load cell was reset to zero so that the effects of confining pressures on the loading ram would not be reflected in the stress measurement. The test was run at a constant strain rate of $0.05 - 0.10mm$ per minute $(3.25 - 6.5\%/hr)$. The necessity of the low strain rate was caused by unexpected pressure buildup during shear. It was desired to keep the changes in pore pressure to within 2% of the effective confining pressure as suggested by Lacasse and Berre [56]. This is not expected to be of concern in the testing of sands as they are considered to experience instantaneous drainage [36]. However, the fine Ottawa Sand did not drain immediately, requiring careful adjustment of the strain rate. The samples were generally sheared until the strain reached 30%, the radial strain caused the diameter of the sample to exceed that of the enlarged platens or constant volume conditions were reached. None of the samples showed evidence of shear bands or other heterogeneous behaviour with the exception of slight bulging

Upon completion of the triaxial test, the axial strain was ceased concurrent to the closure of the sample drainage valve. The confining and internal pressures were then reduced to zero, the cell drained and the triaxial cell base holding the sample was frozen for a period of 24 hours. After complete freezing, the sample was removed from the membrane, weighed, dried and weighed again. From the dry and wet mass,

the final void ratio was determined.

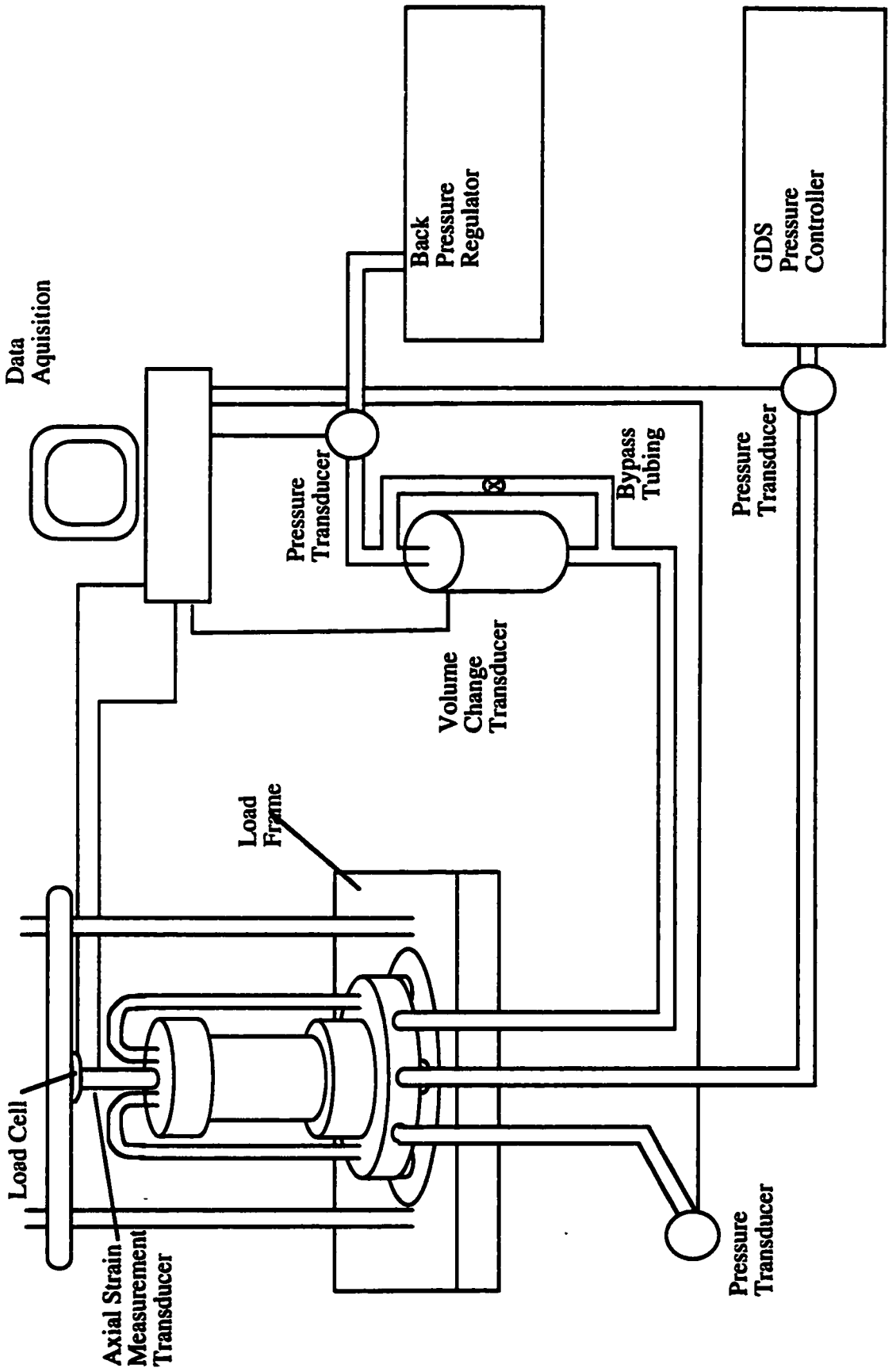

Figure 3.1 Schematic of Triaxial Testing Apparatus

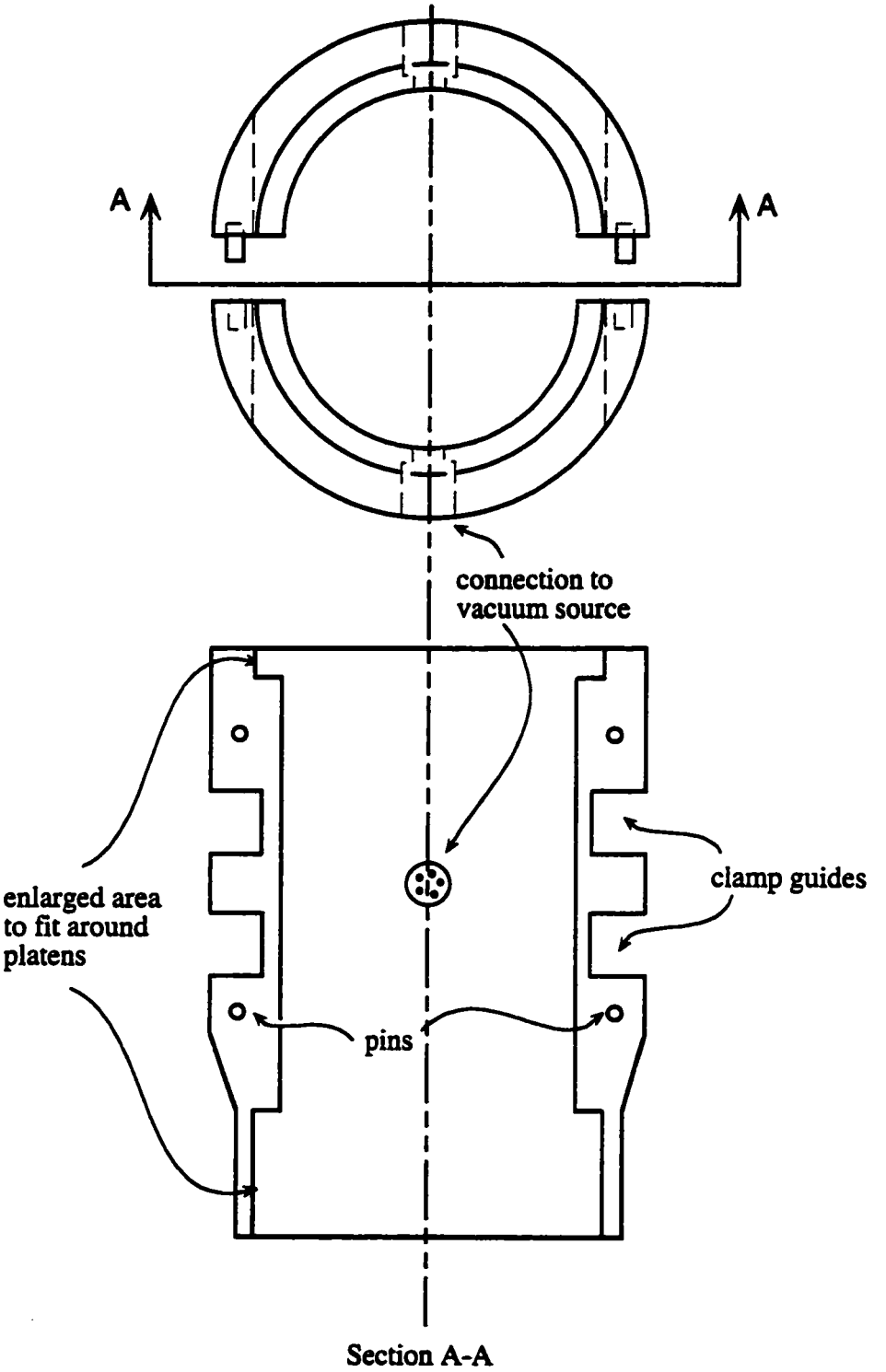

Figure 3.2 Split Mold Design

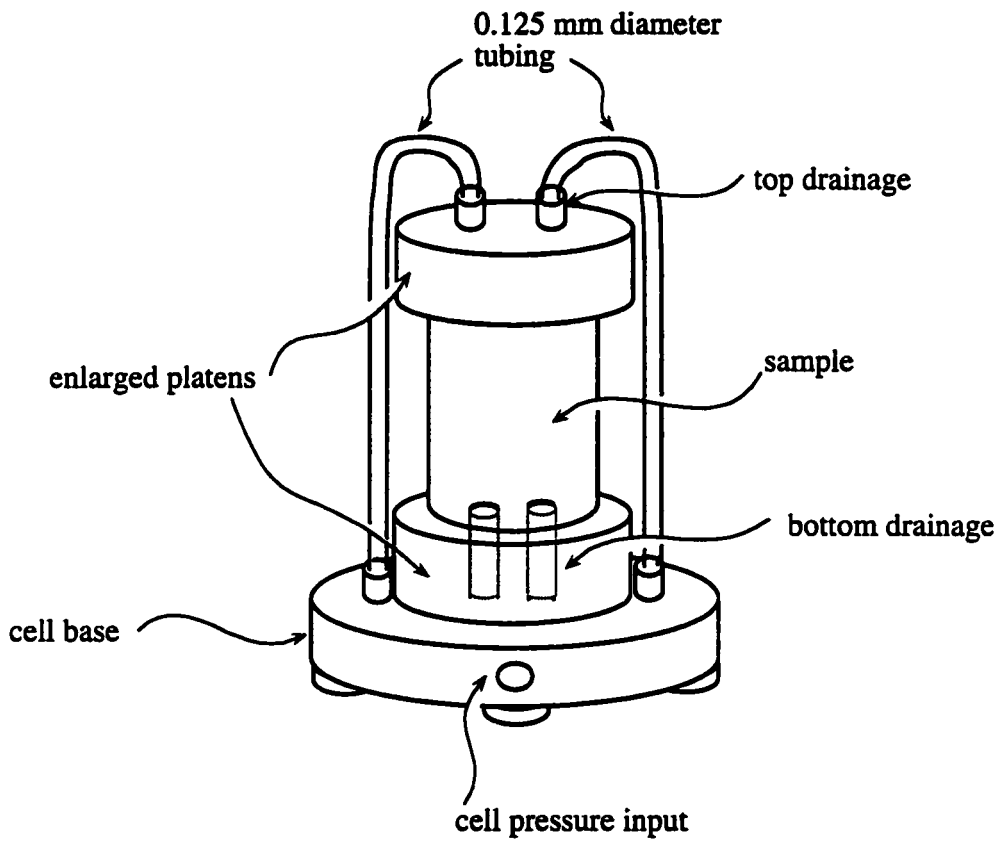

Figure 3.3 Triaxial Cell and Sample

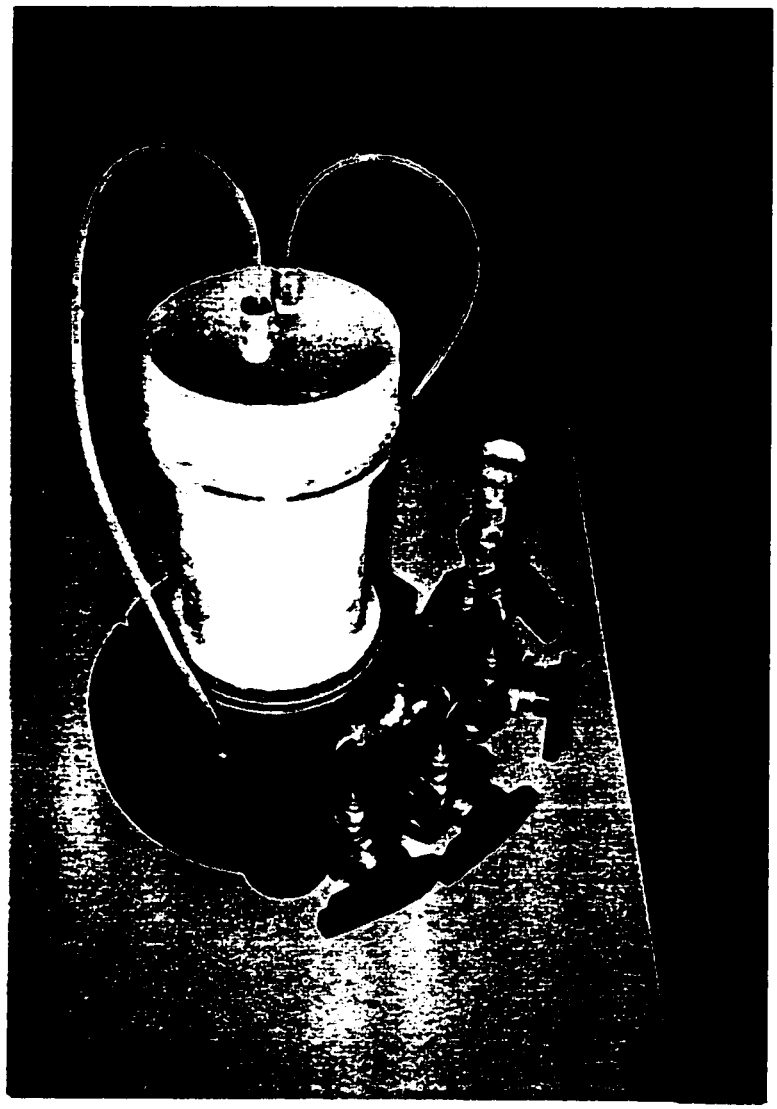

Figure 3.4 Triaxial Cell and Sample (Photograph)

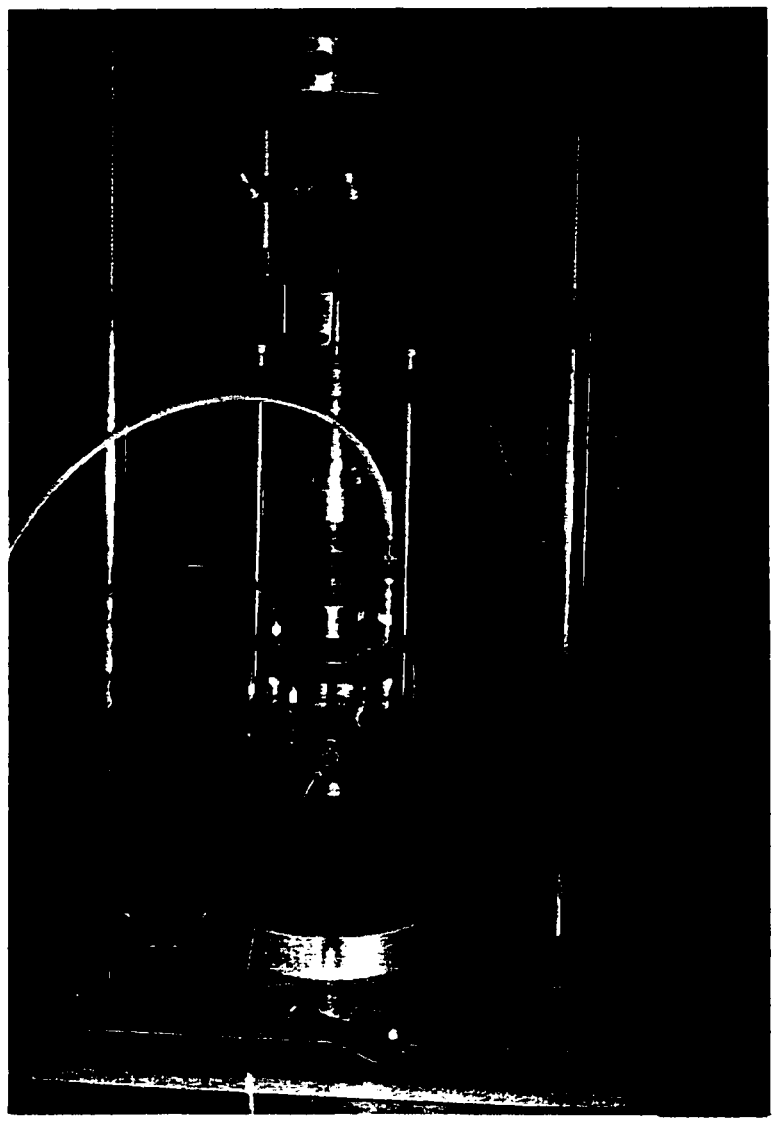

Figure 3.5 Triaxial Cell and Load Frame

Figure 3.6 Load Frame and Pressure Controller

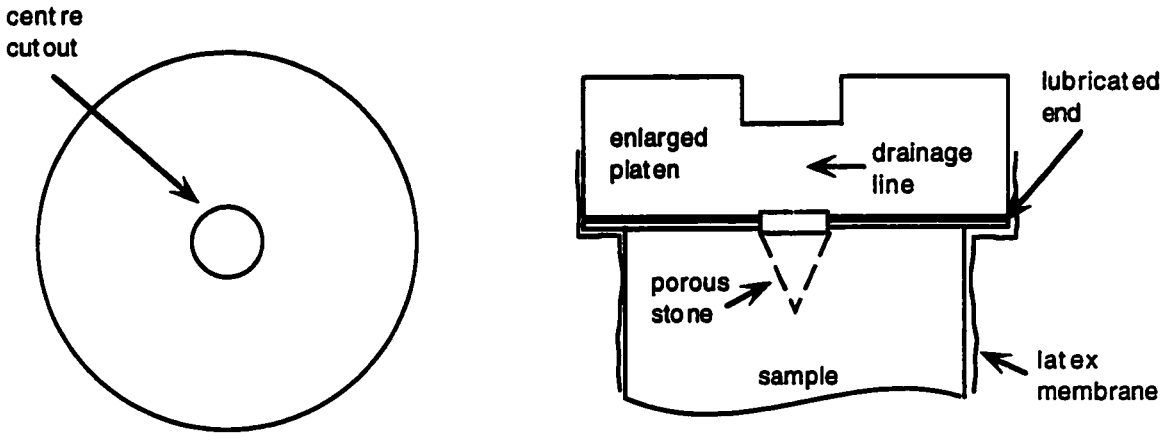

(a) plan view of free end

(b) side view of arrangement

Figure 3.7 Typical Free End Design Arrangement
(after Colliat-Dangus *et al.*, 1988)

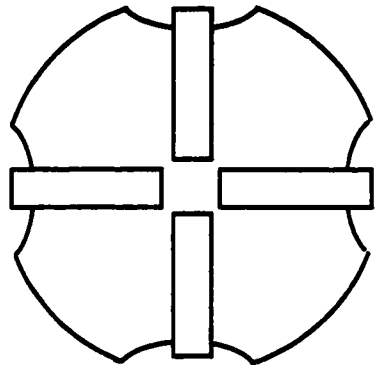

(a) plan view of free end

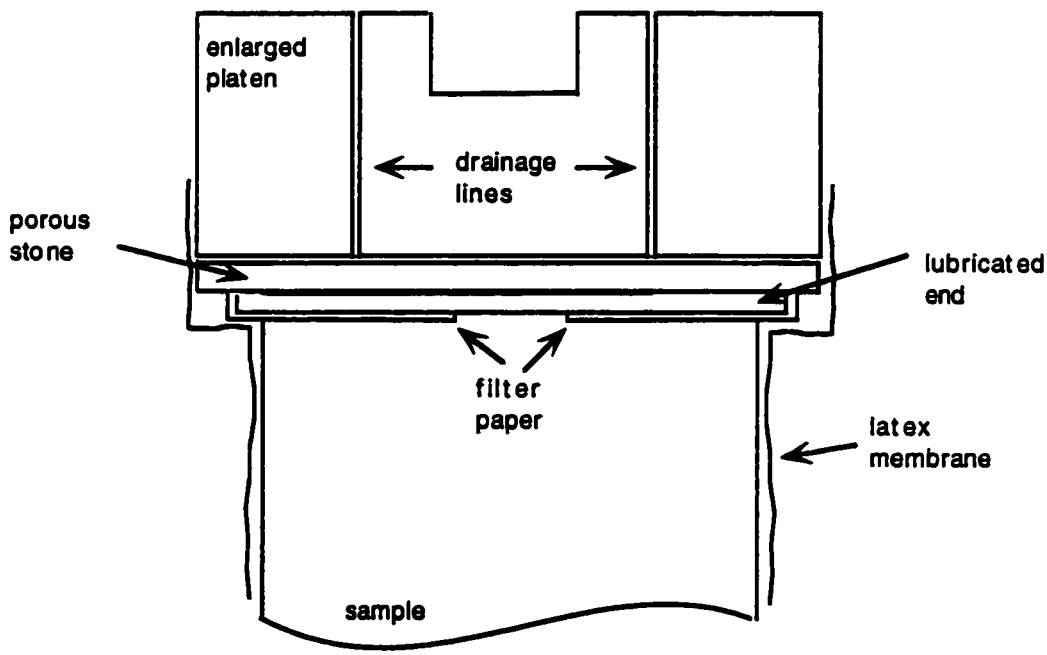

(b) side view of arrangement

Figure 3.8 Free End Design Arrangement used in Experimental Program

Chapter 4

THE BEHAVIOUR OF FINE OTTAWA SAND

4.1 General

Ottawa Sand is a commercially available quartz sand with rounded grains and is a standard material used in laboratory testing of granular materials. The determination of the physical material parameters as well as the behavioural characteristics of Ottawa Sand provides insight into the development of the proposed stress-dilatancy model. From this information, all model parameters are determined and their accuracy is crucial to the model outcome.

Extensive testing has been conducted on granular materials for purposes of material parameter determination. However, the reliable testing of a sand required to verify the proposed model is not as readily available. Common intentions of triaxial results are the independent determination of elastic parameters or peak strength (Mohr-Coulomb) parameters or, more recently, critical state conditions. Rarely are these three states extensively explored in one test. A wide range of initial conditions is preferred to determine the model's capability to predict material behaviour. Precise measurements of stress and volumetric changes from initial conditions through peak behaviour to the critical state were undertaken. The results of these experiments are presented in the following sections.

Sieve Analysis	Specific Gravity	Void Ratio
$D_{10} = 0.235mm, D_{30} = 0.305mm$		$e_{max} = 0.74$
$D_{50} = 0.335mm, D_{60} = 0.390mm$	$G_s = 2.65$	
$C_u = 1.66, C_c = 1.02$		$e_{min} = 0.52$

Table 4.1: Results of Preliminary Physical Parameter Determination

4.2 Physical Material Parameters

The preliminary testing conducted to determine the physical characteristics of the fine Ottawa Sand included the measurements of grain size distribution, specific gravity and maximum and minimum void ratios. The plot of particle size is shown in Figure 4.1. Table 4.1 summarizes the remaining test results where D_{10}, D_{30}, D_{50}, and D_{60} represent the grain diameters at 10, 30, 50 and 60% passing, respectively. The C_u and C_c values indicate the coefficient of uniformity and coefficient of curvature.

Under the Unified Soil Classification System, the material is classified as a rounded fine uniform sand [54]. The specific gravity, G_s of 2.65 is consistent with common measured values. The expected maximum void ratio, e_{max} of 0.80 [50] was slightly higher than the value of 0.74 measured herein; likely due to inconsistencies in the practiced test procedures. These inconsistencies easily develop between different laboratories, especially in the determination of maximum void ratio, as the test involves the measured volume of sand after shaking it in a graduated cylinder. The determined value of minimum void ratio, $e_{min} = 0.52$, is typical of measured values.

4.3 Behaviour of Ottawa Sand

The measured characteristics of Ottawa Sand during the drained monotonic triaxial testing provided results characteristic to those of a uniform fine granular material. The initial packing and confining pressures of the sand is shown to greatly influence both the strength and the volumetric responses of the sand. Loose samples showed no evidence of dilatancy or strain softening while the dense samples portrayed opposite results of expansion and peak strengths.

4.3.1 Stress-Strain Response

Figures 4.2(a), 4.3(a), and 4.4(a) show the stress-strain response curves of Ottawa Sand at various initial densities and confining pressures. The plots are typical of Ottawa Sand at the given void ratios and confining conditions. The much steeper initial slopes of the curves indicate the much higher strength of dense materials which also show strong evidence of strain-hardening and softening effects. At 'large' axial strains, the critical state is approached and the three curves converge to the constant volume stress value, $(\sigma_1/\sigma_3)_{cv}$. The initial density also seems to influence the rate of strain hardening with the highest value corresponding to denser states.

The influence of confining pressure is not as great on the stress-strain curves as that of initial density. However, with increasing cell pressures the initial slope of the principal stress ratio, the peak stress ratio declines. Thus, an elevated confining pressure results in an apparently weaker material.

4.3.2 Volumetric Strain Response

Volumetric strain is plotted against axial strain in Figures 4.2(b), 4.3(b), and 4.4(b). Dilatant behaviour is obvious in the dense sands while contraction is prevalent for the looser materials. Samples sheared from void ratios close to that of critical experience little change in volume during testing. It is of interest to note the path these sands follow when they experience volume change. Contraction occurs initially in all samples as particle rearrangement occurs and the contact forces are established. From there, the loose sands continue to densify as the axial strain is applied until the constant volume is reached. The dense sands quickly reach a minimum volume and thereafter begin to expand as a result of grain overriding. The volumetric strain curve reaches a maximum slope at a point which is close to or at peak on the stress-strain curve. The slope then gradually reduces and strives towards achieving a zero value. Had the test continued, this slope would have eventually exhibited a horizontal trend, a common critical state characteristic.

The medium dense sands tested in this program were prepared at initial void ratios close to the critical values. Observation of the experimental results show that they experience very little volumetric strain throughout the triaxial test when compared to the loose and dense samples. For example, the medium dense sand tested at a confining pressure of $800kPa$ has an initial void ratio of 0.639, almost equal to the critical value of 0.637. Theoretically, even though the initial void ratio is at its critical value, the material is not at critical state since there is no shear stress and the mobilized friction angle ,φ_m, is not equal to the constant volume friction angle, φ_{cv}. Hence, as the material is sheared measurable volumetric strain

(Figure 4.4(b)) shows initial contraction followed by dilation with the void ratio finally reaching its critical value. The volume change curves of the loose material seem to maintain a horizontal slope at a much lower axial strain than the medium dense material. However, the actual volume change that the loose sands exhibit is much greater than that of the medium dense sands. An explanation of this could be that the energy required to move the grains against the confining pressure to cause even a slight amount of dilatancy is much greater than that needed to move the grains in the direction of the confining pressure.

The volume changes experienced by Ottawa Sands are also influenced by confining pressure. As the cell pressure becomes greater, dense sands produce less dilation. Loose sands also reflect the same trend, compressing with shear as the confining pressure is increased.

4.3.3 Dilatancy

The stress-dilatancy relationship also shows trends consistent with expected granular material behaviour. The plots shown in Figures 4.5 through 4.7 give a clear picture of dilatancy evolution for each test. Based on the definition of dilatancy D as being $(1 - d\varepsilon_v^p/d\varepsilon_1^p)$ with volume expansion represented by negative values of $d\varepsilon_v^p/d\varepsilon_1^p$, a dilatancy value less than one describes contractive behaviour. The loose material remains in this region through the duration of shear application. Alternately, dense particulate materials will achieve dilatancy values both below and above unity as they experience contractive and expansive stages.

The direct measurement of dilatancy cannot be taken during the triaxial test.

It is instead calculated from the slope of the plastic volumetric strain versus the plastic axial strain curve. Mathematical difficulties in defining this slope are caused by sensitive measurements in that the changes in strains, while following a general curve, are not uniform from one set of readings to the next. If, for example, the change in plastic axial strain between readings is zero, the solution for dilatancy is undefined. Graphical definition of the plot of plastic volume change against plastic axial strain is also a complicated task as polynomial curve fitting procedures can estimate the shape of the curve but do not accurately depict the slopes. Large discrepancies result from using these methods to determine dilatancy, even with large order polynomial estimation. In this research, the best results of dilatancy curves were observed when calculating strategic positions, such as initial, maximum and final slopes, of the plastic volumetric strain curves independently. Although the entire dilatancy plot is not captured, a depiction of the curve is achieved which is adequate for comparison with the determined model values as presented in Chapter six.

4.3.4 Summary of Results

Table 4.2 summarizes the triaxial test conditions and results given in terms of confining pressure σ_3, initial void ratio e_o, void ratio at failure e_f, critical void ratio e_{cr}, principal stress ratio at failure $\left(\frac{\sigma_1}{\sigma_3}\right)_f$ and principal stress ratio at critical state $\left(\frac{\sigma_1}{\sigma_3}\right)_{cv}$.

σ_3	e_o	e_f	e^*_{cr}	$\left(\frac{\sigma_1}{\sigma_3}\right)_f$	$\left(\frac{\sigma_1}{\sigma_3}\right)^*_{cu}$
200	0.693	0.664	0.664	3.20	3.20
500	0.684	0.647	0.647	3.25	3.25
800	0.690	0.637	0.637	3.28	3.28
200	0.642	0.642	-	3.45	-
500	0.639	0.649	-	3.43	-
800	0.639	0.639	-	3.39	-
200	0.528	0.559	-	4.20	-
500	0.537	0.564	-	4.10	-
800	0.535	0.564	-	4.04	-
* critical values were determined for loose samples only. The remaining tests did not reach reliable critical conditions prior to completion.					

Table 4.2: Table Triaxial Test Results

4.4 The Influence of Free Ends

The necessity of free ends in triaxial testing has been previously discussed in this thesis. Although free ends were incorporated in all experiments used to calibrate the modified stress-dilatancy model, the experimental program also included procedures which omitted the use of lubricated ends. The purpose of these tests were to provide insight into the influence of lubrication on the stress-strain-volumetric characteristics as well as the dilatant behaviour of granular materials.

The interaction between the platens and the soil in samples with initially high void ratios does not greatly affect the strength measurements of the samples. Volume changes in these specimens show consistent contraction with no dilatant behaviour exhibited. The contraction mutes the effect of the rigid ends as the radial extension against the platen is much smaller than in the case of dilation. Observation of the volumetric strain for the loose sample in Figure 4.8(b) gives an indication of the slight effect that the use of free ends has on a loose sample. The compaction of the rough end specimen is minutely constricted when compared with the lubricated end. It is obvious that the use of free ends is not of great concern in the triaxial testing of low density samples.

The importance of free ends becomes significant when viewing the comparative figures for a dense sand (Figure 4.9(b)). The predominantly dilatant behaviour causes potential for a large interactive localized stress zone between the platen and the soil surface. As the increase in volume is reflected only in radial movement, the soil has to move considerably farther against the platen than for a loose sand, creating frictional effects such as bulging. The frictional effects are reflected in both

the stress and volumetric behaviour. Figure 4.8(b) displays the stress-strain curves for dense sand with and without free ends. While the initial slopes of the curves appear to be similar, the absence of lubrication promotes an exaggerated effect on both the peak strength and on the strain-softening of the soil.

The greater stress required to fail the sample results from the interaction between the platen and soil. The apparent increase in strain softening is likely due to the localization of failure around the sample ends. This requires a lower residual stress to cause the large axial strain as the overall strength of the soil is reduced.

Restrictions to the ends of the dense soil during shear also result in reduced volumetric effects. The volumetric strain for both lubricated and frictional ends is shown in Figure 4.9(b). Both the contraction and expansion portions of the curve are hindered by the frictional ends. Heterogeneity is once again evident as the soil is restricted, bulging occurs and local conditions govern the behaviour of the sample.

In summary, it can be said that the differences in volumetric strain curves exhibited under different end plate conditions can be attributed to the influences of end constraints. For example, if rough end plates are used, the soil particles have reduced freedom of movement at small strains (or small shear stresses) while trends of localized deformation are accentuated at 'large' strains.

The dilatancy plot comparisons (Figure 4.10) of the rough and free ends show typical results expected from volumetric strain curves. As the slope of the volume change is consistently less for the frictional ends than for the lubricated ends, the $d\varepsilon_v^p/d\varepsilon_1^p$ term in the dilatancy expression is also less. It follows that for values of dilatancy less than unity, the frictional ends will be more dilatant, while for values

greater, these ends will be less dilatant than the free end samples.

4.5 Membrane Correction

The influence of the membrane on experimental results can be, in many cases, quite substantial. For this reason, correction factors can be implemented to ensure accurate results. The two major effects caused by the use of a membrane in triaxial testing are membrane penetration and additional stress application. The former effect causes a slight offset in the volumetric strain due to the pressure applied on the outside of the membrane causing it to push into the voids around the exterior of the sample. The volume of water expelled from these areas will influence the values of volumetric strain.

Linton *et al.* [57] suggest a crude calculation intended to describe the depletion of water due to membrane penetration

$$\varepsilon_v = 4 \cdot \frac{D_{10}}{D} \left(\frac{1}{2} - \frac{\pi}{12 \cdot \cos 30^\circ} \right) \tag{4.1}$$

where ε_v is the volumetric strain due to membrane penetration, D_{10} is the diameter of the grains at the 10 percent finer mark of the grain size distribution curve and D is the diameter of the sample. It is based on the voids caused by a hexagonal close-packed structure and is influenced only by particle size and diameter of the sample.

Using Equation 4.1, a three inch diameter sample of Ottawa sand with a D_{10} of 0.235 mm exhibits a 0.0025% offset on the volumetric strain due to membrane penetration. In comparison with the measured values of volumetric strain, this correction factor is very small and can be considered negligible.

The effects of membrane inflicted stress on the sample are also minimal. The calculation of the initial confining pressure which is exerted on the soil as the membrane is first positioned, p_{om}, is dependent on the modulus of the membrane, M, the diameter of the specimen, d_o, at the end of consolidation and the initial diameter of the membrane, d_{im} [58]

$$p_{om} = 2M\frac{d_o - d_{im}}{d_o d_{im}}. \tag{4.2}$$

From Equation 4.2, the stress inflicted on the experimental triaxial specimens is extremely small. This results from the use of a membrane with a fairly low modulus and a diameter close to that of the sample.

La Rochelle *et al.* [58] also suggest methods for calculating the influence of the membrane on two common type of failures. As the peak stress is reached, the sample will exhibit either a bulging type failure or a shearing failure, or a combination of the two. A solution for each of these failure modes is included in La Rochelle's [58] paper. The triaxial tests carried out in this program show mainly bulging as failure occurs with very little shearing evident. Once again, the effects on stress were negligible.

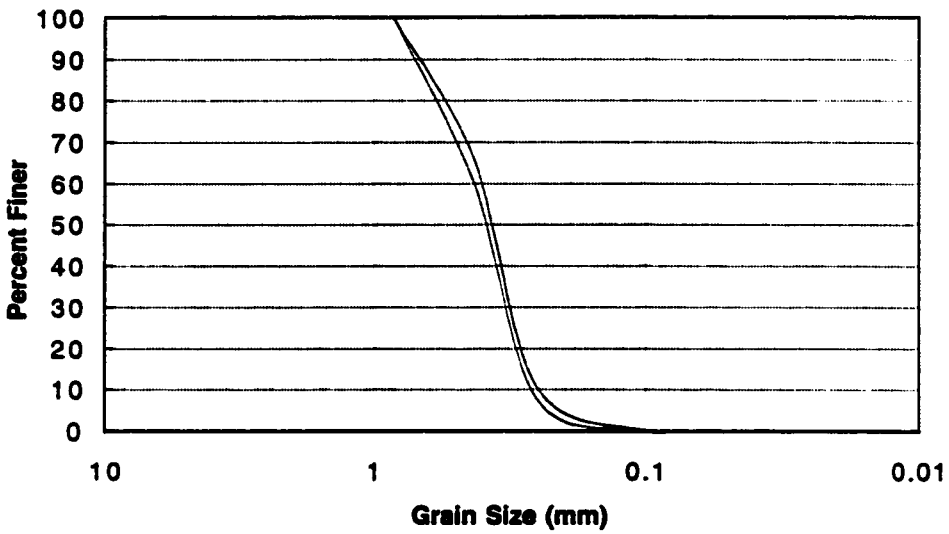

Figure 4.1 Grain Size Distribution of Ottawa Sand

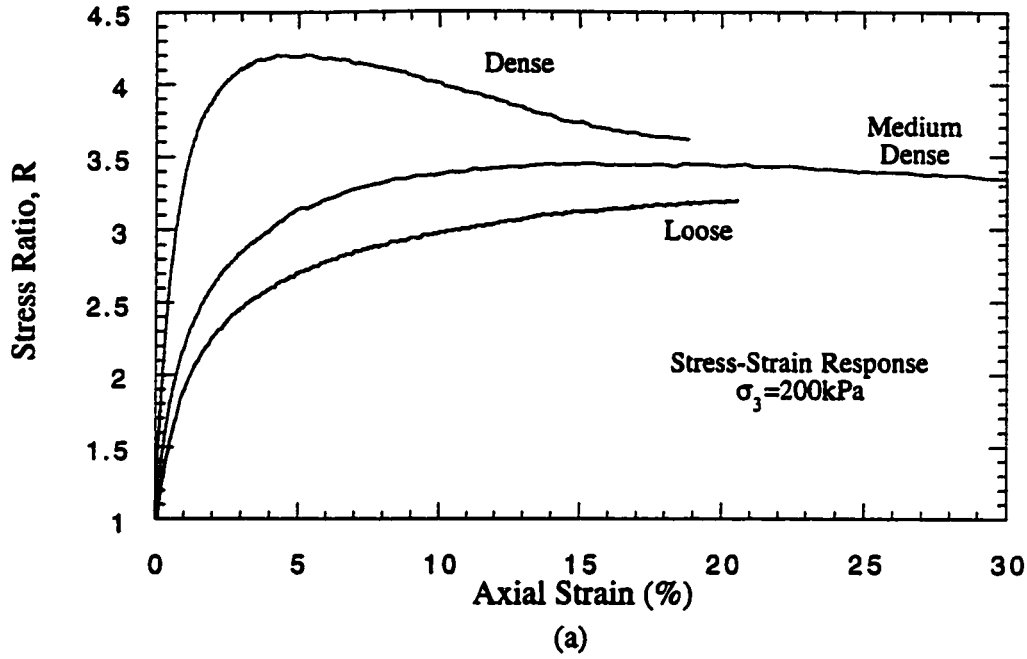

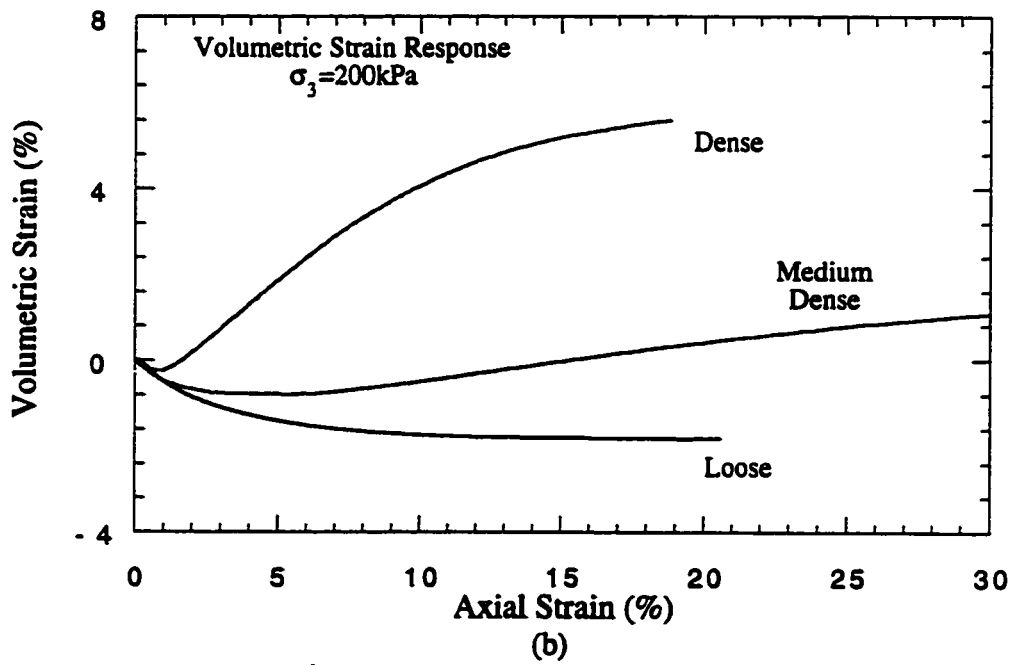

Figure 4.2 Monotonic Triaxial Testing Results on Ottawa Sand; σ_3 = 200kPa

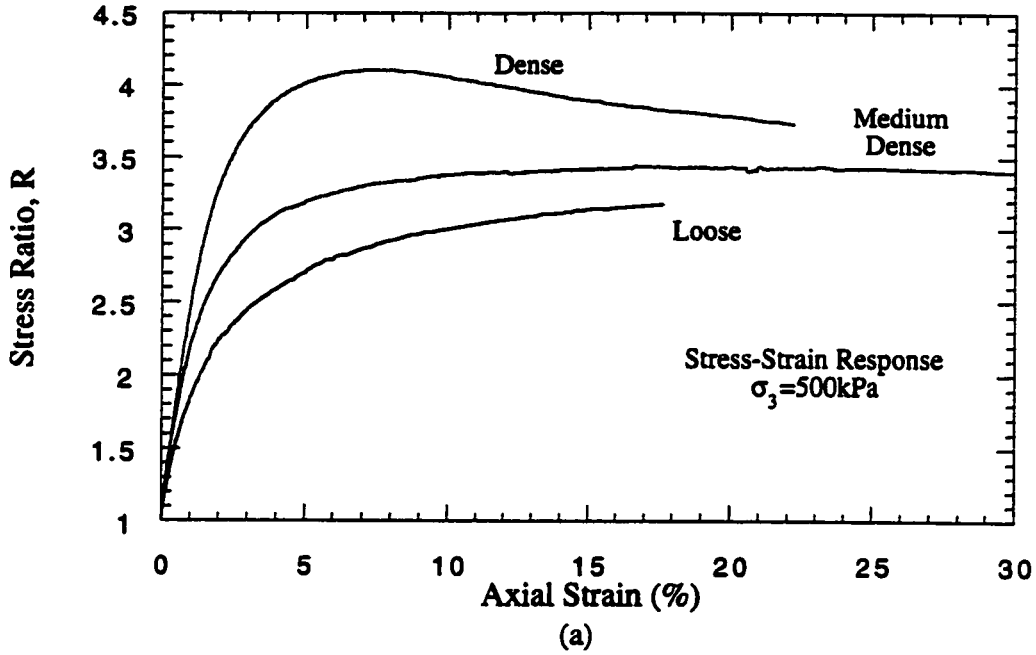

(a)

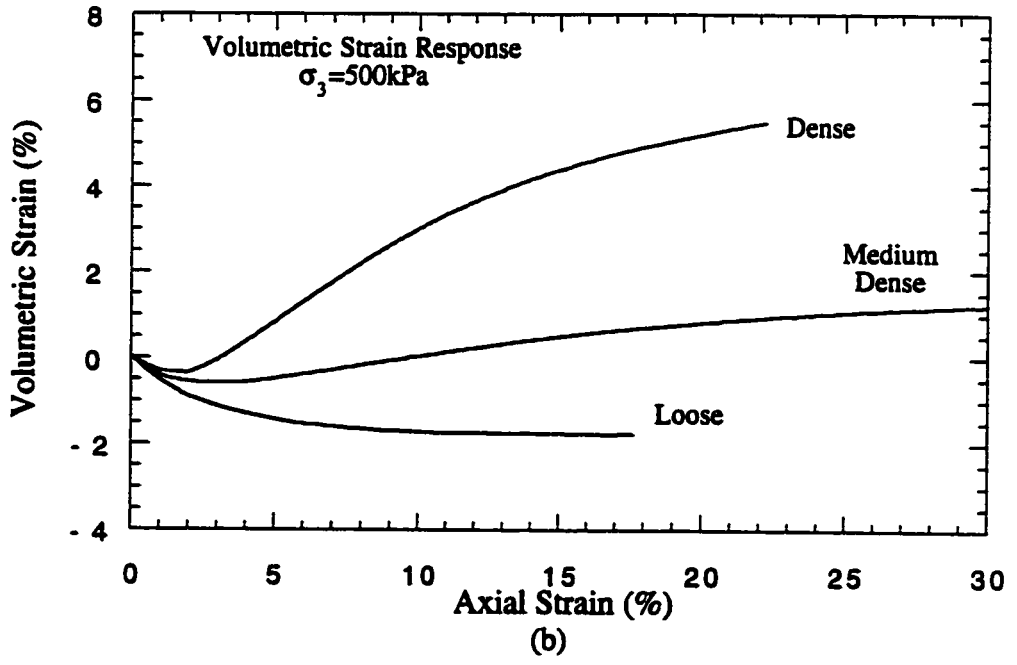

(b)

Figure 4.3 Monotonic Triaxial Testing Results on Ottawa Sand; σ_3 = 500kPa

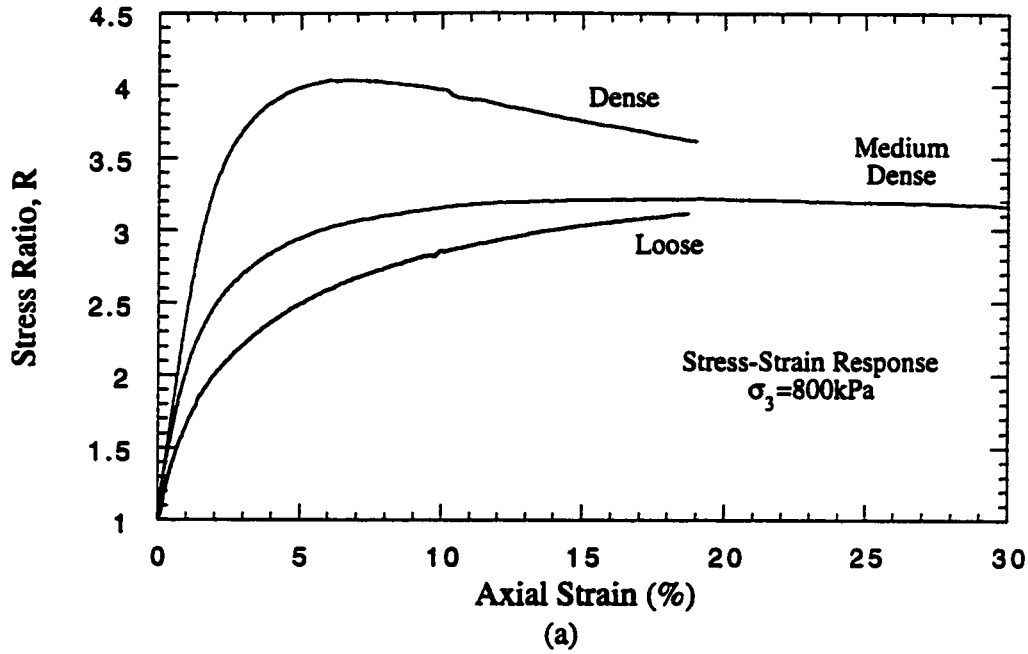

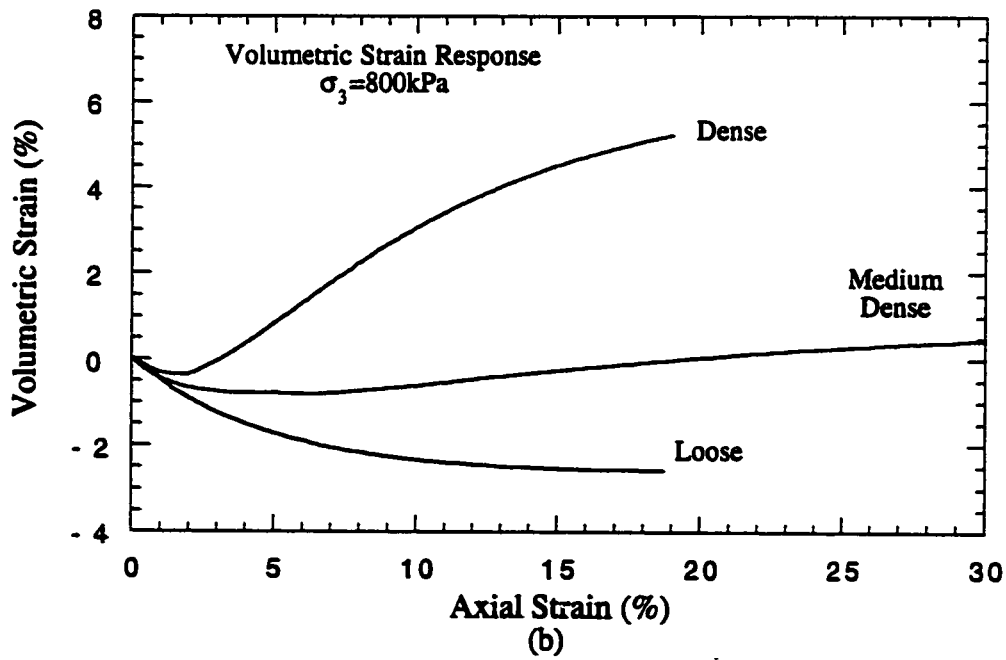

Figure 4.4 Monotonic Triaxial Testing Results on Ottawa Sand; σ_3 = 800kPa

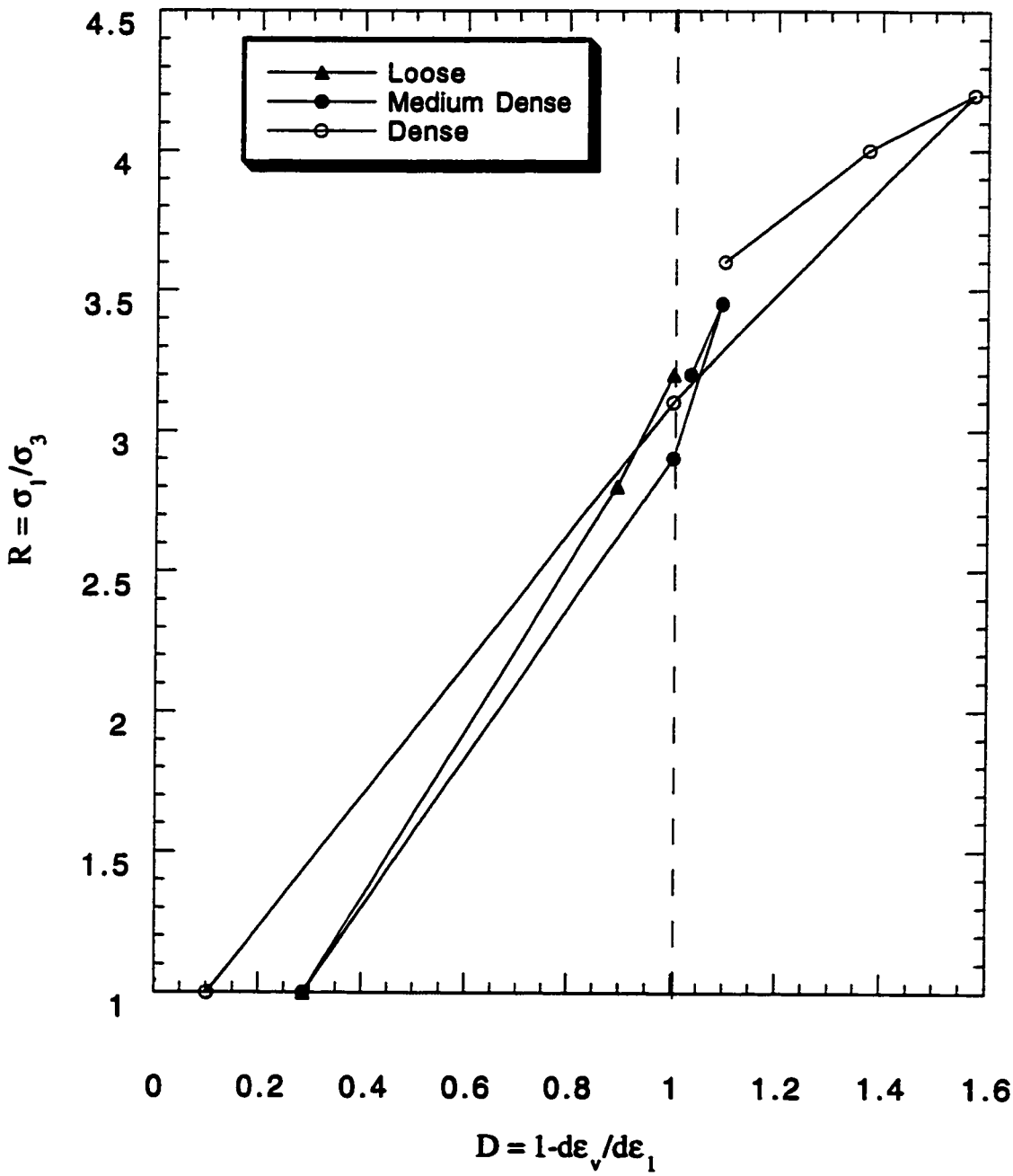

Figure 4.5 Monotonic Triaxial Testing Results on Ottawa Sand; R - D Plots, $\sigma_3 = 200kPa$

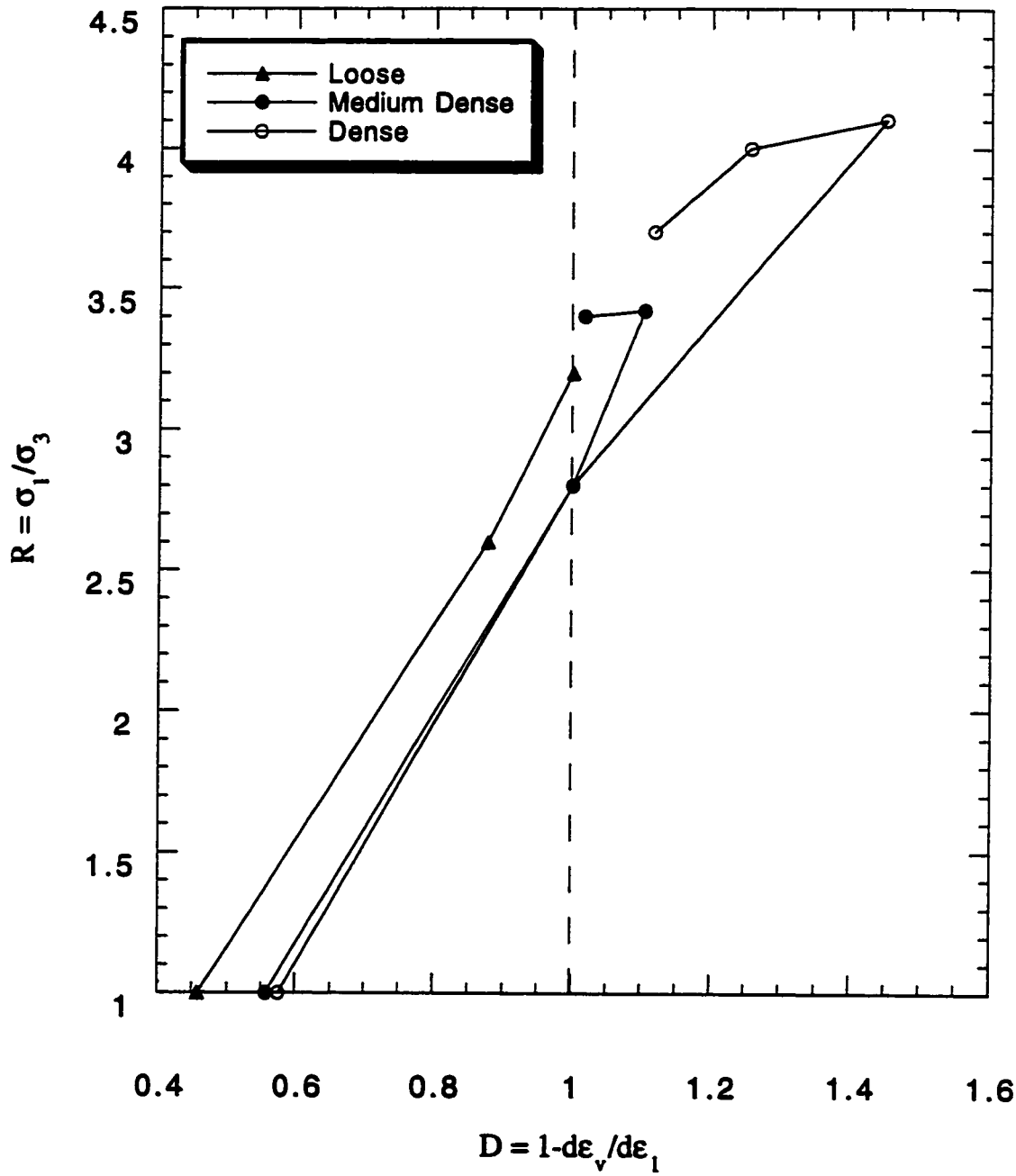

Figure 4.6 Monotonic Triaxial Testing Results on Ottawa Sand; R - D Plots, $\sigma_3 = 500kPa$

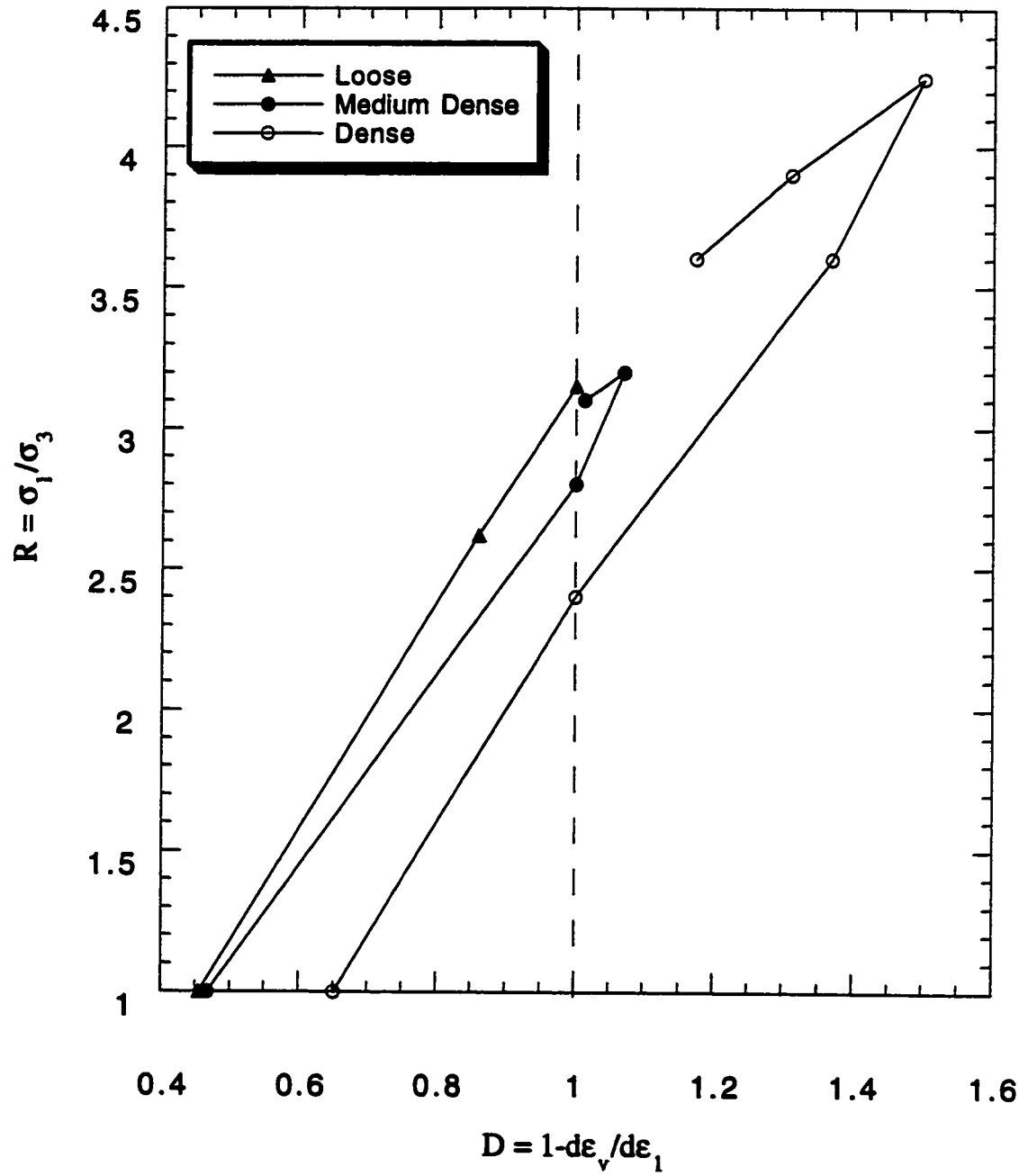

Figure 4.7 Monotonic Triaxial Testing Results on Ottawa Sand; R - D Plots, σ_3 = 800kPa

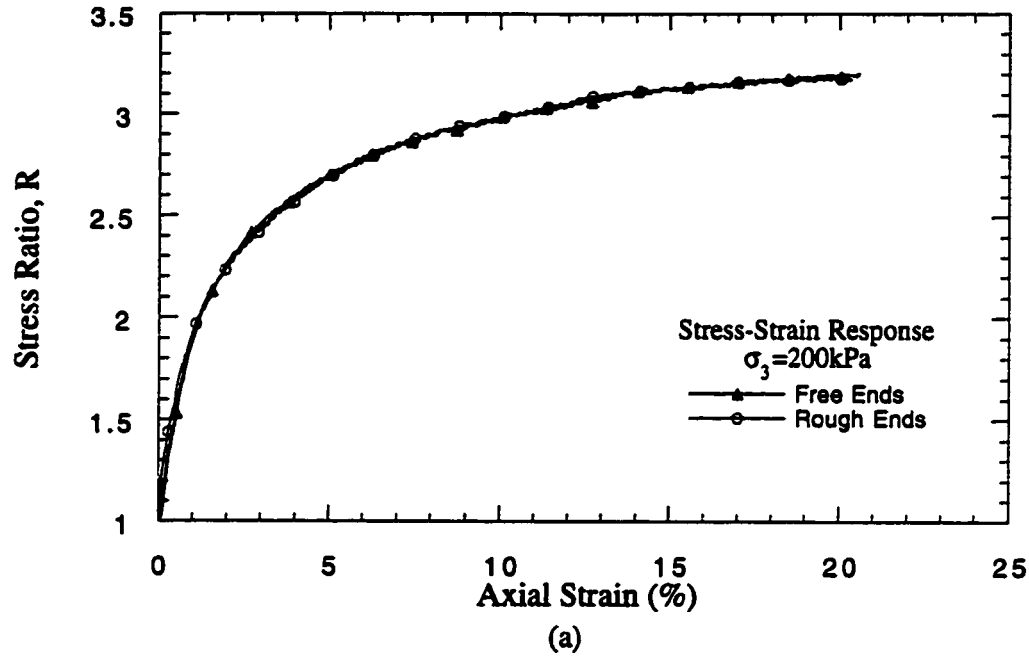

(a)

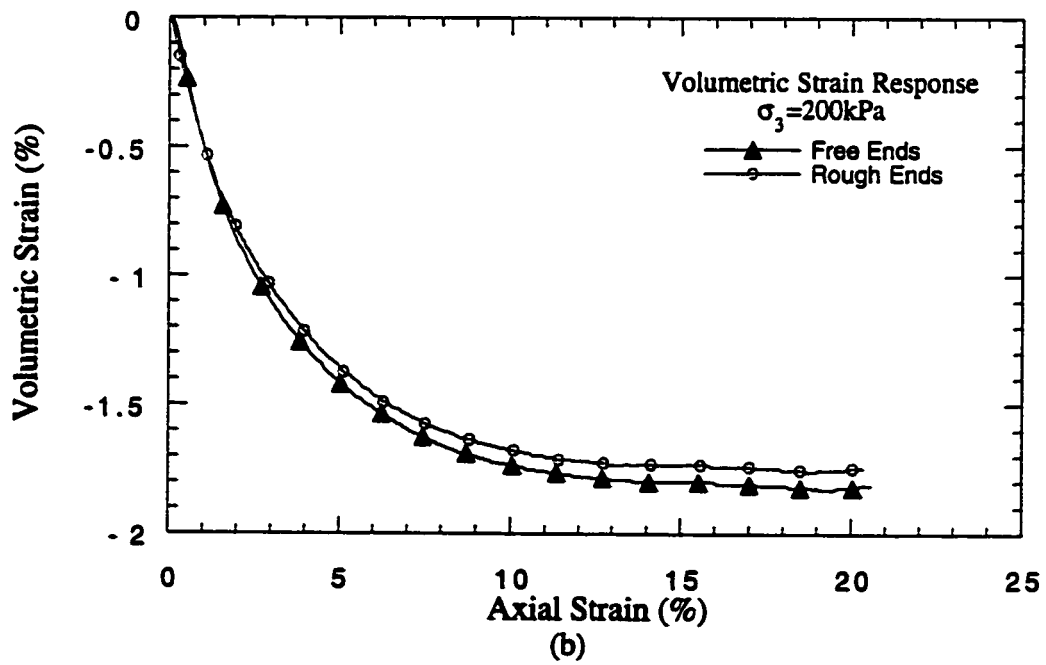

(b)

Figure 4.8 Effects of Free Ends on Loose Ottawa Sand

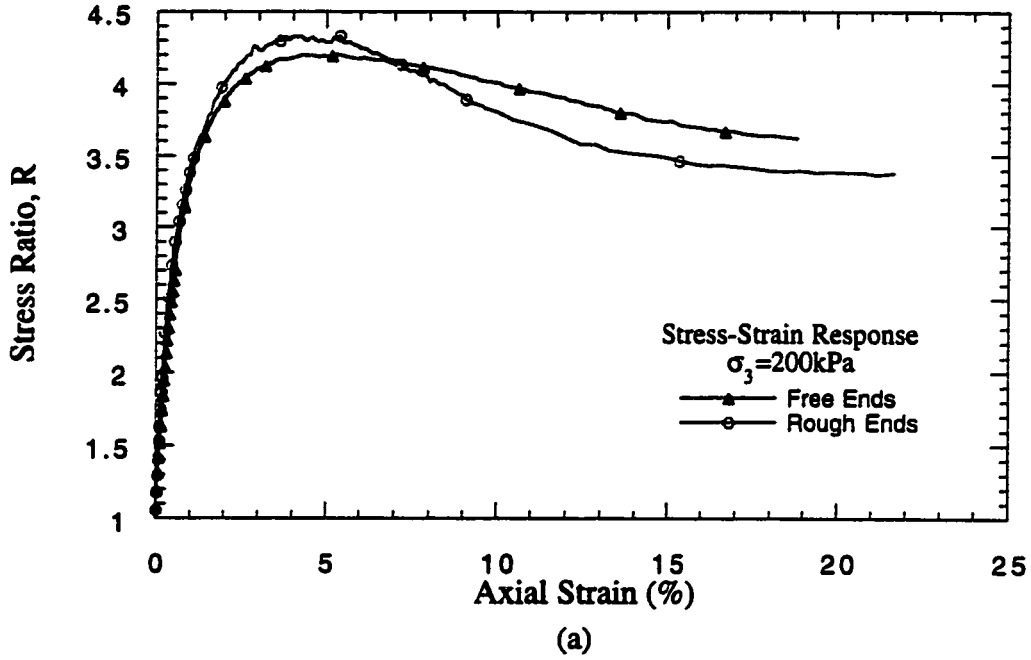

(a)

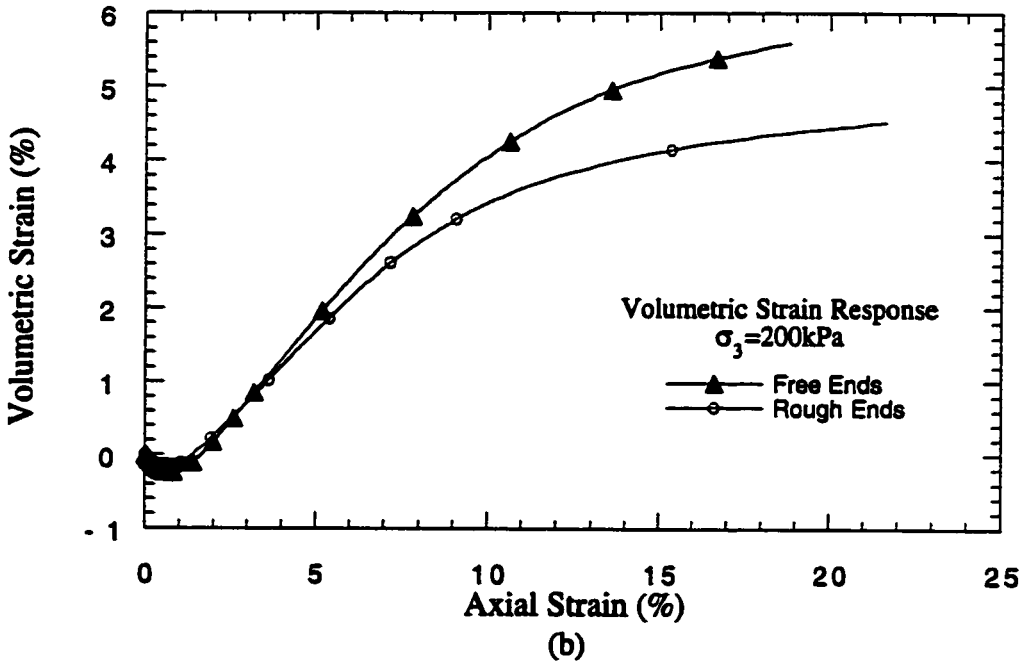

(b)

Figure 4.9 Effects of Free Ends on Dense Ottawa Sand

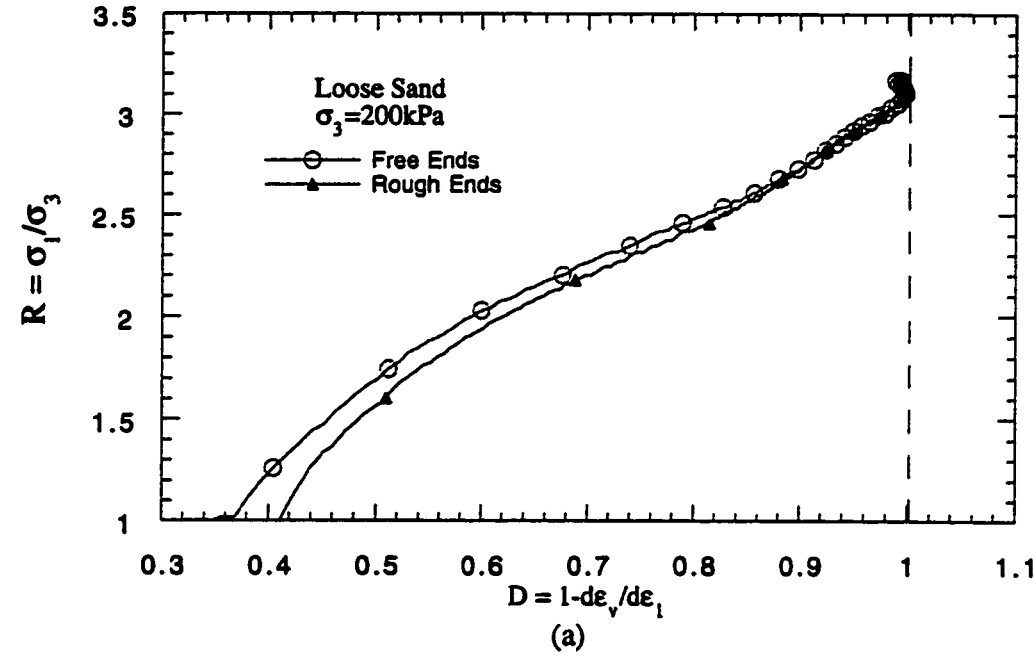

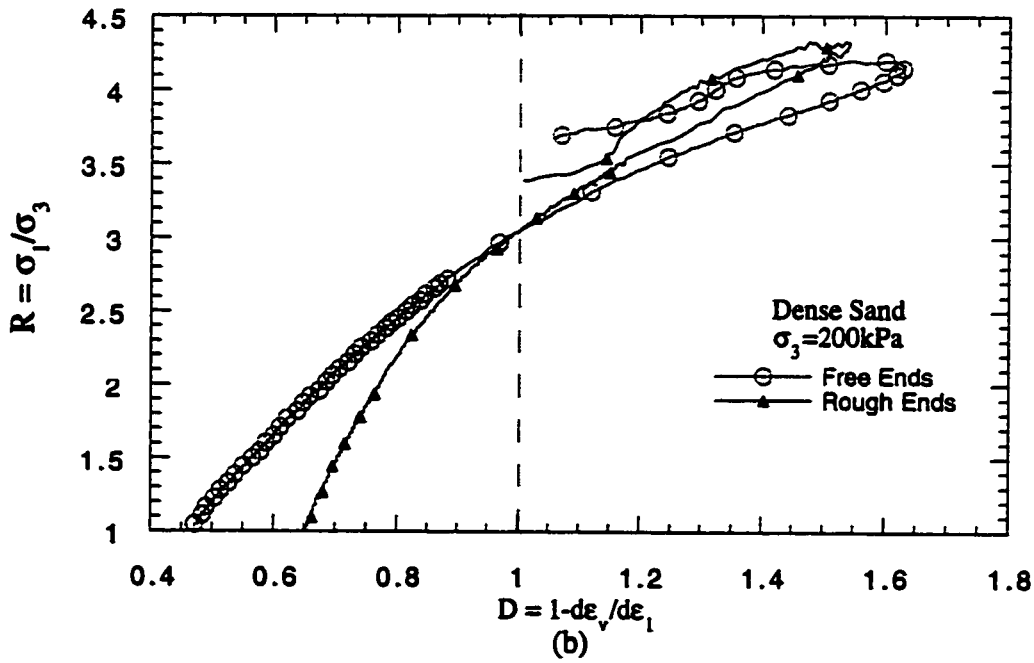

Figure 4.10 Effects of Free Ends on Dilatancy Responses of Ottawa Sand

Chapter 5

DESCRIPTION OF MODIFIED

STRESS-DILATANCY MODEL

5.1 General

The shortcomings of Rowe's [2] 1962 stress-dilatancy theory, as presented in Chapter two, become evident when comparing it to experimental results. The omission of material characteristics such as pressure and density dependencies, strain softening, peak and post-peak behaviour and stress induced anisotropy results in a simplified description of granular material dilatancy. However, the use of the equation requires only the value of the constant volume friction angle and the mobilized friction angle. Since this initial attempt to describe granular material behaviour, variations have been presented which incorporate the above mentioned characteristics ([6], [59], [60], [61], [62]). The limitations of these models have prevented their widespread use, as each one either omits relevant material characteristics or becomes too complicated to be advantageous.

A relationship has recently been developed [7] which incorporates pressure and density and strain hardening and softening effects. While the use of stress-induced

anisotropy of the influence of cyclic loading are not considered, a balance between simplicity and accuracy must be achieved in a functional constitutive model. This chapter presents the model, as well as the development of the required parameters. Chapter 6 then compares the model results with the experimental plots.

5.2 Modified Stress-Dilatancy Model

The purpose of Wan and Guo's [7] 1996 constitutive model for granular soils is to provide a method of accurately describing material behaviour by using a reasonable number of easily determinable parameters with clear physical meaning. The equations presented herein are those suggested and developed by Wan and Guo [7] using concepts of coupled plastic hardening-softening and stress-dilatancy to capture the effects of void ratio and stress level on granular responses. The stress-dilatancy relationship takes into account the slip and overriding of soil particles but does not include particle rotation in the consideration of plastic volume changes.

5.2.1 Deformation Characteristics

The framework of the model incorporates non-linear elasticity and the plastic flow rule to separate total deformation rates, $\dot{\boldsymbol{\varepsilon}}$, into respective elastic and plastic increments, $\dot{\boldsymbol{\varepsilon}}^e$ and $\dot{\boldsymbol{\varepsilon}}^p$, i.e.

$$\dot{\boldsymbol{\varepsilon}} = \dot{\boldsymbol{\varepsilon}}^e + \dot{\boldsymbol{\varepsilon}}^p \tag{5.1}$$

The plastic volumetric strain rate, $\dot{\varepsilon}_v^p$, which result from Equation 5.1 is further

split into volumetric, $\dot{\varepsilon}^p_{v(c)}$, and deviatoric, $\dot{\varepsilon}^p_{v(s)}$, proportions such as

$$\dot{\varepsilon}^p_v = \dot{\varepsilon}^p_{v(c)} + \dot{\varepsilon}^p_{v(s)} \tag{5.2}$$

The subscripts c and s in Equation 5.2 represent components of the plastic strain due to compaction and to shearing, respectively.

Calculations of elastic shear strain are performed using a non-linear form of the relationship between shear stress, τ, and elastic shear strain,γ^e, i.e.

$$\gamma^e = \tau/G;\ G = G_o \frac{(2.17-e)^2}{1+e}\sqrt{p} \tag{5.3}$$

Notice that the above Equation 5.3 is dependent on both void ratio, e, and mean stress level, p. The mean stress level is an expression used to describe an average stress condition exerted on the soil as $p = (\sigma_1 + 2\sigma_3)/3$ with σ_1 and σ_3 representing the major and minor principal stresses, respectively. Recall that in conventional triaxial stress conditions, the intermediate stress is equivalent to the minor stress and the lateral pressures can be grouped together as $2\sigma_3$. All stresses are considered to be effective as the drained testing does not allow pore pressure buildup. The G_o term is a constant used to define the shear stress at very small strains. The relationship given in Equation 5.3 is well-known as it was first introduced by Hardin [63] based on tests performed in the small strain regime ($\varepsilon \simeq 10^{-5}$). Since then, there have been a number of other relationships (all derived by experimental results) proposed

in the literature, see Iwasaki *et al.* [64]. Recently, some theoretical support has been given to justify the mean stress dependency on the shear modulus. Goddard [65] suggested that at low stress levels, the dependency of mean stress is closer to $p^{\frac{1}{2}}$ until, at a transitional confining pressure, p^*, the dependency becomes closer to $p^{\frac{1}{3}}$.

5.2.2 Failure Surface

The shear failure mechanism is described using a Mohr-Coulomb failure surface, F, as

$$F = \frac{\sigma_1 - \sigma_3}{2} - \left(\frac{\sigma_1 + \sigma_3}{2}\right) \sin\varphi = 0 \tag{5.4}$$

with φ as the friction angle.

The peak and constant volume (critical) states are individually defined by the application of the respective friction angle values, φ_f and φ_{cv} into equation 5.4.

5.2.3 Yield Surfaces

In the same manner, the shear yield surface, F_s, is expressed by employing the mobilized friction angle, φ_m, in equation 5.4 as

$$F_s = \frac{\sigma_1 - \sigma_3}{2} - \left(\frac{\sigma_1 + \sigma_3}{2}\right) \sin\varphi_m = 0 \tag{5.5}$$

The evolution of the mobilized friction angle defined by some hardening law eventually describes the isotropic expansion or contraction of the surface F_s in the

stress space.

On the other hand, the compaction yield surface is simply described by a cut-off surface which is expressed as

$$F = p - p_o = 0 \tag{5.6}$$

in which p_0 provides a limit to the isotropic compaction of the soil dependent upon accumulated plastic volumetric strains.

5.2.4 Flow Rules

As discussed previously in Chapter 2, the use of associated plasticity in the characterization of granular material behaviour leads to an overestimation of plastic volume changes. For this reason, a non-associated flow rule of plasticity theory

$$d\varepsilon_s^p = d\lambda \frac{\partial Q_s}{\partial \sigma} \tag{5.7}$$

is used to calculate plastic shear strain increments, $d\varepsilon_s^p$, in which $d\lambda$ is the plastic multiplier and Q_s is the chosen plastic potential function

$$Q_s = (\sigma_1 - \sigma_3) - (\sigma_1 + \sigma_3)\sin\psi_m \tag{5.8}$$

in which ψ_m is the mobilized dilatancy angle calculated from a stress-dilatancy equation.

On the other hand, plastic compaction, $d\varepsilon^p_{v(c)}$, is calculated by the use of the associated flow rule

$$d\varepsilon^p_{v(c)} = d\lambda \frac{\partial F}{\partial p} \tag{5.9}$$

as plastic isotropic consolidation is well estimated by this means. In this case, the plastic potential function, F, is defined in the same manner as the Mohr-Coulomb yield surface in Equation 5.5.

5.2.5 Modified Stress-Dilatancy Equation

Rowe's original stress-dilatancy equation is written as

$$R = KD \tag{5.10}$$

and relates the stress ratio, R, a value representing the ratio of major and minor principal effective stress, to the dilatancy term, $D = 1 - d\varepsilon^p_v/d\varepsilon^p_1$ by a constant $K = \tan^2(\pi/4 + \varphi_{cv}/2)$.

Another convenient way of expressing equation 5.10,

$$\sin\psi_m = \frac{\sin\varphi_m - \sin\varphi_{cv}}{1 - \sin\varphi_m \sin\varphi_{cv}} \tag{5.11}$$

involves the mobilized friction angle, φ_m, dilatancy angle, ψ_m, and the constant volume friction angle, φ_{cv}.

To integrate the effects of void ratio and pressure changes into Equation 5.11, Wan and Guo [7] used a ratio of the current to critical void ratios, e/e_{cr}, a term which envelopes both of the above factors as follows

$$\sin\psi_m = \frac{\sin\varphi_m - (\frac{e}{e_{cr}})^{\alpha}\sin\varphi_{cv}}{1 - (\frac{e}{e_{cr}})^{\alpha}\sin\varphi_m\sin\varphi_{cv}}. \tag{5.12}$$

The material parameter α determines the degree to which the constant volume friction angle, φ_{cv}, is corrected for density effects. The incorporation of confining pressure dependencies are indirectly related through the values of e_{cr}, the elastic shear strain and the yield surfaces. The current void ratio is found by combining the distortional volume changes with hydrostatic compaction as given by

$$e = e_o \exp\left[-\left(\frac{p}{h_l}\right)^m\right] \tag{5.13}$$

with e_o as the initial void ratio, p as mean pressure, and h_l and m as material constants found from experimental data. The critical void ratio is determined from the exponential relationship

$$e_{cr} = e_{cro} \exp\left[-\left(\frac{p}{h_{cr}}\right)^{n_{cr}}\right] \tag{5.14}$$

dependent on the pressure, p, and the critical void ratio at very small confining stresses, e_{cro}, usually assumed to be equal to the maximum void ratio, e_{max}. The h_{cr} and n_{cr} values are material constants. It can be demonstrated the e/e_{cr} term becomes equal to one at constant volume state, the condition applied to Rowe's stress-dilatancy equation. Indeed, Equations 5.11 and 5.12 become identical as the effects of current density are ignored.

5.2.6 Hardening and Softening

The hardening and softening mechanism is controlled in the mobilized friction angle relationship with the use of void ratio, e, and plastic shear strains, γ^p as

$$\sin\varphi_m = \frac{\gamma^p \left(\frac{e}{e_{cr}}\right)^{-\beta}}{a + \gamma^p} \sin\varphi_{cv} \tag{5.15}$$

with a and β as material constants measured by simple triaxial testing. Both hardening and softening effects are incorporated by the void ratio factor, e/e_{cr}. Peak states are achieved when the current void ratio, e, is greater than the constant volume void ratio, e_{cr}. Subsequently, as the two values become closer, softening is demonstrated.

5.3 Determination of Model Parameters

The laboratory test results presented in Chapter four are highly significant in model parameter determination. The measured values of initial and final void ratios, stress,

$G_o = 2750kPa$	$\nu = 0.29$	$e_{cro} = 0.74$	$\varphi_{cv} = 32°$
$a = 0.004$	$\alpha = 1.69$	$\beta = 1.3$	$h_l = 426.8MPa$
$m = 0.43$	$h_{cr} = 2867MPa$	$n_{cr} = .232$	

Table 5.1: Model Parameters for Ottawa Sand

strain, volumetric strain and confining pressures used together with the equations from the preceding section provide the 11 model parameters. These parameters can be classified into three groups describing elastic behaviour, shear dilatancy and compaction characteristics. The determined values are summarized in Table 5.1 and further elaboration on the methods used to obtain the parameters is given in the subsequent sections.

5.3.1 Elastic Parameters

The non-linear elastic portion of strain is measured to separate the elastic and plastic strains. The values of Young's Modulus and Poisson's ratio are computed at very low axial strains, between 0 and 0.5% after adjustment for seating errors. The assumption that Poisson's ratio remains constant allows an average value to be used to convert the initial Young's modulus into the initial shear modulus using the relationship $G = E/2(1+\nu)$

With various initial shear modulus values for given void ratio and pressure conditions, the constant G_o can be calculated with Equation 5.3. The value of G_o determined by this method, was found to be very low for an Ottawa Sand. This can be explained by the inaccurate methods used to measure the small strains. An

external linear displacement transducer was attached to the loading ram of the tri-axial cell in the experimental program. This, coupled with the need to measure axial stress and strain behaviour up to constant volume conditions reduced the sensitivity of the small stress and small strain measurements.

Adjustment to the value of G_o from the measured $1250kPa$ to the model value of $2750kPa$ which is compatible with taking the initial unloading modulus produced more accurate theoretical curves. Had the measurement of small strains been possible, it is likely that the G_o value used in the model could have been more effectively backed by the experimental program.

The critical void ratio at very low confining pressures, e_{cro}, is simplified to the maximum void ratio, e_{max}, as determined by the physical material testing. The parameters h_{cr} and n_{cr}, describing the dependence of critical void ratio on stress level, are found to be $2867MPa$ and 0.232, respectively, by taking the double log of equation A.1 as follows,

$$\ln\left[\ln(e_{cro}/e_{cr})\right] = -n_{cr}\ln(p) + n_{cr}\ln(h_{cr}). \tag{5.16}$$

The development of this expression, and the corresponding plots of the experimental values are given in Appendix A. Because constant volume conditions are achieved only by the loose material in the experimental results of this research, the critical void ratios and corresponding confining stresses used are from these data only.

The friction angle at constant volume conditions, φ_{cv}, is also taken from the

results of loose sands. The value of 32° is calculated from the following relationship

$$\left(\frac{\sigma_1}{\sigma_3}\right)_{cv} = \tan^2\left(\frac{\pi}{2} + \frac{\varphi_{cv}}{2}\right) \tag{5.17}$$

where the $(\sigma_1/\sigma_3)_{cv}$value is determined directly from the stress ratio at constant volume conditions of the tested loose Ottawa Sand.

5.3.2 Shear Dilatancy Parameters

The parameters α, a and β govern the shear dilatancy behaviour. The influence of a and β are seen in the hardening-softening mechanism (Equation 5.15). The solutions of these constants can be found by imposing peak conditions on the equation. This is represented in two ways; by replacing $sin\varphi_m$ with $sin\varphi_f$ and by equating the slope of the mobilized friction curve to zero with the expression

$$\frac{d(\sin\varphi_m)}{d\gamma^p} = 0. \tag{5.18}$$

The resulting two equations,

$$\frac{\sin\varphi_f}{\sin\varphi_{cv}} = \frac{\gamma_f^p}{a + \gamma_f^p}\left(\frac{e_f}{e_{cr}}\right)^{-\beta} \tag{5.19}$$

and

$$a = \frac{\beta(1+e_o)(e_{cr})(\gamma_f^p)^2 \sin\psi_{\max}}{e_f - \beta(1+e_o)(e_{cr})\gamma_f^p \sin\psi_{\max}} \tag{5.20}$$

can be solved simultaneously with $\sin\psi_{\max} = (-d\varepsilon_v^p/d\gamma^p)_f$.

The a and β values resulting from the solutions of the above equations did not result in accurate mobilized friction angle plots when compared with the measured curves. The values were subsequently adjusted to $a = 0.004$ and $\beta = 1.3$ to provide a closer representation of the experimental values.

The α parameter controls the degree of influence that void ratio holds on the modified stress-dilatancy relationship. It is determined by relating the mobilized frictional angle with the mobilized dilatancy angle in Equation 5.12. By manipulating this equation, and taking the log values of both sides, α is given by

$$\alpha = \frac{\log X}{\log(e/e_{cr})} \text{ with } X = \frac{\sin\varphi_m - \sin\psi_m}{(1-\sin\varphi_m \sin\psi_m)\sin\varphi_{cv}}. \tag{5.21}$$

Because the mobilized values of the friction and dilatancy angles, φ_m and ψ_m, did not yield satisfactory parameter values, the peak measurements, φ_f and ψ_f, were instead substituted. These offered a better description of α, producing more accurate theoretical predictions. The determination of $\alpha = 1.69$ by the linear relationship in Equation 5.21 is given in Appendix A.

5.3.3 Compaction Parameters

The cap parameters h_l and m were taken from the volume changes during the hydrostatic compaction of the samples prior to shear. The double log of Equation 5.13 was calculated to determine isotropic volumetric changes with confining pressure. The calculated values of $h_l = 426.8MPa$ and $m = 0.43$ are determined in Appendix A.

Chapter 6

STRESS-DILATANCY MODEL VERIFICATION

6.1 General

This chapter compares the theoretical and measured responses of the Ottawa Sand behaviour in conventional triaxial stress conditions. Wan and Guo [7] have previously evaluated the capability of the model with promising results using the published data of authors such as Cornforth [66], Bishop and Green [67] and Lee and Seed's [45] extensive article on the behaviour of Sacramento Sand. However, incomplete information provided in these publications gave need for an experimental program designed exclusively for the particular material parameter determination.

The parameters calculated in the previous chapter are used to obtain the predicted responses of the stress and volumetric characteristics of fine Ottawa Sand. These responses are then compared to the measured experimental curves given in Chapter four.

6.2 Model Responses

The presentation of the model validity is given in this section. Special care must be taken when attempting to calibrate the model due to the complicated interactions

and dependencies of the parameters. Each of the parameters governed by plastic behaviour is automatically dependent on the initial shear modulus constant, G_o, as this is used to characterize the plastic strains of the experimental data. Because the calculation of the mobilized friction and dilatancy angles are each based on plastic measurements, the model values of these material characteristics become dependent on many variables. For example, the determination of the dilatancy angle, ψ_m, as given by

$$\sin\psi_m = \frac{\sin\varphi_m - \left(\frac{e}{e_{cr}}\right)^{\alpha}\sin\varphi_{cv}}{1 - \left(\frac{e}{e_{cr}}\right)^{\alpha}\sin\varphi_m\sin\varphi_{cv}} \tag{6.1}$$

varies either directly or indirectly with all of the 11 parameters a, β, α, φ_{cv}, G_o, ν, h_{cr}, n_{cr}, h_l, m and e_{cro}, most of which are also interrelated.

It becomes obvious that the complicated interaction between the parameters cause a 'chain reaction' through the calculations of model responses, causing the balance of variables which describe the predicted model behaviour to become a difficult process. However, this inter-dependence of material parameters has the benefit of allowing an accurate prediction of sand over varying void ratio and confining pressure ranges using only one consistent set of material parameters.

6.2.1 Stress-Strain-Volumetric Responses

The comparisons of predicted with measured behaviour of fine Ottawa sand are shown in Figures 6.1, 6.2 and 6.3 for confining pressures of 200, 500 and $800kPa$ respectively. The first plot of each figure displays stress ratio against axial strain, while the second shows volumetric strain with axial strain.

The constitutive model depicts reasonably accurate curves describing granular material behaviour with pressure and density dependencies. In viewing the comparison of stress-strain relationships, discrepancies arise in the initial slope of the curve. The model estimates a stronger material than the measured values allow, creating premature peaks in the curves. The model prediction also exaggerates the effects of strain-softening in the dense sand.

The volumetric predictions are also reasonable when plotted along with the experimental values. The differences in the two sets of curves cannot be corrected with alteration of the parameter values, as the attempted adjustment of these constants merely results in the movements of all the curves, see Figures 6.2 and 6.3. This is due to the previously mentioned interdependence of the model parameters.

The differences in the experimental and theoretical curves stem from both laboratory error and model simplicity. Although great care was taken to achieve homogeneous, reproducible results in the experiment, the testing program and applied corrections could not compensate for every possible discrepancy. The use of free ends did much to prevent localized behaviour, but could not completely eliminate the bulging effects. The method of area correction was indirect, using external measurements of axial strains together with volumetric strains to calculate the lateral movements assuming its equality in both the intermediate and minor principal directions.

The constitutive model parameters which are determined from the experimental data are also responsible for the discrepancies between the measured and calculated curves. The three parameters with the most influence on the model outcome are G_o,

a and β. The elastic shear modulus constant, G_o, is used initially to separate elastic and plastic strains from the total experimental values. It is also implemented in the determination of elastic strain in the model. In this way, the theoretical curves are twice dependent on the value of G_o.

The mobilized friction angle parameters, a and β also control the model outcome. The calculation of mobilized friction angle, $\sin\varphi_m$, as given by

$$\sin\varphi_m = \frac{\gamma^p \left(\frac{e}{e_{cr}}\right)^{-\beta}}{a + \gamma^p} \sin\varphi_{cv} \tag{6.2}$$

is affected by a, β, γ^p and the current to critical void ratio. Later work with the model showed more accurate responses and better agreement with experimental data when the value of a was made dependent on void ratio. At this stage, the modification has not been included and was deemed outside the scope of this thesis. However, the desire to keep the number of parameters to a minimum and the relatively satisfactory results with the constant a value gave reason to leave the parameter as it was originally determined.

6.2.2 Stress-Dilatancy Responses

The predicted responses of the stress-dilatancy relationships are shown in Figures 6.4 through 6.6. The loose and medium dense behaviour is depicted well by the model, however, the tests which experience a high degree of dilatancy show some anomalies. The sensitivity of the dilatancy factor, D, is quite high as the measurement of the

slope is dependent on the volumetric strain curve. While a fairly close fit of the volume change characteristics can be easily achieved, it is difficult to recreate its respective slope everywhere on the curve. The large dilatancy causes the slope to reverse sign in the dense curves and creates a much more sensitive slope than the loose curves exhibit. This leads to greater room for error in the analysis of the dense material. Overall, the dilatancy response curves fitted quite reasonably with the experimental data capturing the essential features over a range of initial void ratios and confining pressures. It is emphasized here that trying to match exactly both volume change curves and their respective slopes with only one set of material parameters constitutes very tight fitting conditions and can be an intensely difficult exercise.

6.3 Further Model Predictions

The model can be extendend to predict stress-strain-volumetric behaviour under extreme void ratio and confining pressure conditions. Figure 6.7 is the calculated response of a very loose sand at confining pressures ranging from $50kPa$ to $3MPa$. The material becomes more ductile with increasing confining pressure with all the curves tending toward the same critical stress ratio corresponding to critical state.

The influence of pressure on the volume change characteristics is quite evident (Figure 6.7(b)), with a much lower critical void ratio reached at very high confining stresses. Dilatancy plots of the model prediction of loose sand are shown in Figure 6.9(a). Once again the behaviour of the sand becomes more like that of a ductile

material as the confining pressures increase.

The corresponding behaviour of dense sand as generated by the model is shown in Figure 6.8. As confining stresses are increased, the material behaviour becomes more ductile with a decreasing trend for the peak stress ratio value. Moreover, the peak and strain-softening segments of the stress-strain plots are eliminated at pressures of $10MPa$. Also at this pressure, dilative volume changes are muted as the high contact forces between the sand grains do not allow for much expansion of the sand mass as a whole. The dilatancy plots also show the sand to exhibit behaviour of a looser sand with pressure increase (Figure 6.9(b)). The dilatancy factor, $1 - d\varepsilon_v^p/d\varepsilon_1^p$, is greater than two at a confining pressure of $50kPa$ but does not achieve values much greater than one at $10MPa$.

The trends of the Ottawa Sand given by the model at very high confining pressures may not be an accurate depiction of the granular material behaviour observed in experimental testing. The model predictions are based on the premise that the individual grains remain intact during sliding throughout the loading regime. High external pressures however, may cause the contact forces between grains to become greater than the strength of the individual particles. Crushing of the grains would result, and measurements of the strength of the experimental sand would be less than the apparent strength of the model sand.

6.4 Conclusions

The interpretation of the model predictions of the behaviour of fine Ottawa Sand can be summarized as follows:

1. Predictions of Ottawa Sand behaviour in the stress-strain and volumetric strain plots captures the trend of the measured experimental values. However, the model is less capable of representing stress-dilatancy behaviour.

2. The inclusion of particle slip and override considerations in the model is sufficient to describe the behaviour of the Ottawa Sand under compressive conventional triaxial conditions. If the testing involved a change in principal stress direction however, the influence of particle microstructure and rolling effects may require the modification of the model.

3. The integration of the parameters and their dependencies on one another create difficulties in the model calibration as the adjustment of a single variable will be echoed in both the stress and volumetric responses of the model.

4. The sensitivity of a model representation of the slope of the plastic volume change curve suggests that although the modified stress-dilatancy relationship is an adequate means to extract theoretical stress-strain-volumetric characteristics of granular materials, a direct stress-dilatancy response is difficult to recreate.

5. The constant, a, used in the calculation of the mobilized friction angle, would better represent the experimental data if it was made a function of the ratio

of current to critical densities, $\left(\frac{e}{e_{cr}}\right)^{\alpha}$.

6. Predictions of Ottawa Sand behaviour outside the experimental testing agenda show typical results, with both the loose and dense samples becoming more ductile with increasing confining pressures. The stress values at high strains tend to reach critical state values regardless of the confining pressures. Volume change however, is highly dependent on the surrounding stresses, with increasing stresses leading to greater contractive tendencies.

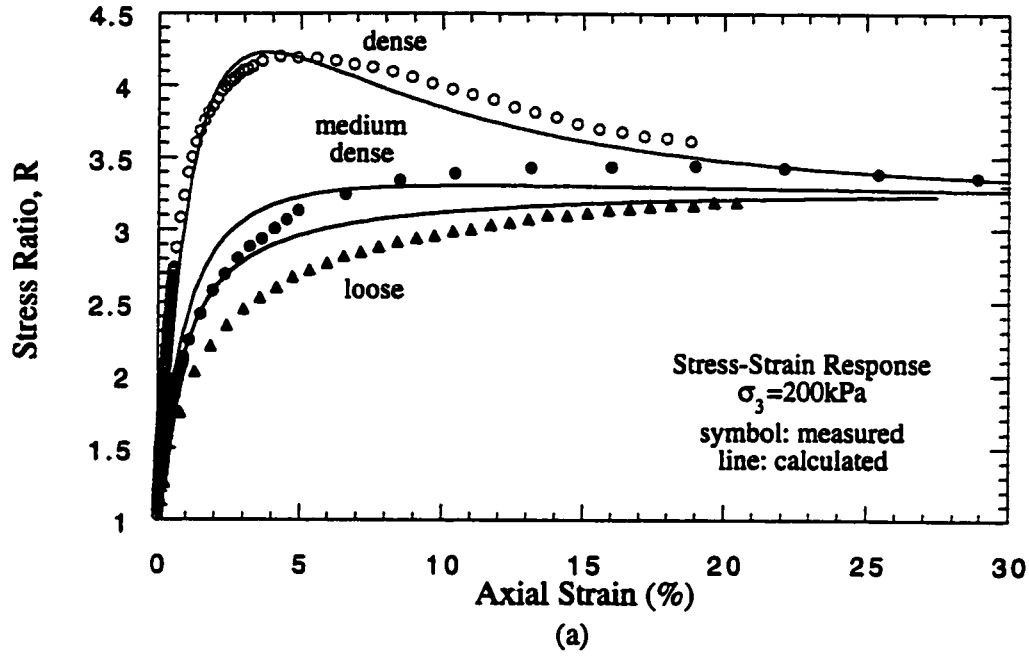

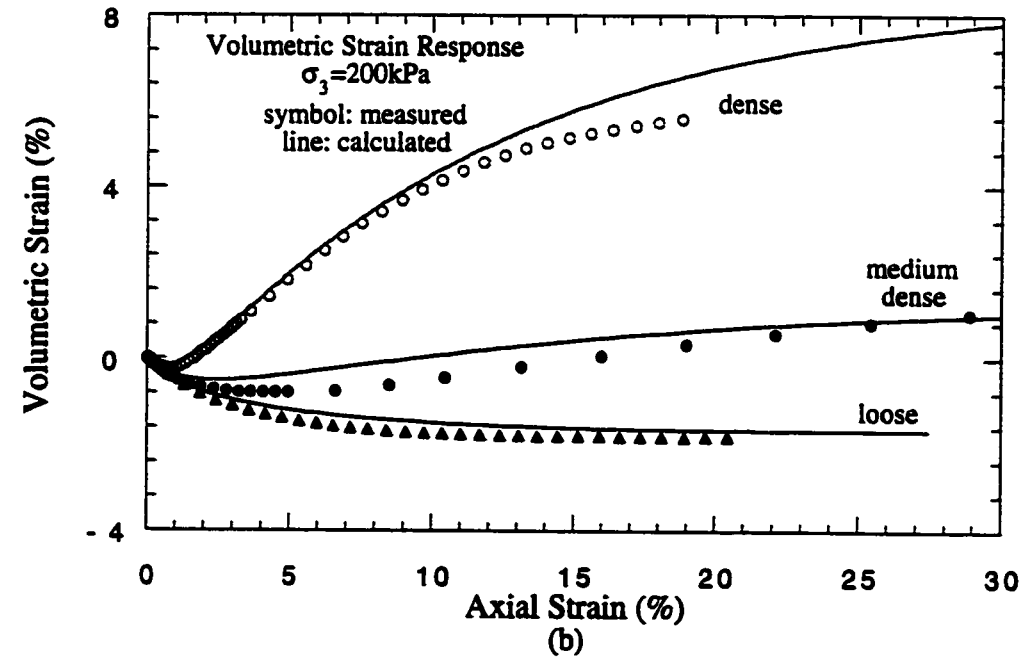

Figure 6.1 Comparison of Model and Experimental Behaviour of Ottawa Sand; $\sigma_3 = 200$kPa

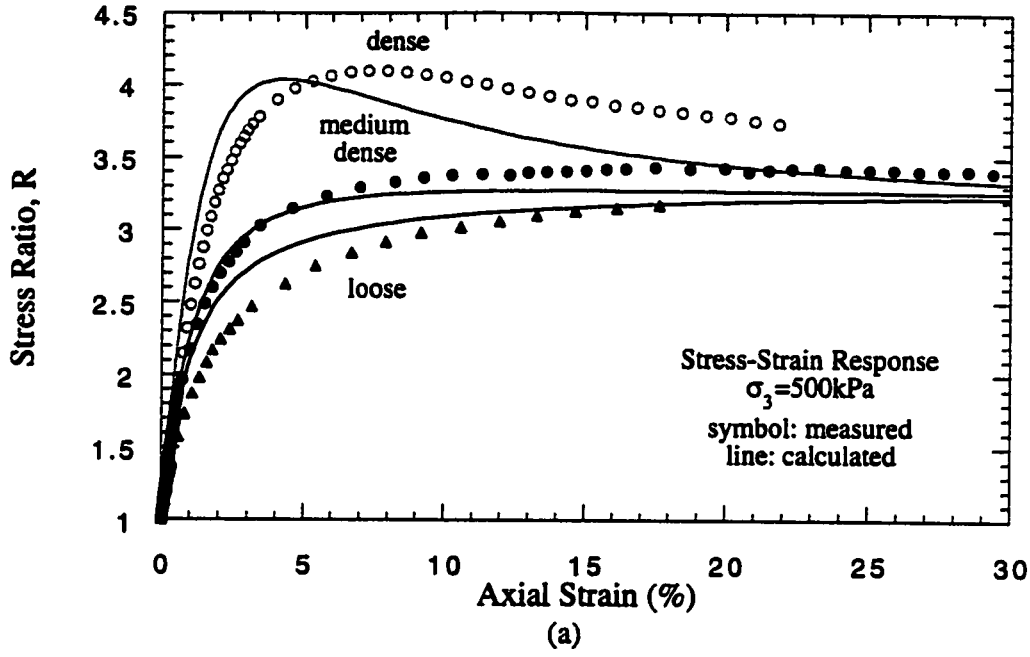

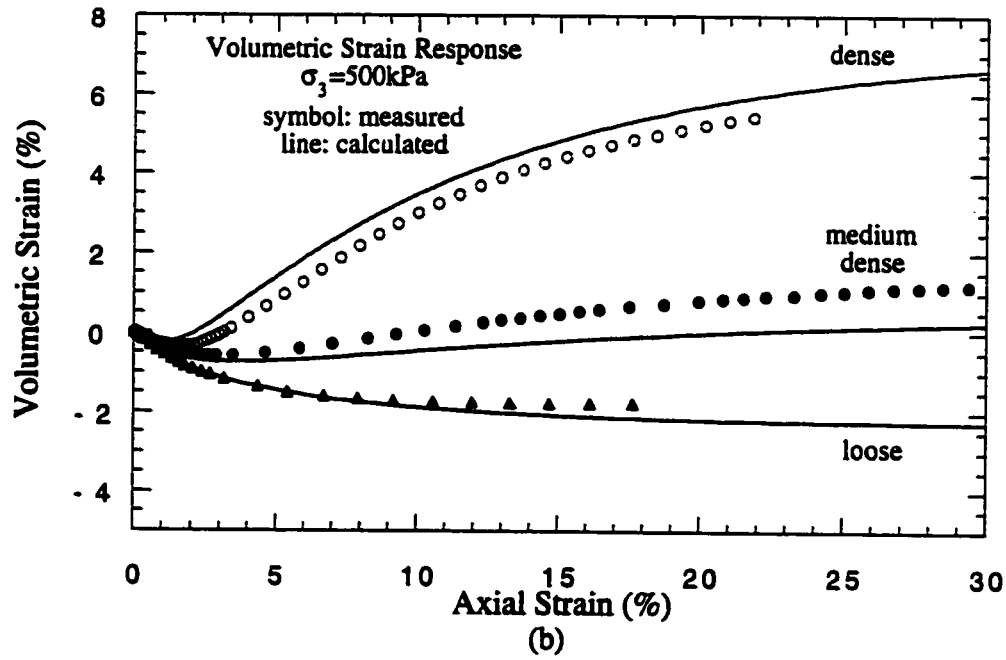

Figure 6.2 Comparison of Model and Experimental Behaviour of Ottawa Sand; $\sigma_3 = 500$kPa

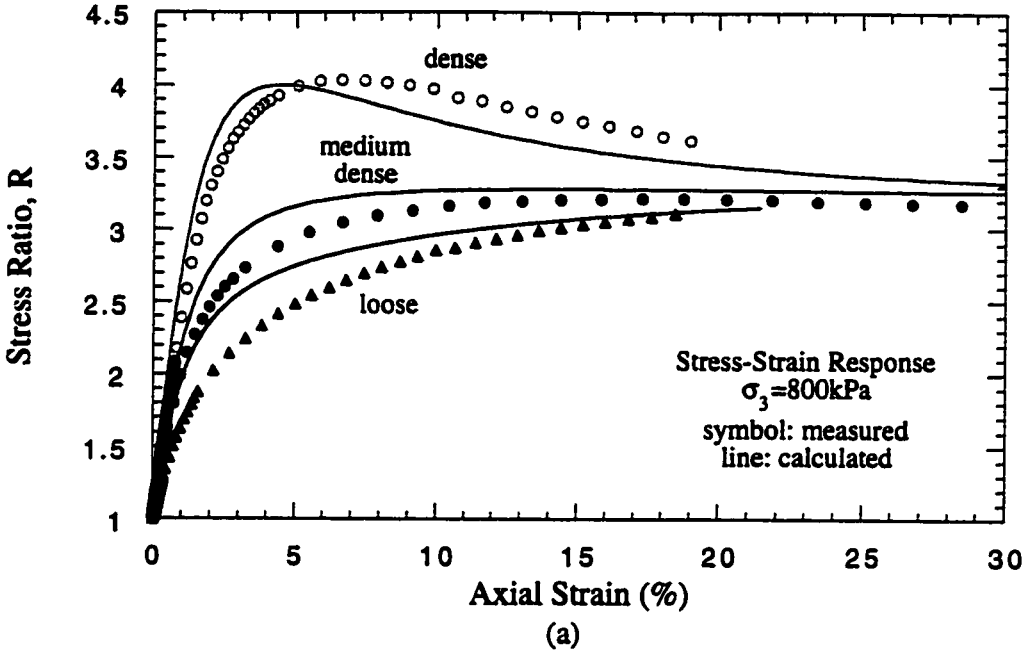

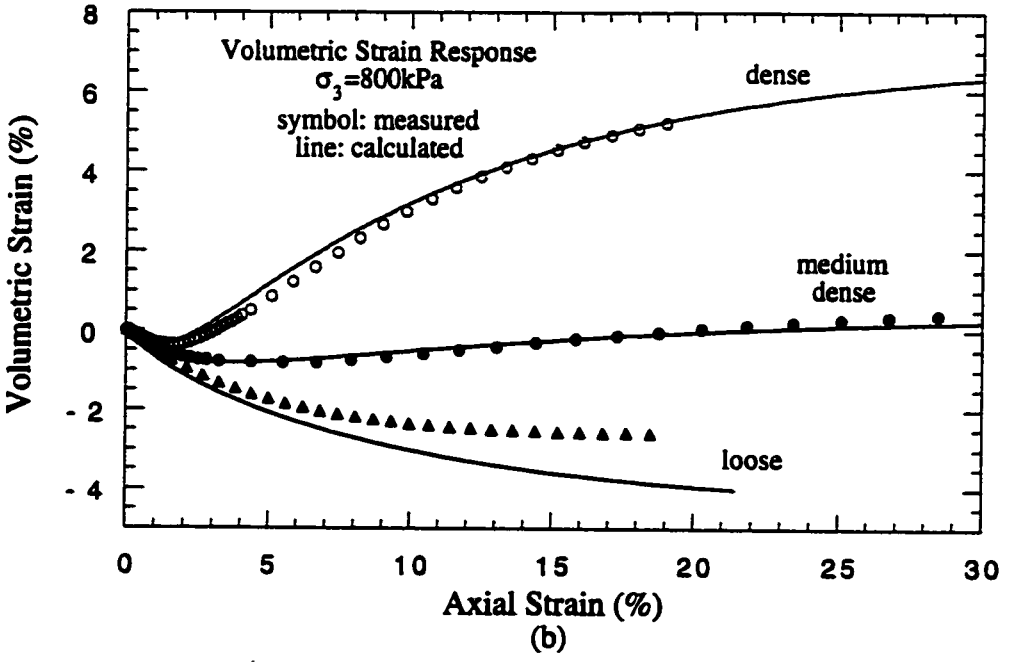

Figure 6.3 Comparison of Model and Experimental Behaviour of Ottawa Sand; σ_3 = 800kPa

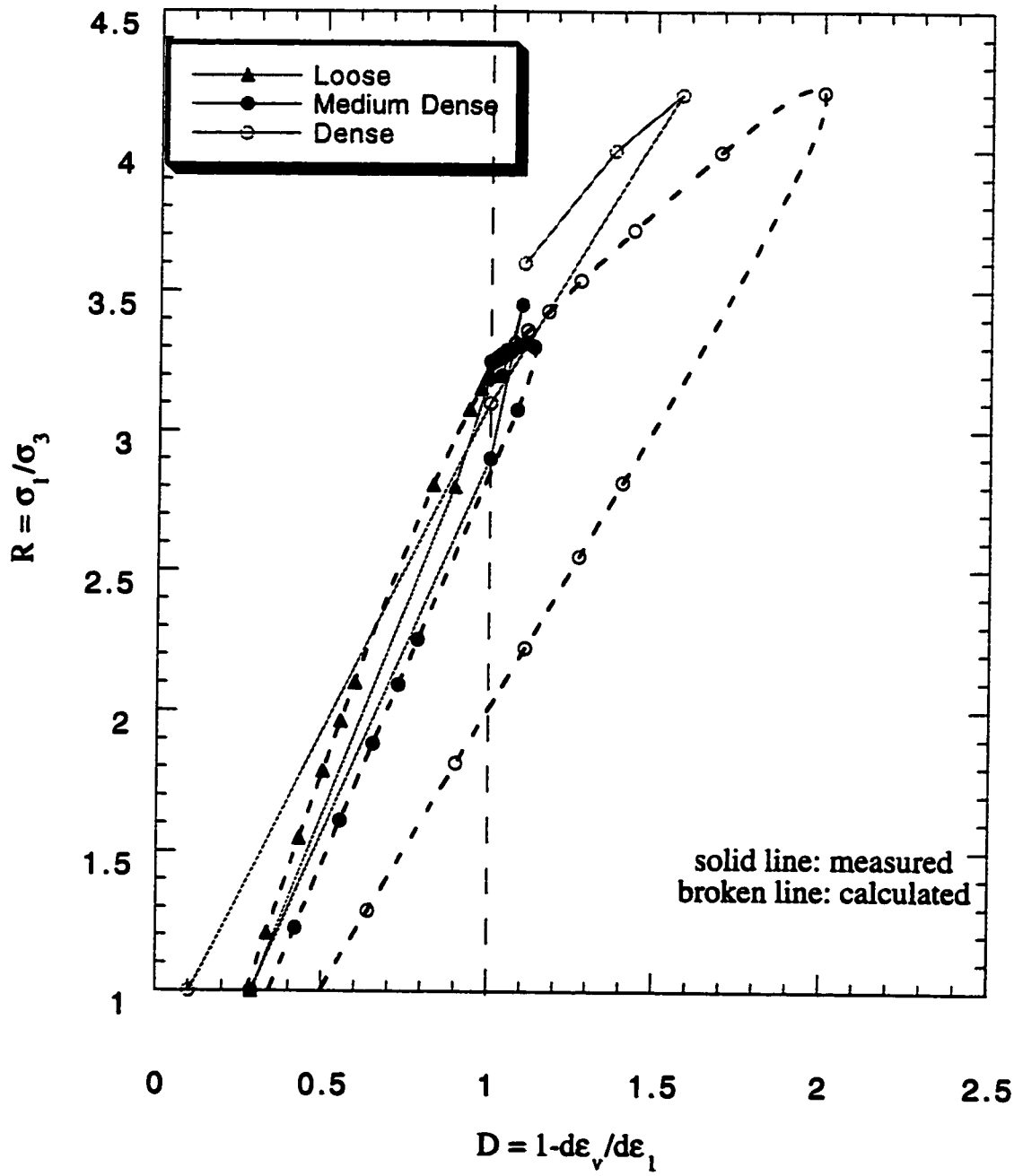

Figure 6.4 Comparison of Model and Experimental Behaviour of Ottawa Sand; R - D Plots, σ_3 = 200kPa

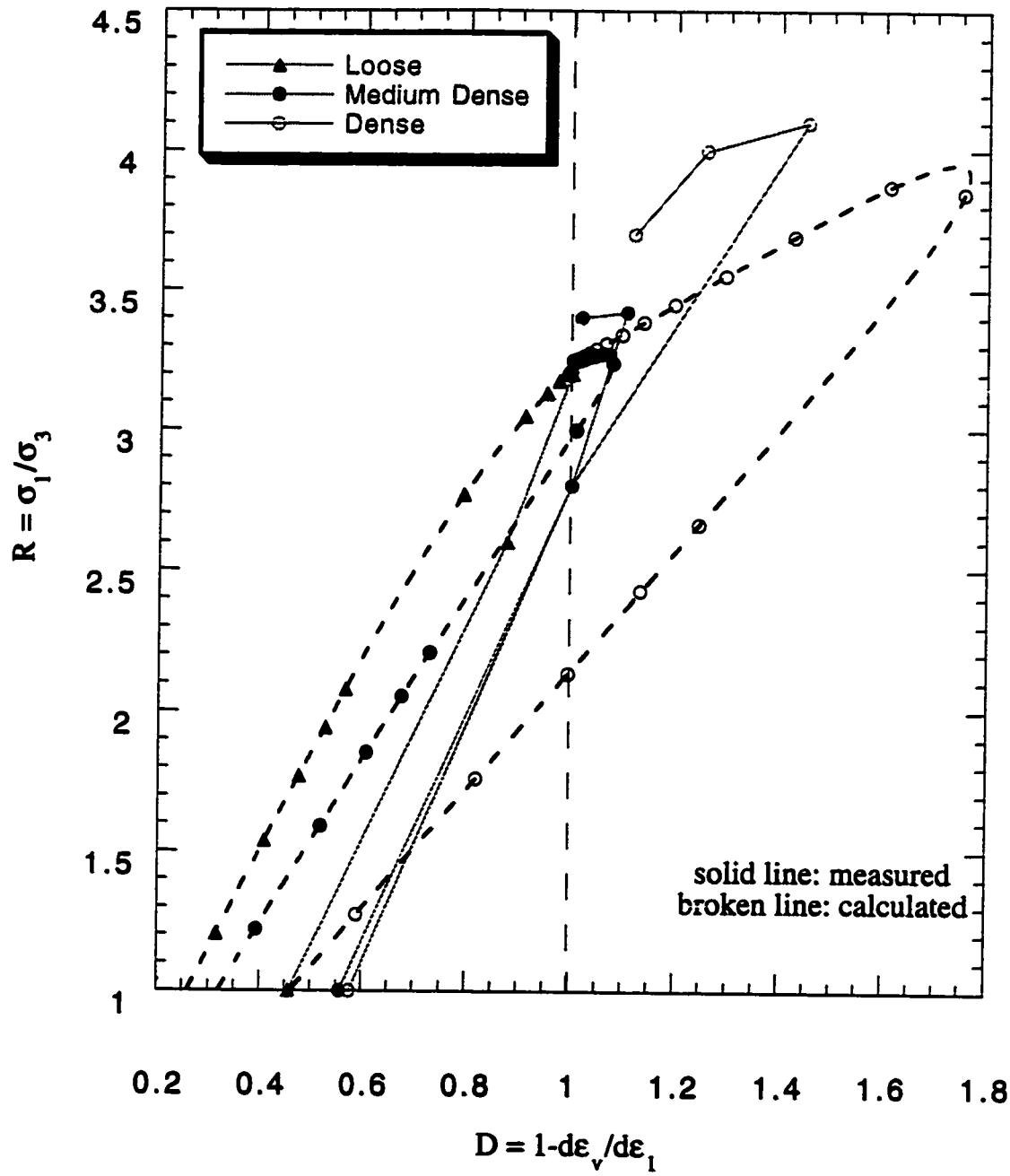

Figure 6.5 Comparison of Model and Experimental Behaviour of Ottawa Sand; R - D Plots, σ_3 = 500kPa

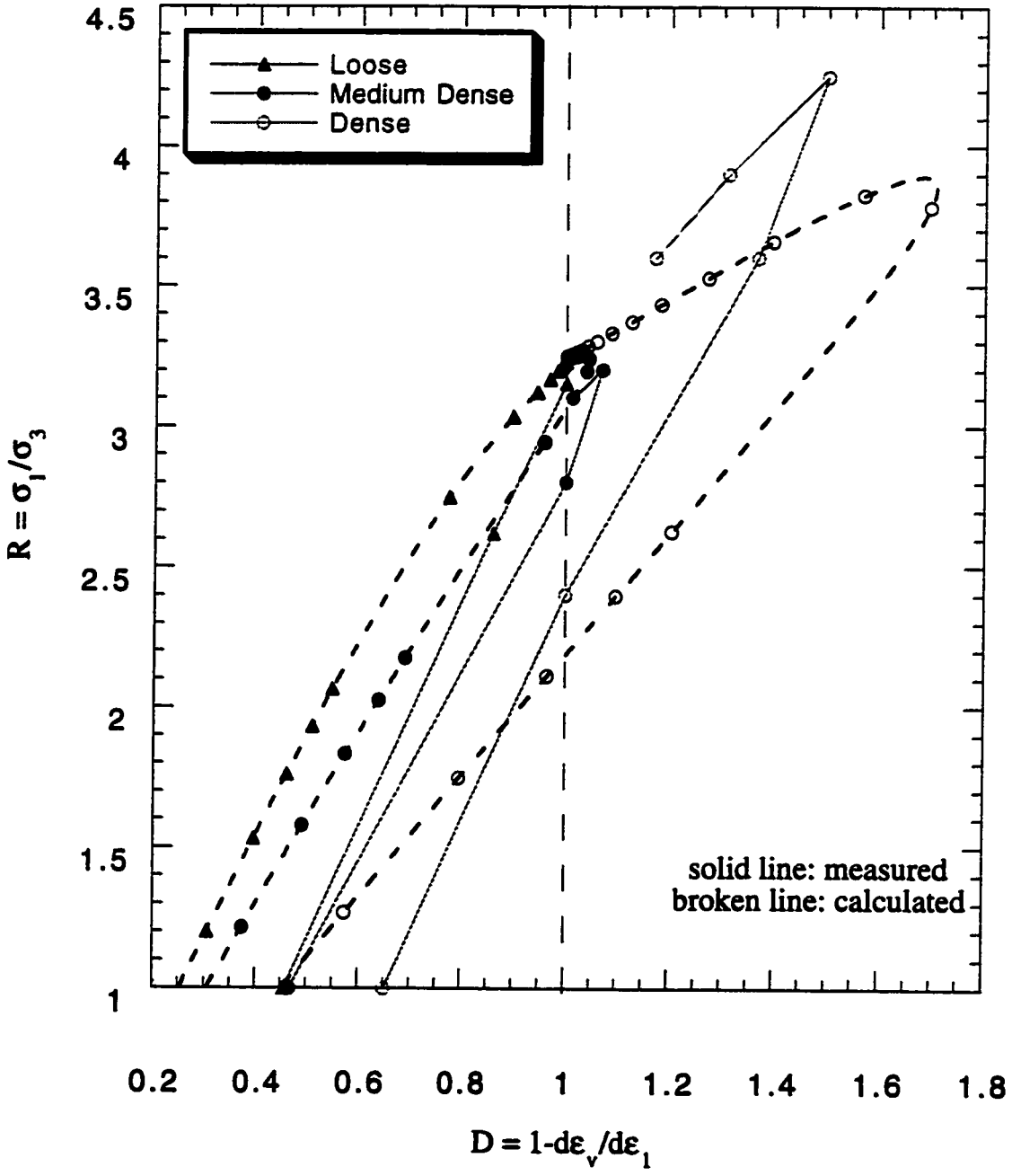

Figure 6.6 Comparison of Model and Experimental Behaviour of Ottawa Sand; R - D Plots, σ_3 = 800kPa

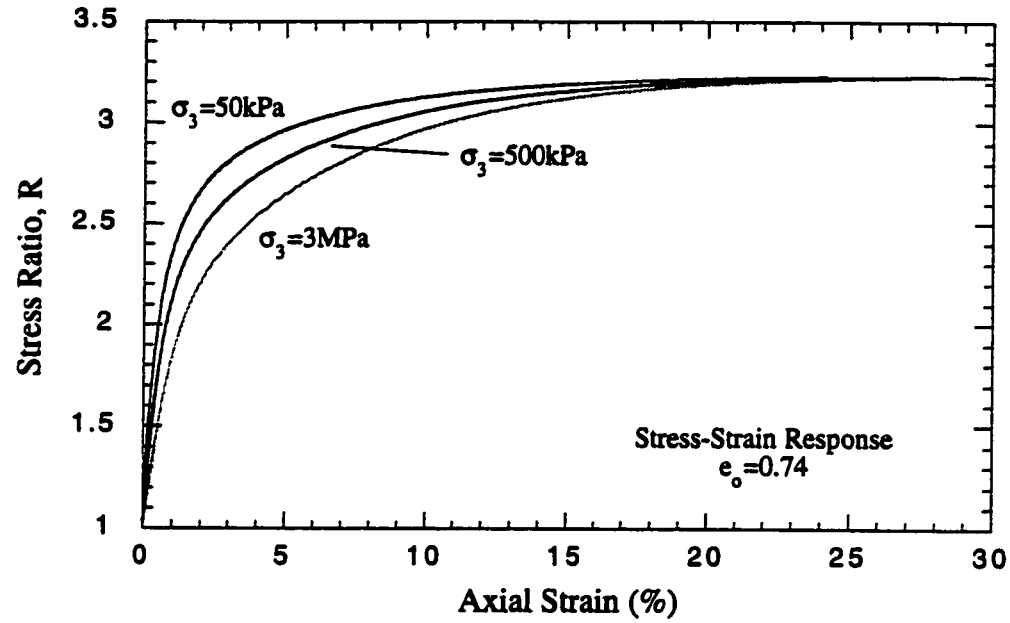

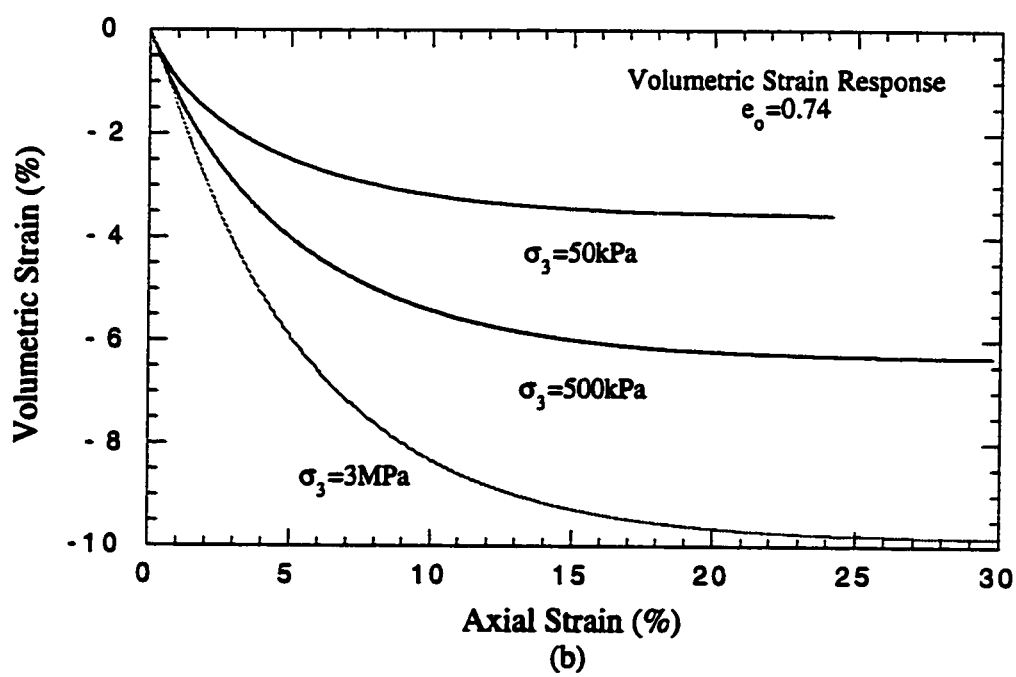

Figure 6.7 Model Prediction of Loose Ottawa Sand Behaviour at Various Confining Pressures

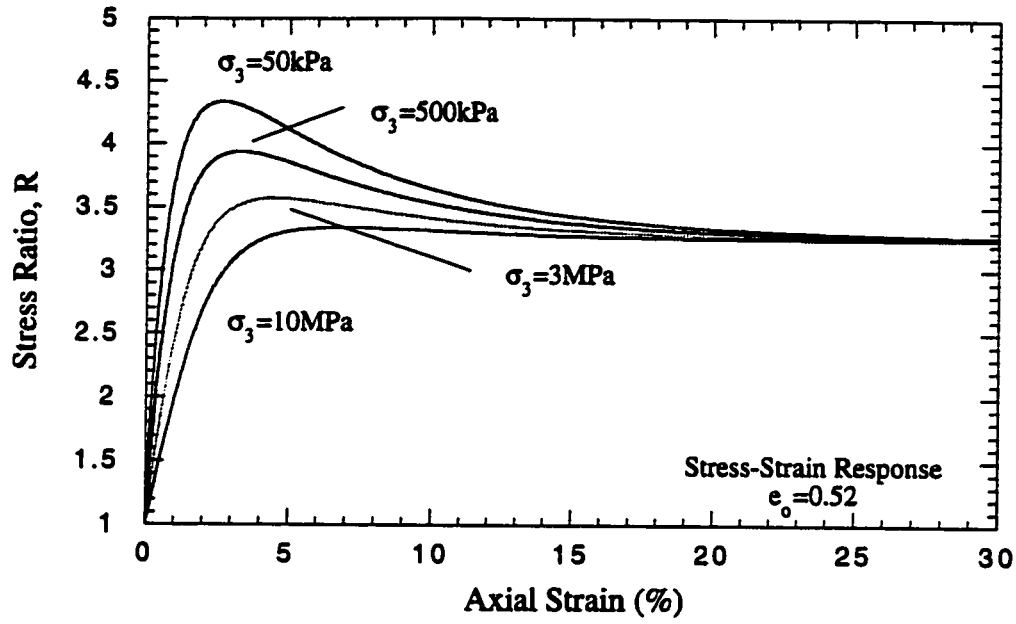

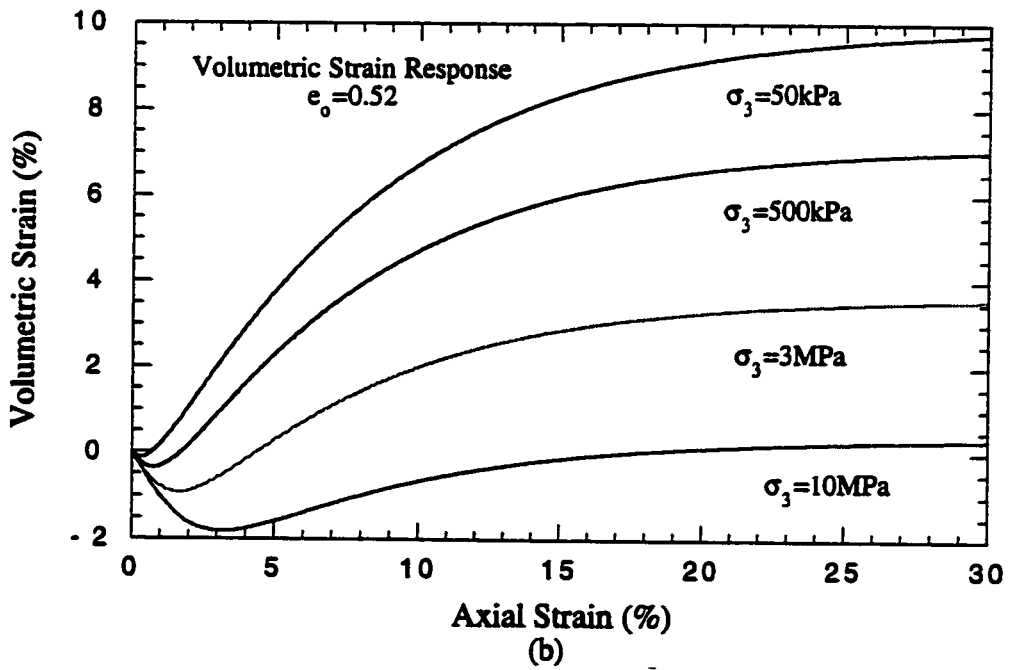

Figure 6.8 Model Prediction of Dense Ottawa Sand Behaviour at Various Confining Pressures

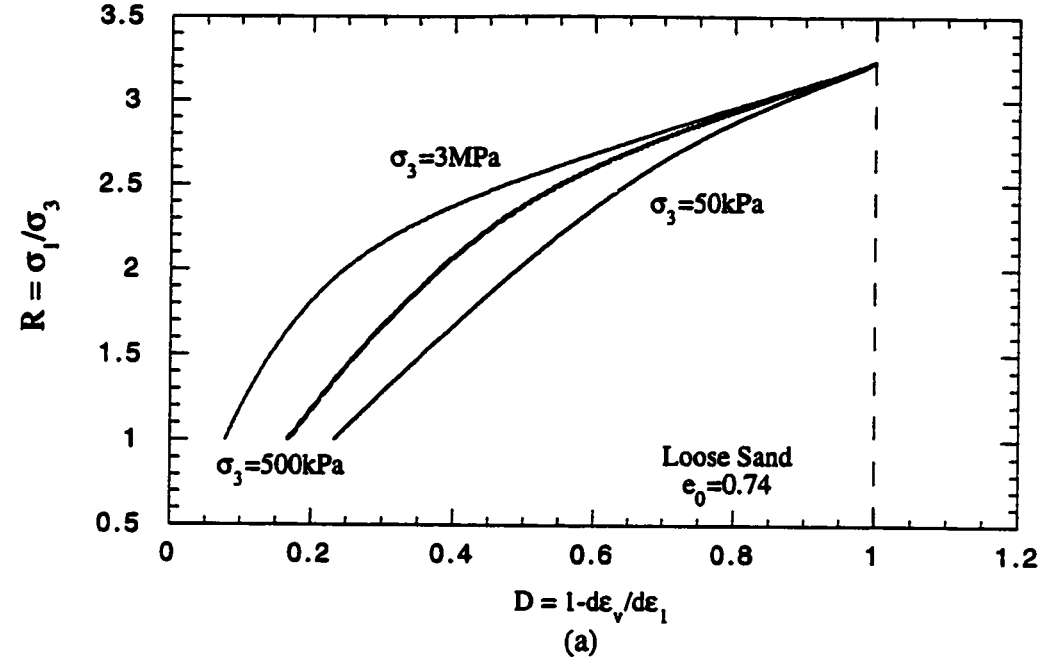

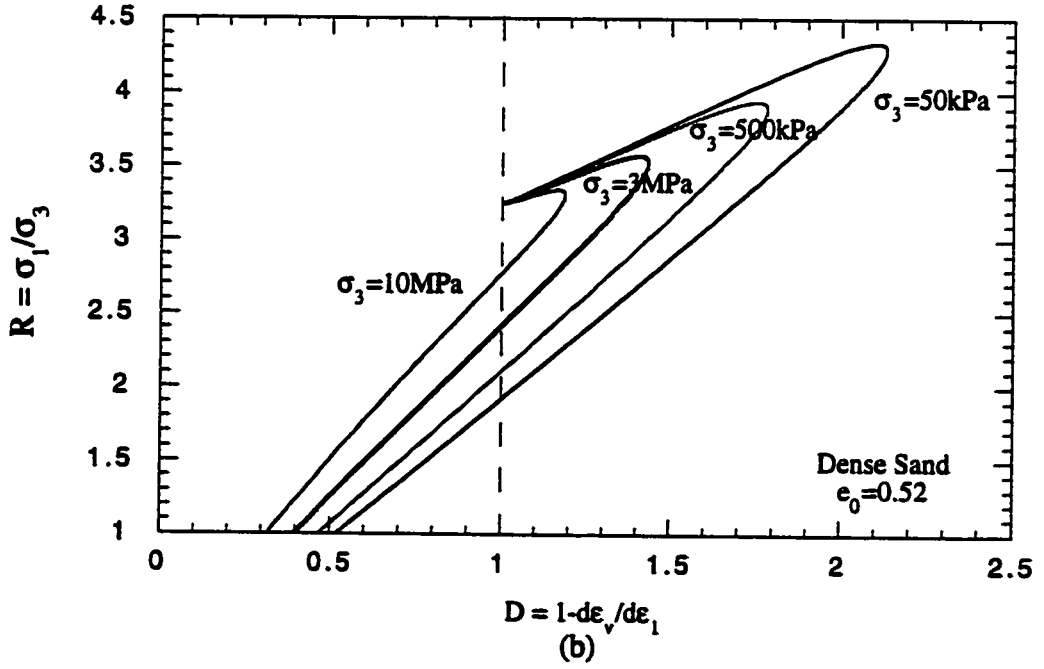

Figure 6.9 Model Prediction of the Dilatancy of Ottawa Sand at Various Confining Pressures

Chapter 7

EXPANSION OF TESTING TO CYCLIC LOADING

7.1 General

The decision to expand the triaxial testing program to incorporate cyclic loading stemmed from a desire to eventually modify the constitutive model discussed in Chapter five to integrate the effects of cyclic loading on the behaviour of granular materials. The ability to ensure an accurate depiction of this behaviour is dependent on an understanding of evolution of the cycles in terms of changes in behaviour with void ratio and confining pressure including shakedown and runaway condition requirements. Although complicated, a model capable of defining cyclic, low frequency volume changes in granular materials will be of great value to the geotechnical engineering field. A notable example is the case of retaining walls imposing low frequency cyclical loads on to the backfill material due to the action of repetitive cooling and heating from the environment.

Extensive cyclic testing has been carried out in recent years for the purposes of understanding liquefaction behaviour. These tests were generally performed at high

frequencies and/or under undrained conditions to allow for the pore pressures to build up in the sample. Once these pore pressures approached the applied confining pressure, failure would occur as effective stresses tend to zero. Although earthquake loading is often an important factor when considering granular material strength, another form of cyclic loading is beginning to be considered with some interest. Low frequency loading, while not generally responsible for catastrophic failures like those caused by earthquakes, can create subtle volume changes and, over time, may damage or even fail the affected structures under the complete absence of any pore pressures. It is not a strength failure as with liquefaction, but instead a deformation failure resulting from a long period of reoccurring movement which induce a change in microstructure in the material. Caused by such things as temperature and other climate effects and vehicular traffic, low frequency loading is relatively obscure and can initially occur subtly without recognition.

The aforementioned conditions, shakedown and runaway, are used to describe stable and unstable soil behaviour in both stress and strain controlled cyclic loading. Shakedown defines the condition where the sample densifies and becomes stronger with cyclic load application, eventually reaching a state in which the volumetric expansive portion of each cycle equals the contractive portion. The net volume change per cycle becomes zero and further changes in energy input requirements are eliminated. Runaway conditions are opposite, as an unstable state will cause the soil to continue to experience volume changes as plastic deformations accumulate with increasing number of cycles. Runaway behaviour is generally expected for cyclic testing in which the cyclic loading begins after strain-softening is exhibited by the

sample. As strain-softening occurs, the sample is more prone to an accumulation of plastic strains over the cycles, thus leading to an unstable condition.

7.2 Modification of Triaxial Testing to Incorporate Cyclic Procedures

The sample preparation techniques used in the cyclic loading program were identical to those used in the monotonic loading regime. The differences in the experimental agenda were reflected in the need for a stress-controlled load application which could be slowly cycled for longer time periods.

7.2.1 Testing Objectives and Specifications

The testing program for cyclic loading involved a reduction in the variety of initial specimen conditions to allow for a more comprehensive understanding of the effects of cyclic loading on the Ottawa Sand samples. The mid-range void ratio and confining pressure tests were eliminated, leaving loose and dense samples, each confined to 200 and $800kPa$ prior to shear. A monotonic loading pattern was used to strain the soil up to a strategic point on the axial strain curve before switching the loading to a cyclic pattern. This pattern proceeded until it became evident that shakedown conditions would occur.

Figures 7.1 through 7.4 show the condition of the sand at the commencement of cyclic loading. Four tests were carried out dense sands, and two on the loose

Test #	σ_3	Strain Position	e_o	$e_{o(cyclic)}$	Figures
1	200	1	0.703	0.684	7.1, 7.8
2	200	4	0.693	0.662	7.1, 7.9
3	800	1	0.689	0.670	7.2, 7.10
4	800	4	0.683	0.650	7.2, 7.11
5	200	1	0.547	0.542	7.3, 7.12
6	200	2	0.545	0.557	7.3, 7.13
7	200	3	0.551	0.566	7.3, 7.14
8	200	4	0.537	0.580	7.3, 7.15
9	800	1	0.548	0.543	7.4, 7.16
10	800	2	0.540	0.545	7.4, 7.17
11	800	3	0.540	0.560	7.4, 7.18
12	800	4	0.537	0.574	7.4, 7.19

Table 7.1: Summary of Cyclic Trialxial Testing Conditions

sands with the two different confining stresses, 200 and $800kPa$, used for each test. Table 7.1 provides a summary of the conditions of the sand prior to cyclic loading. The 12 testing conditions are described by confining pressure, σ_3, the position of the commencement of cyclic loading along the axial strain axis as given by the numbered values, 1 to 4, in Figures 7.1 - 7.4, the void ratio of the sample prior to the monotonic loading, and the void ratio of the sample just prior to the commencement of cycles. The respective Figures which display the strength and volume change characteristics of the specimens are also named in the final column of Table 7.1.

Figure 7.5 better describes the soil conditions before cyclic loading. Points 1, 2, 3 and 4 are the strategic positions on the stress-dilatancy plot chosen to represent initial soil conditions.

The change in loading pattern on the loose samples was begun at two stages. One at approximately 2% axial strain (point 1), where contractive volume changes were quite high, and one at approximately 20% strain (point 4), at constant volume conditions. These two locations were considered adequate for the loose material, as contraction occurs throughout the monotonic loading regime. The dense sand however, required four tests due to the more complicated nature of dilatant behaviour. Cyclic loading commenced at approximately 1, 3, 5 and 17% to attempt to capture initial contraction (point 1), initial dilation (point 2), near peak (point 3) and constant volume (point 4) conditions, respectively. It should be noted that the peak condition does not necessarily correspond to maximum dilation as the influence of elastic behaviour and material structure are omitted in the measurement of dilatancy. At the onset of load reversal, the stress was reduced completely and brought to the lowest possible stress on the sample without lifting the loading ram from the platen.

7.2.2 Testing Equipment

The ELE Digital Tritest load frame proved inadequate for use with the required stress controlled cyclic loading regime. Its limited capabilities allowed only for manual displacement controlled movement, creating a need for constant supervision and surveillance of the measured stress. While some tests required only a few hours,

many lasted for 16 to 20 hours, leading to the desire for an automated testing method. The MTS load frame provided this automated service and was therefore used in the cyclic portion of the research. Figures 7.6 and 7.7 show the MTS system and the surrounding experimental setup.

Some simple changes were made to the data acquisition capabilities to allow for the measurement to exhibit a greater or lesser sensitivity at given times during testing. The desired cyclic results required accurate data to be captured during the initial cycles in the test while the stress-strain-volumetric response prior to cyclic loading, and later in the cyclic portion were not as crucial. To prevent large, unmanageable data files, a voltage controlled switch was integrated directly into the data acquisition system. This switch allowed the reading intervals to be toggled between 30, 10 and 2 seconds. With this system, a wide degree of accuracy could be obtained when desired.

The other testing equipment remained identical to that used in the monotonic loading procedure as outlined in Chapter three.

7.2.3 Cyclic Triaxial Testing

The cyclic triaxial testing procedure differed from the monotonic in that the necessity of control on stress limits caused a stress-controlled rather than strain-controlled method of testing. The upper and lower load limits were pre-programmed into the MTS system. As the test proceeded, load was cyclically applied and released in a sinusoidal pattern through the load range.

The load limits were periodically adjusted to account for area changes in the

sample. The rate at which the test was carried out was controlled by the frequency of the cycles. Ranging between 0.005 and $0.5Hz$, the frequency setting was dependent on the stress limits and the buildup of pore pressures in the sample. A test that required a greater stress range was conducted at a lower frequency, primarily because of the desire to keep a consistent strain rate but also because of the length of time allowing pore pressure buildup in each direction of loading. For example, a low stress range will cause the axial conditions to alternate between compression and expansion quite frequently. Accompanying volume changes will likewise alternate as these responses are shown to closely follow the axial strain (Figures 7.8 to 7.19). Thus, the pore pressures are only able to build up for a short period of time before the load direction changes and internal pressure effects are reversed. On the other hand, for a test with a large stress range, the time required between load direction changes is much greater, allowing pressures to gradually change for a long period before reversal.

Although the strain rates in the cyclic loading regime were higher than those used in the monotonic testing, the suggestions of Lacasse and Berre [56] were followed and the maximum allowable deviation of the internal sample pressures from the original measured value was 2% of the effective confining pressure. At these pressures, the cyclic testing results should not have experienced any strain rate effects different from the monotonic results.

7.3 Experimental Results

Enlarged views of the cyclic responses are shown in Figures 7.8 through 7.19. These plots depict the evolution of stress and volume changes throughout the testing. Several visual observations can be made from the graphs and behaviour is found to be pressure, density and cyclic evolution dependent.

It should be noted that the near consistent responses of the Ottawa Sand subjected to cyclic triaxial testing may suggest that these responses were controlled by the testing apparatus and not the material characteristics of the sand. Further tests should be performed to determine the influence of the system and therefore the accuracy of the results obtained herein. However, a general trend could be deduced from the tests obtained in this research.

7.3.1 Stress-Strain Characteristics

Characteristics common to all cyclic behaviour observed include shakedown conditions, an increase in the slope of the stress-strain loops and contraction trends in the volume change curves. The shakedown conditions were predicted to occur in most cases. However, for the loading that began in the post peak portion of the curves (Figures 7.3 and 7.4), complete failure, termed the runaway condition, of the soil was expected. In this area, the soil had already lost its largest resistance and would have experienced strain-softening under monotonic conditions being unable to withstand the current stress level.

Reasons for the unexpected shakedown for post-peak conditions are obscure but

could involve the method of loading, the type of sand used or the sample preparation techniques. The MTS system was not capable of performing cyclic tests on post-peak samples because of its inability to incorporate both stress-control and strain-control in the same test. For this reason, the ELE Digital Tritest was manually controlled through the stress cycle. With this procedure, sinusoidal loading was impossible, and a ramp pattern was used instead where the direction of loading was reversed immediately without slowing the loading speed. Although this should theoretically not have any effect on the outcome of the testing, other unexpected time-rate effects have been shown to influence the sample and may be extended to the cyclic loading responses.

The absence of runaway (ratcheting) behaviour for post-peak conditions can also be attributed to the rebuild of internal structure which masks the accumulation of residual plastic strains as a result of a decrease in particle slippage recovery with the number of cycles at such high stress ratio. A change in internal structure during the cycles does not necessarily lead to large plastic strains especially in the case when the structure is tending toward a stable, 'strong' configuration such as at steady state condition. The above discussion must be verified by measuring the structure evolution during the test. Although this is outside the scope of this work, it can be addressed in future research

An increasing slope in the stress-strain curves with the progression of number of cycles is also evident in the behaviour of the Ottawa Sand. This is simply explained by the reduction in strain limits with cycles. As the soil becomes stronger with progressive loading, the rebound and contraction of axial length diminishes.

The contraction trend in the volume change curves is another product of the shakedown or strength-gain phenomenon. With each additional cycle, the soil becomes closer to steady state conditions until eventually the dilatant portion of the curve equals that of the contractive and no further net volume changes occur.

7.3.2 Volume Change Characteristics

Density (initial grain packing), confining pressure, number of cycles and location of commencement of cycles all have an effect on the behaviour of the volume changes in granular materials. The following sections will define these dependencies and show comparisons between the various plots.

Density

Density dependencies can be seen when comparing loose and dense samples at strain position (1) in Figures 7.8, 7.10, 7.12 and 7.16. At this position, the behaviour of the samples can be compared as they are both in a contractive state prior to cyclic loading. The differences between the behaviour of the two initial densities are witnessed in the first cycles of the volume change plots (see Figures 7.8, 7.10, 7.12 and 7.16). The unloading curves of the dense sand show dilation while those of the loose sand show a slight contraction. This results from the structure of the sample at the first unloading curve. The loose sand has not yet built up much structural strength and the sample continues to contract slightly with the release of load. The dense sample however, builds up strength and has few void spaces, causing it to rebound as the incremental load direction is reversed. At later cycles in the loading regime,

the loose and dense specimens begin to behave in a more similar manner, with both contraction and dilation occurring in each cycle. Another difference in loose and dense behaviour is seen in the global contraction. A loose sand will achieve greater overall compaction for a given number of cycles as shown in Figures 7.1 to 7.4.

Confining Pressure

The increase of confining pressure tends to mute the volume change effects of the loose sands (Figures 7.8 to 7.11) and the dense sands in positions (1) and (2) (Figures 7.12, 7.16, 7.13 and 7.17) when observing individual cycle behaviour. The dense sands in positions (3) and (4) however, tend to show wider ranges of volumetric strains with increasing confining pressure (Figures 7.14, 7.18, 7.15 and 7.19).

On a global level, comparisons of Figure 7.1 with 7.2 and Figure 7.3 with 7.4 show the increased axial strain range for cycles at higher confining pressures. A possible explanation of this behaviour could be the increased ductility of sands as in the monotonic loading regime at large confining pressures as discussed in Chapter six. This allows for increased irrecoverable strains at higher confining pressures.

The accumulation of plastic strains is witnessed in Figures 7.1 and 7.4 by the trend of movement to the right in the volume change curves. The observation of the dense samples show that at lower confining pressures (Figure 7.3) plastic strain accumulation occurs in every sample while at higher confining pressures (Figure 7.4) this accumulation is evident only in the samples tested at higher stress ratios. To explain this phenomenon, monotonic behaviour is once again used, as increases in confining pressure tend to cause the sample to exhibit a less brittle behaviour. Strain

per cycle is be a result of recoverable elastic strains, with few accumulated plastic strains incurred. At the higher confining pressure the increased stress ratios are sufficient to strain the soil through the elastic range and into the range of plastic behaviour, giving rise to the accumulated plastic strains in these samples over the cycles.

Trends of the Unloading-Reloading Curves

While the global trend of all volume change curves in the cyclic triaxial experiments is contractive, the tendencies of the individual loops also present interesting behaviour of sands. To better explain this behaviour, the loose sand is divided into strain positions (1) and (4), representing initial contractive and constant volume conditions. The dense sand is divided into positions (1), (2 and 3) and (4) representing initial contraction, dilation and constant volume conditions. The confining pressure, while reflected in the amounts of volumetric and axial strain in the individual cycles, does not show a significant influence on the directional trends of the unloading and reloading curves. The cyclic behaviour is studied both at the onset of repetitive loading and later on in the loading regime as the behaviour of the cycles becomes consistent.

Initial Cyclic Behaviour (2-4 cycles) The loose sand at point (1) (Figures 7.8 and 7.10) shows contraction throughout unloading. The reload curve gives a slight initial dilation, followed by contraction. At position (4) (Figures 7.9 and 7.11), the unloading trend is contractive and then dilatant while an increase in load gives purely contractive volumetric strain.

In the initial curves of the dense specimens at position (1) (Figures 7.12 and 7.16), a release of the axial load causes contraction and subsequent dilation. The reapplication of stress causes dilation, then contraction. Positions (2) and (3) (Figures 7.13, 7.14, 7.17 and 7.18) result in almost pure dilation in the unloading curve, and contraction in the reloading curve. In the final position (4) (Figures 7.15 and 7.19), the sample shows a mild expansion before exhibiting a contractive trend during unloading, and contracts initially with reloading before exhibiting dilatant behaviour.

Behaviour in the Later Cycles(10+) The trends of the volume change curves in the later cycles become less dependent on density and the previous monotonic loading. The unloading curves show contraction followed by dilation, with the opposite observed in the reloading regime. The only exception is the dense sands nearing constant volume conditions (position 4). In this case, pure dilation is caused by the release of axial stress and contraction by the subsequent stress application.

Another substantial trend in the later cycles is that the position of the reload curve is entirely above the unload curve on the volumetric strain versus axial strain plot. This merely shows that the volumetric changes throughout the cycle can be maintained even as the global volume changes of the sample near negligible values.

7.4 Conclusions

The conclusions drawn from the triaxial cyclic loading regime are as follows:

1. The effect of density on the cyclic behaviour is seen when comparing loose and dense responses at position (1) when both are in a contractive state. The loose sand shows additional contraction with unloading as the sample has not yet reached a state where much particle slippage has occurred. The dense sample exhibits dilation with the release of stress. The large scale behaviour is also influenced by density. Loose samples experience greater contractions per cycle than dense samples because of the ease of contraction in sands with void ratios greater than critical.

2. Confining pressure effects on cyclic results reflect monotonic findings. Dilatant sections of the loops are more defined at the lower confining pressures as these smaller stresses allow for greater expansion. Volume change (contraction) per cycle is not as great and the axial strain ranges are more narrow at the lower confining pressures. Accumulations of plastic strains are greater at small confining stresses when compared to larger stresses. These results reflect the monotonic sand behaviour which shows an increased ductility in a sample which is sheared at higher confining pressures. Greater recoverable deformation is exhibited before the onset of plastic deformation.

3. A detailed description of the volume change trends in the individual cycles is difficult to define in terms of pressure and density dependencies for the initial few repetitions of loading. However, the characteristics of the mature cycles are more simply described as they are similar for all of the initial sample conditions with the unloading behaviour showing contraction, then dilation and

the reloading behaviour showing the opposite. In both cases, it is seen that the volume change trends do not closely follow the direction of axial strain. An explanation for this could lie in the grain structure of the sand and the influence of loading on its strength. Material structure rebuild is permitted to occur in the latter portions of the unloading path as the sand is no longer subjected to much axial stress. This rebuild is also evident at the end of the reloading path due the redistribution of grain contact forces from the weaker contacts to the stronger contacts, creating a bridging effect. These structural changes in the sands allow for the continued volumetric trends as the reversal in shear stresses must first overcome the material strength due to structural buildup before it can influence the volume change characteristics of the sand.

4. Based on the discussion in item (3), more work needs to be done in the measurement of microfabric and energy dissipation during a test.

5. Observation described in this study are limited to conventional triaxial stress conditions. In other stress paths such as cases where principal stress directions rotate, grains could have more freedom to move. The material response will be very much biased by microstructure change rather than slip phenomenon.

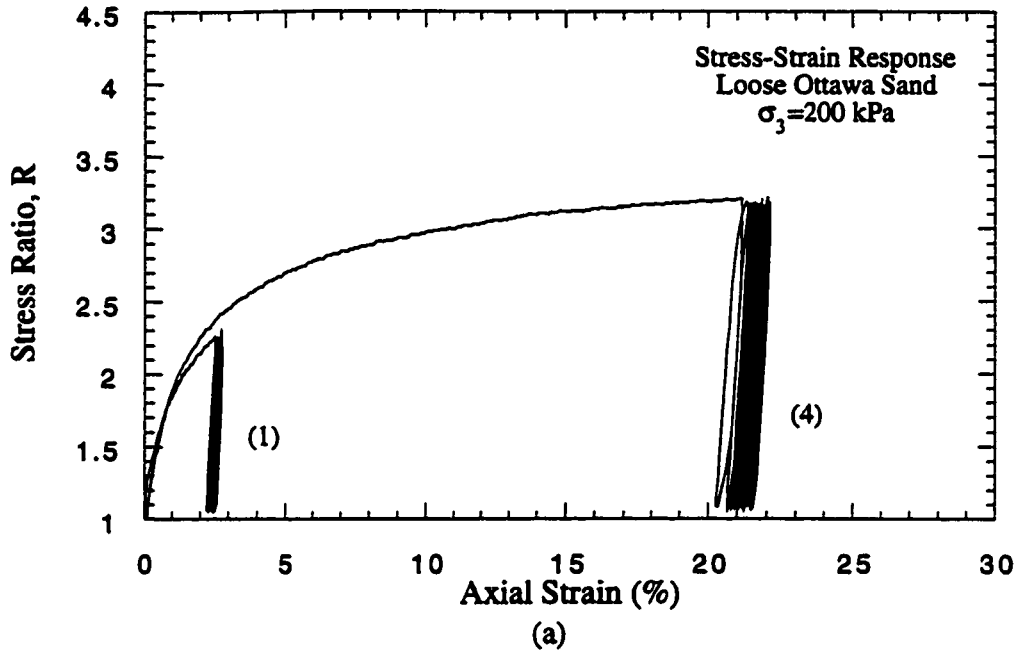

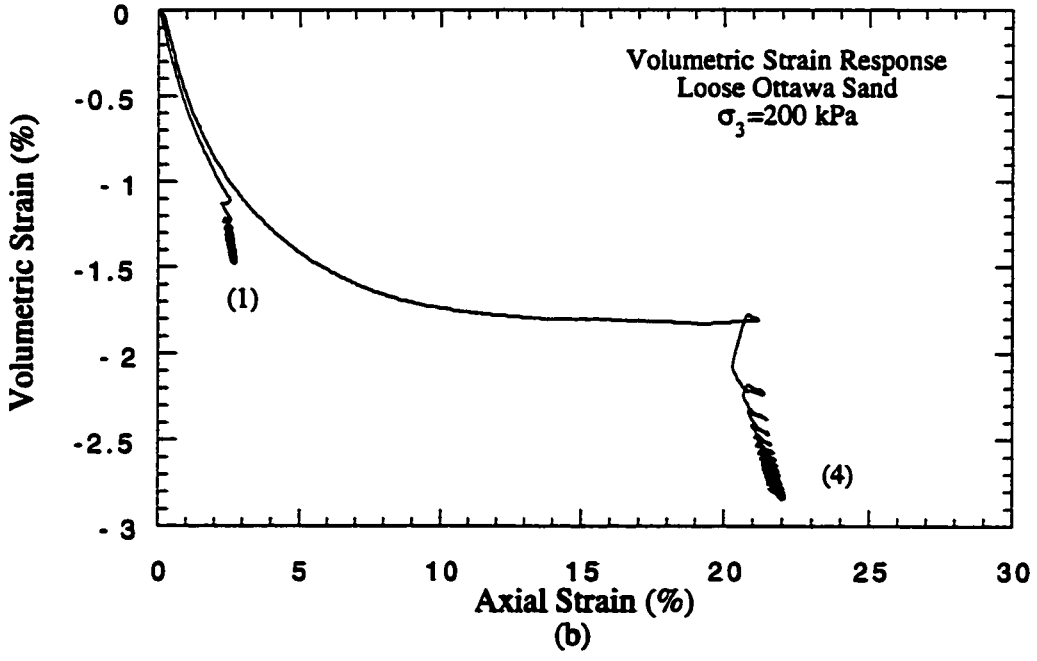

Figure 7.1 Cyclic Triaxial Testing Results on Loose Ottawa Sand; σ_3 = 200kPa

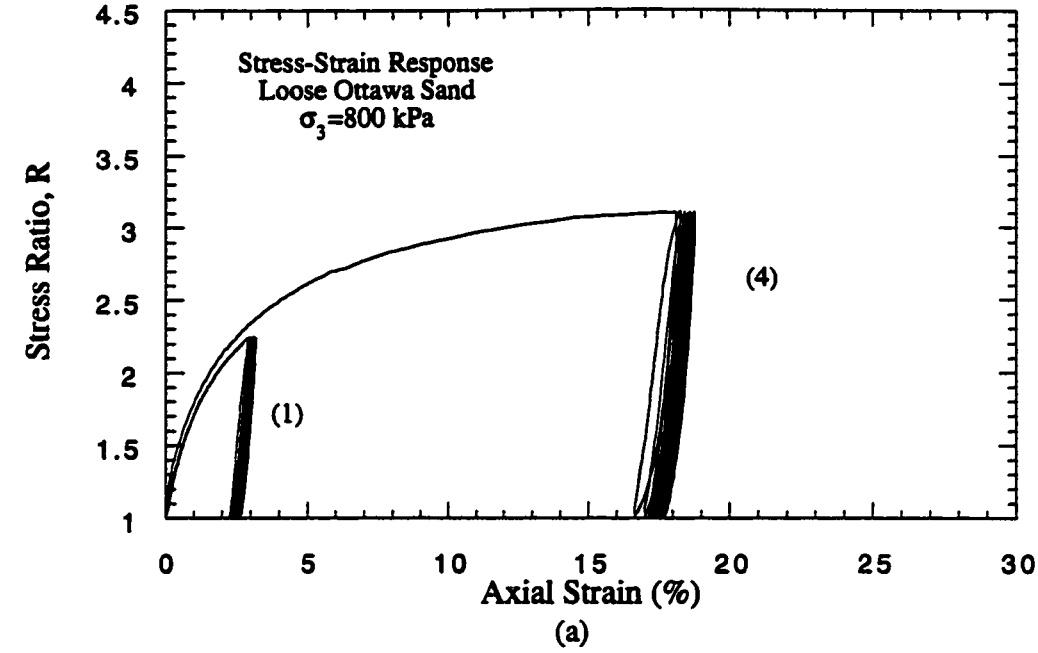

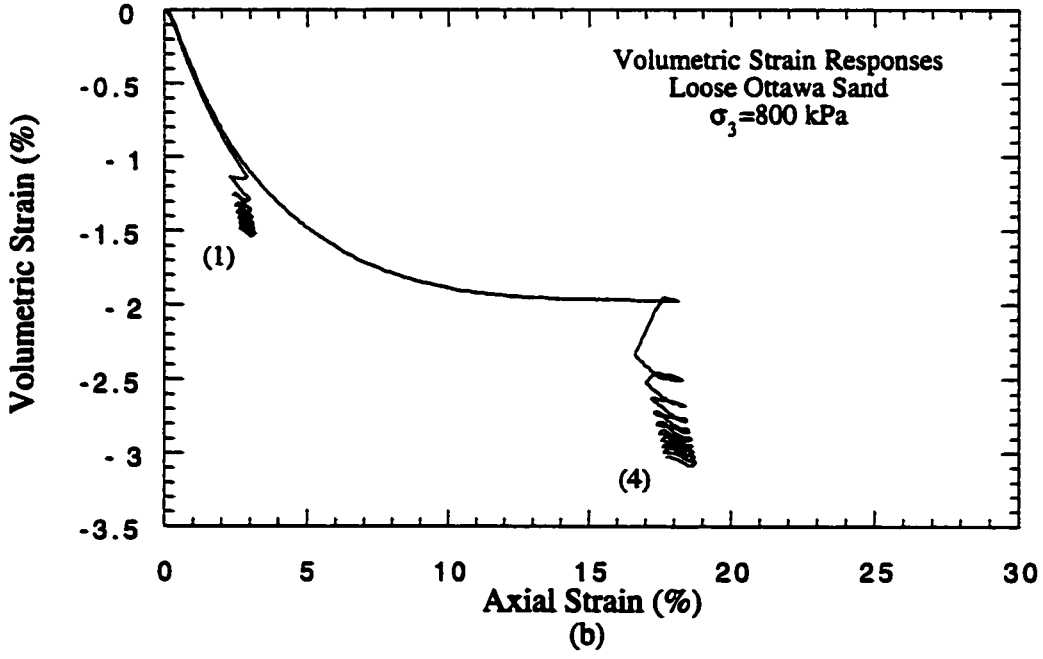

Figure 7.2 Cyclic Triaxial Testing Results on Loose Ottawa Sand; σ_3 = 800kPa

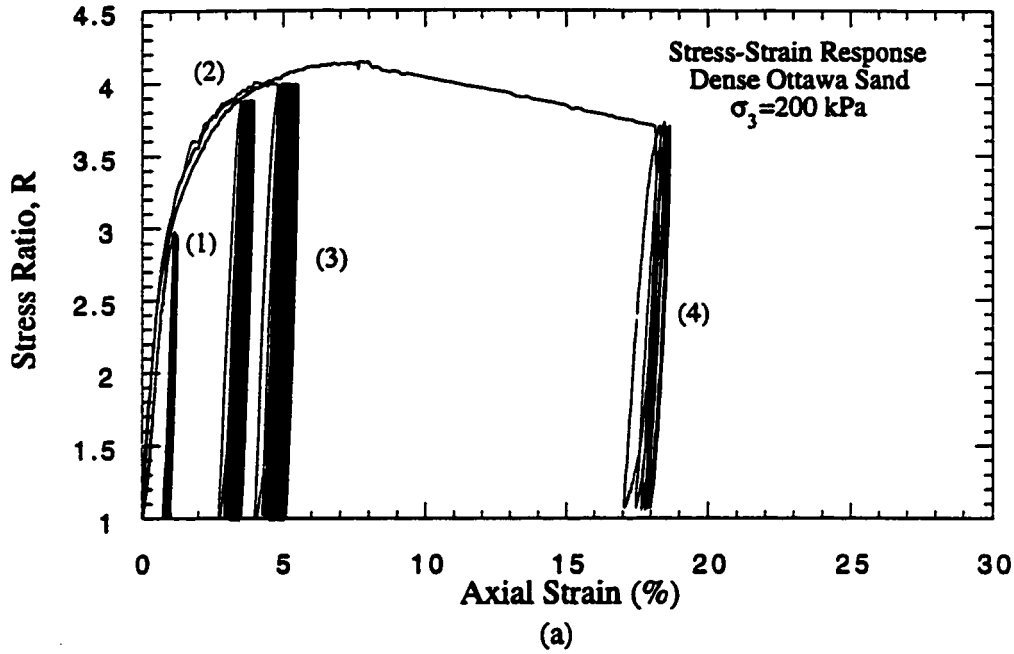

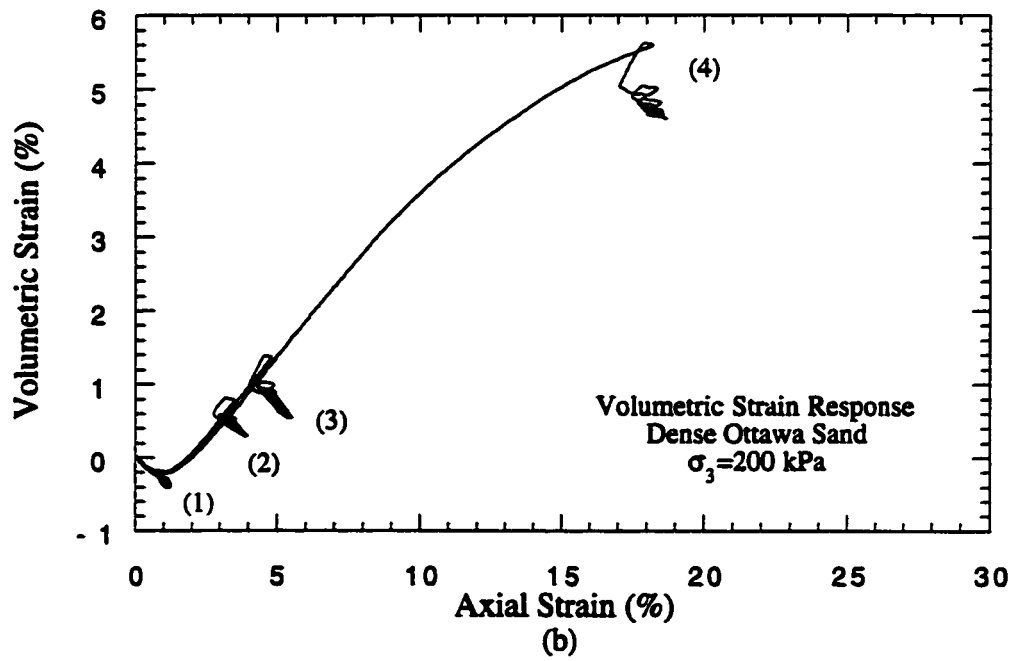

Figure 7.3 Cyclic Triaxial Testing Results on Dense Ottawa Sand; σ_3 = 200kPa

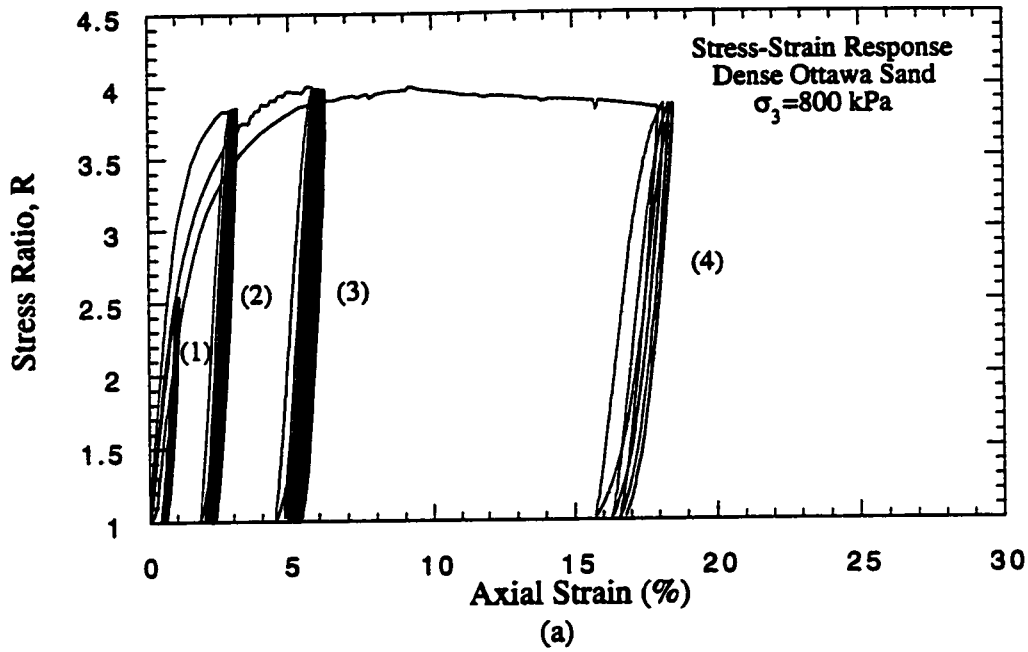

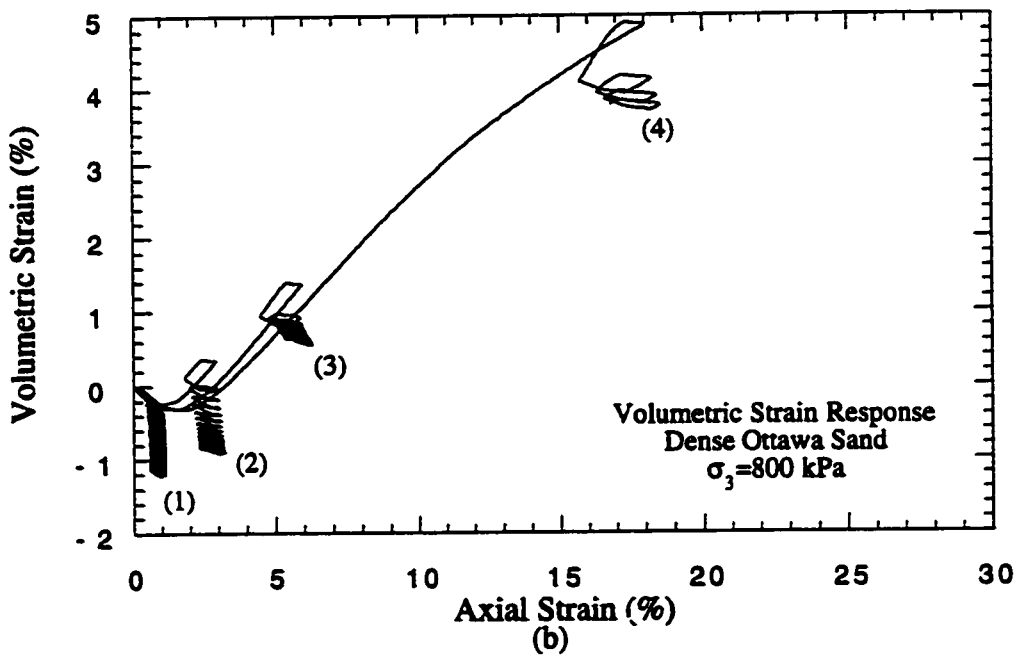

Figure 7.4 Cyclic Triaxial Testing Results on Dense Ottawa Sand; σ_3 = 800kPa

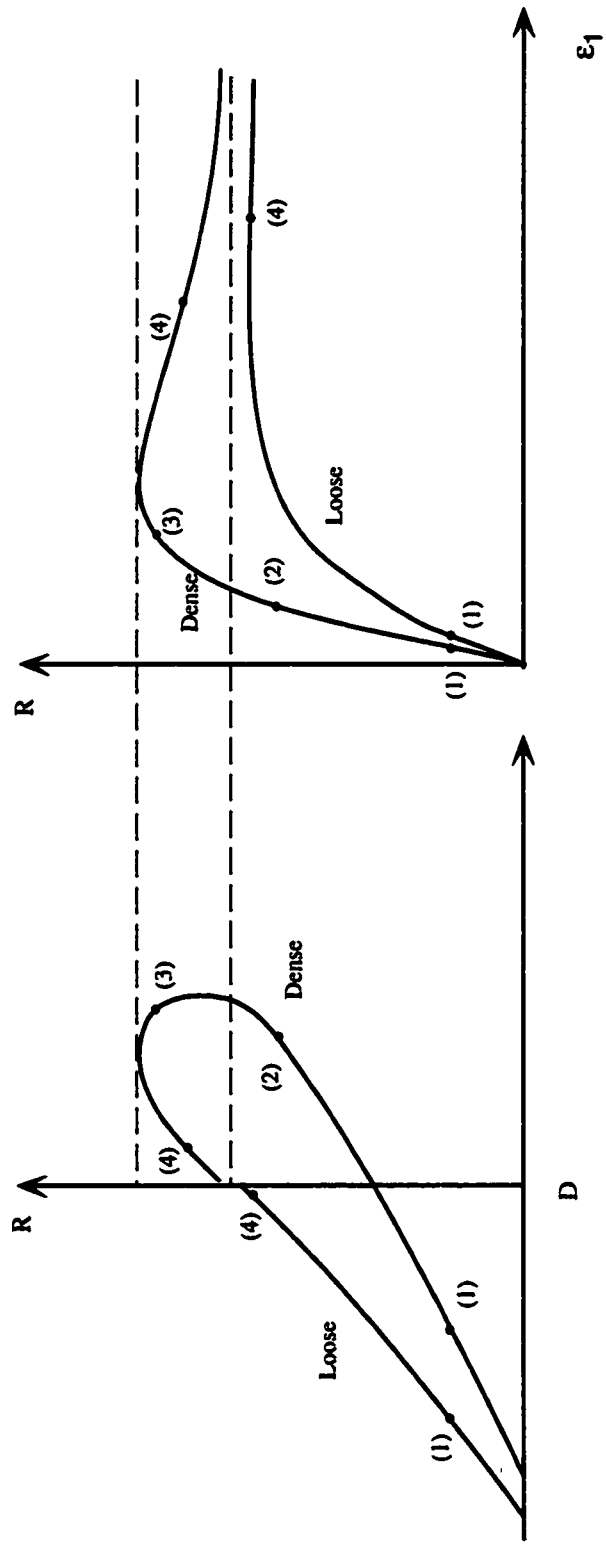

Figure 7.5 Location of Strain Positions

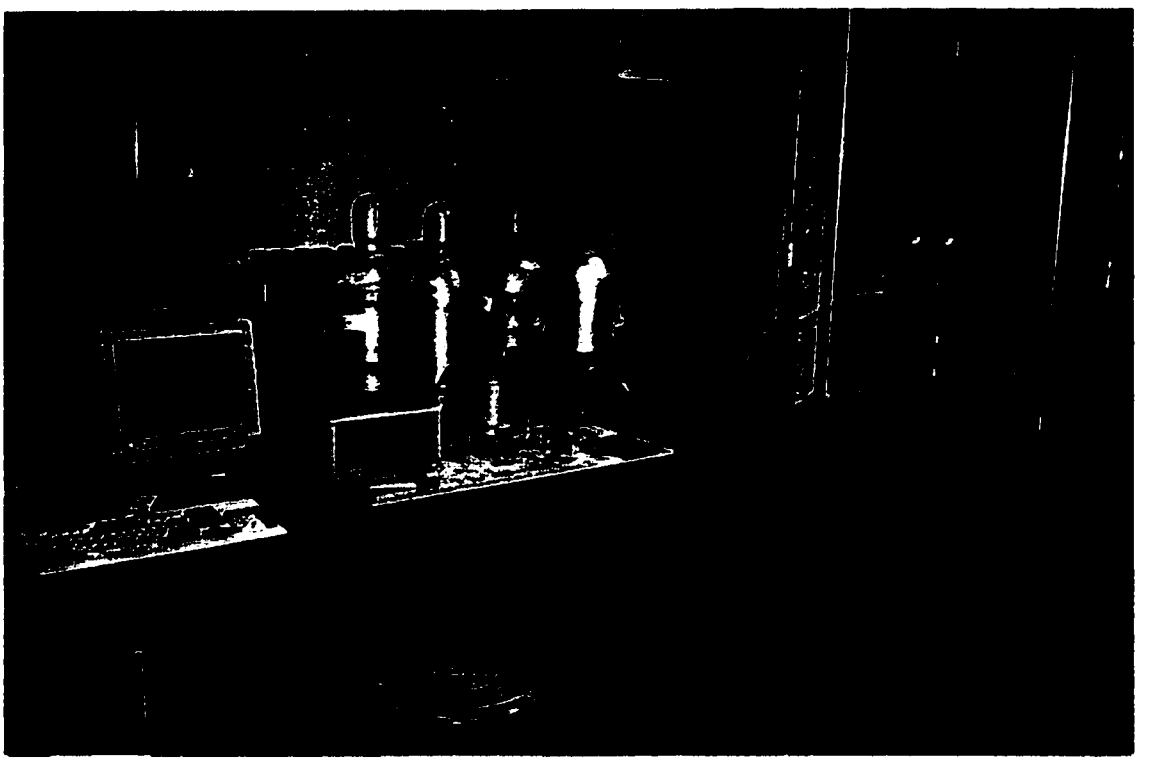

Figure 7.6 Cyclic Testing Apparatus Setup

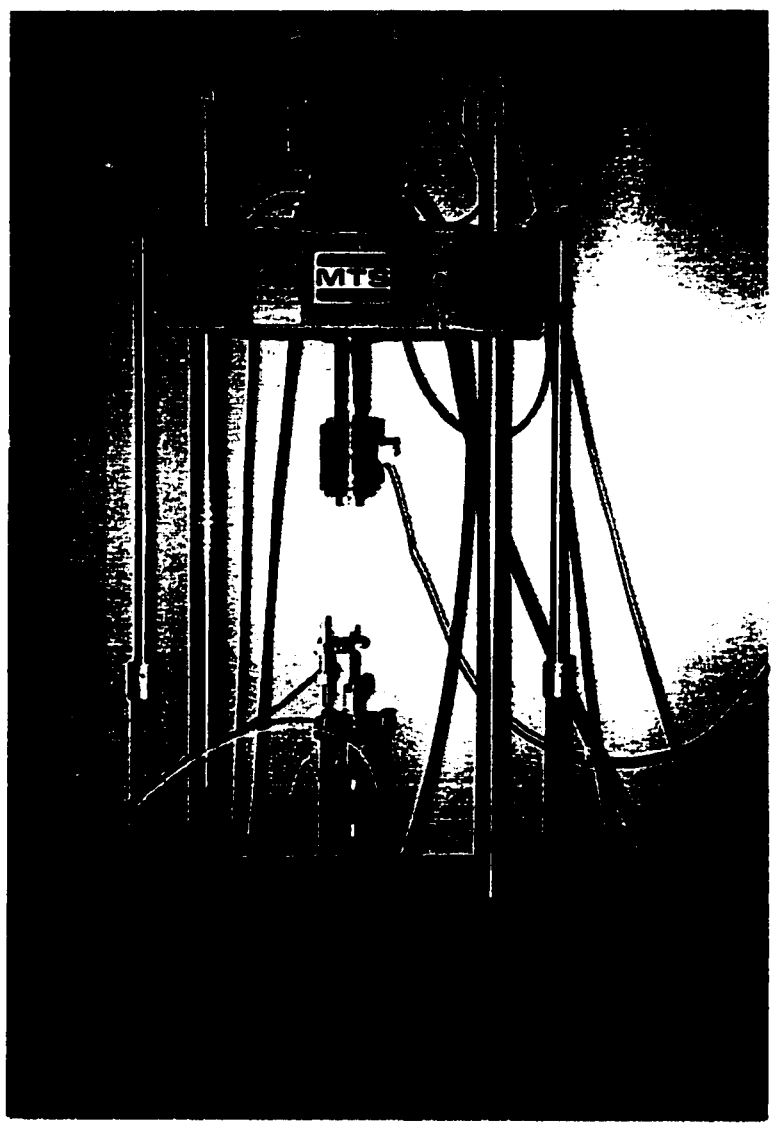

Figure 7.7 MTS Loading Frame

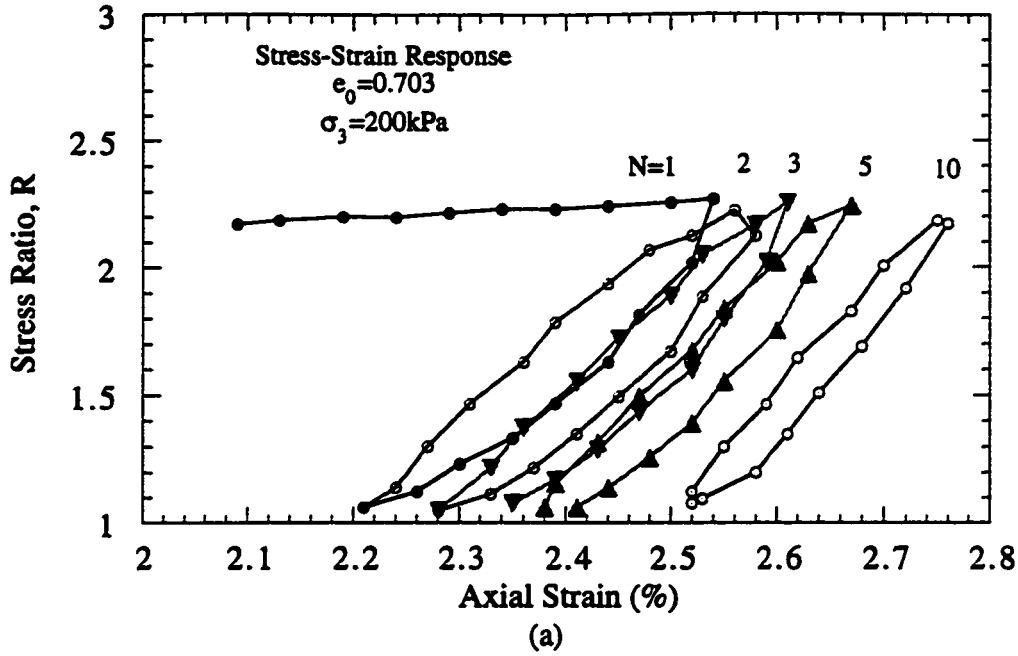

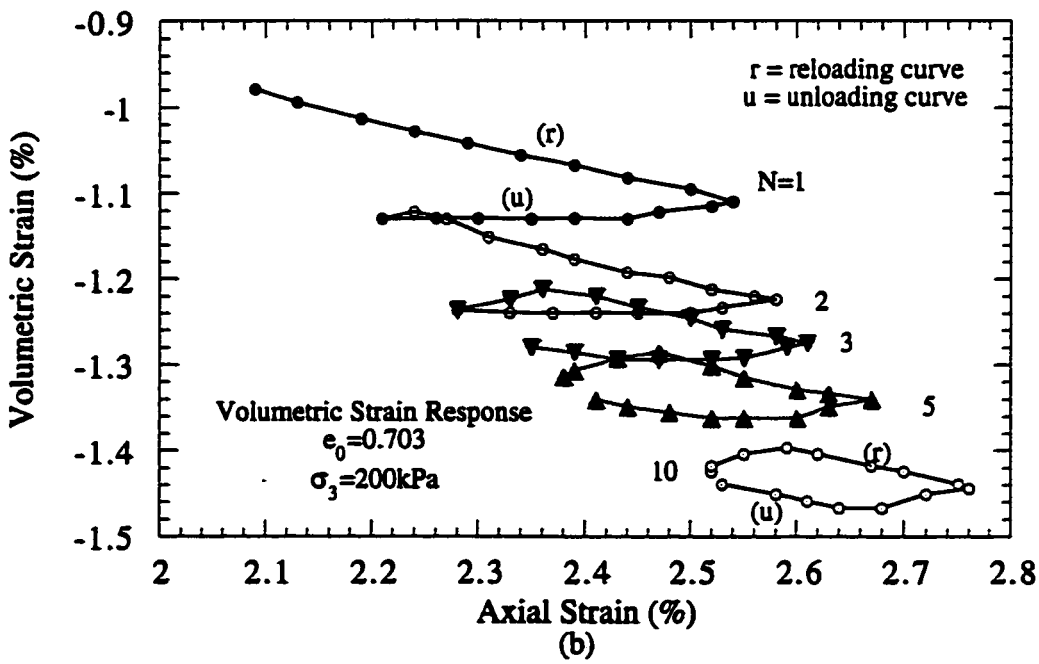

Figure 7.8 Behaviour of Dense Ottawa Sand in the Cyclic Loading Regime (strain position #1); σ_3 = 200kPa

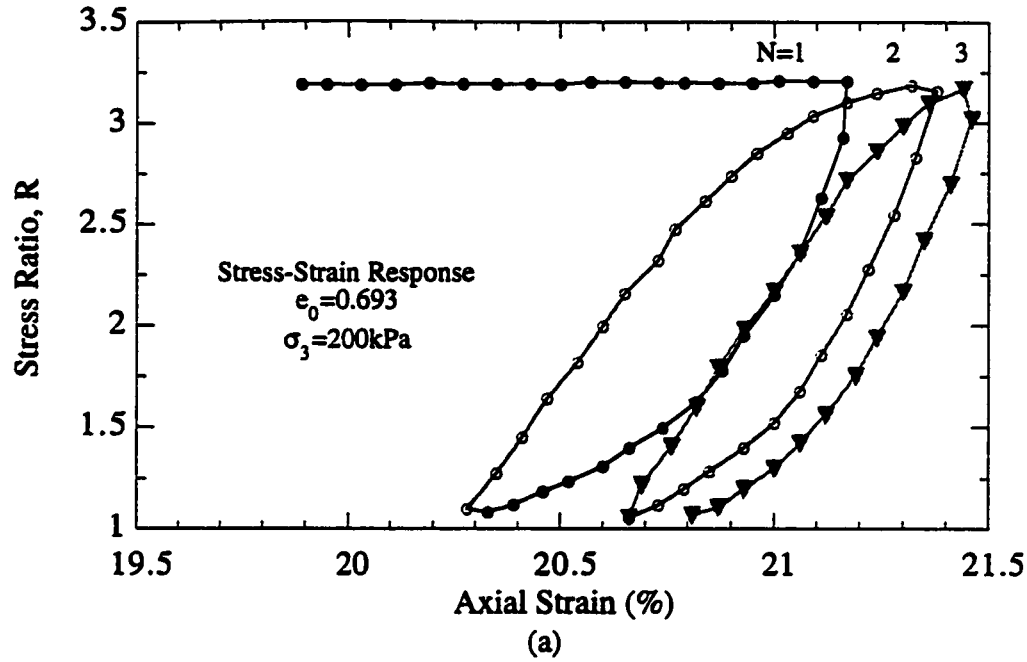

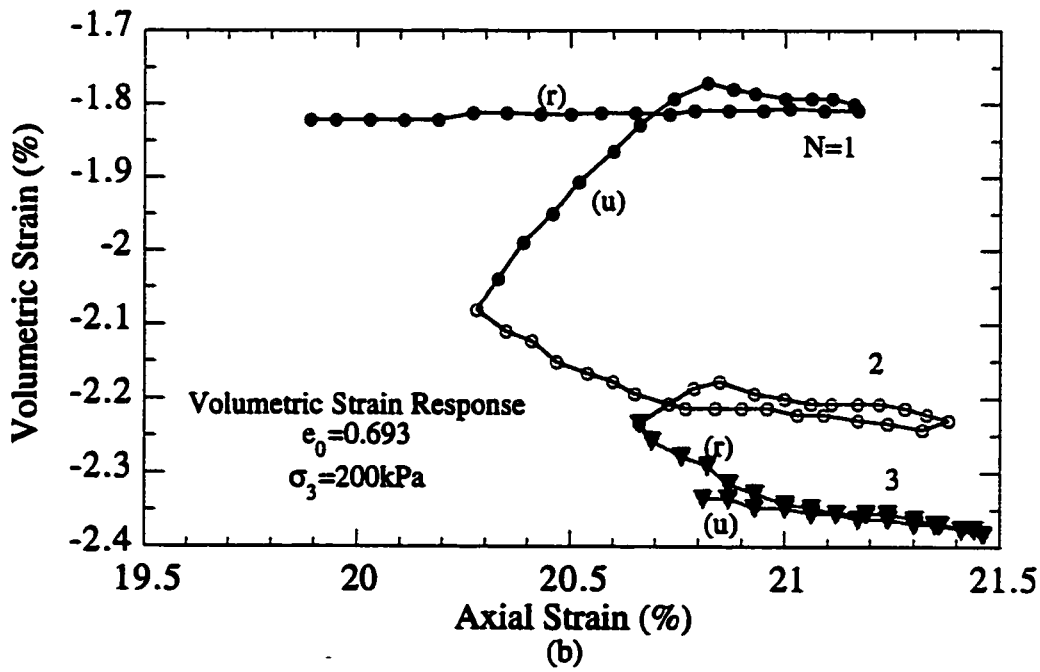

Figure 7.9 Behaviour of Dense Ottawa Sand in the Cyclic Loading Regime (strain position #4); σ_3 = 200kPa

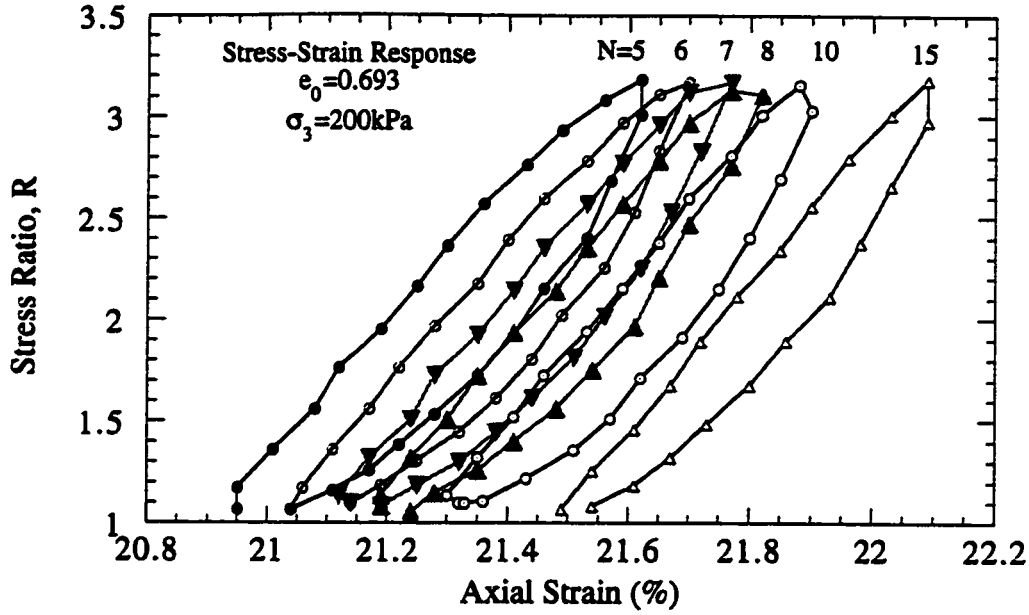

(c)

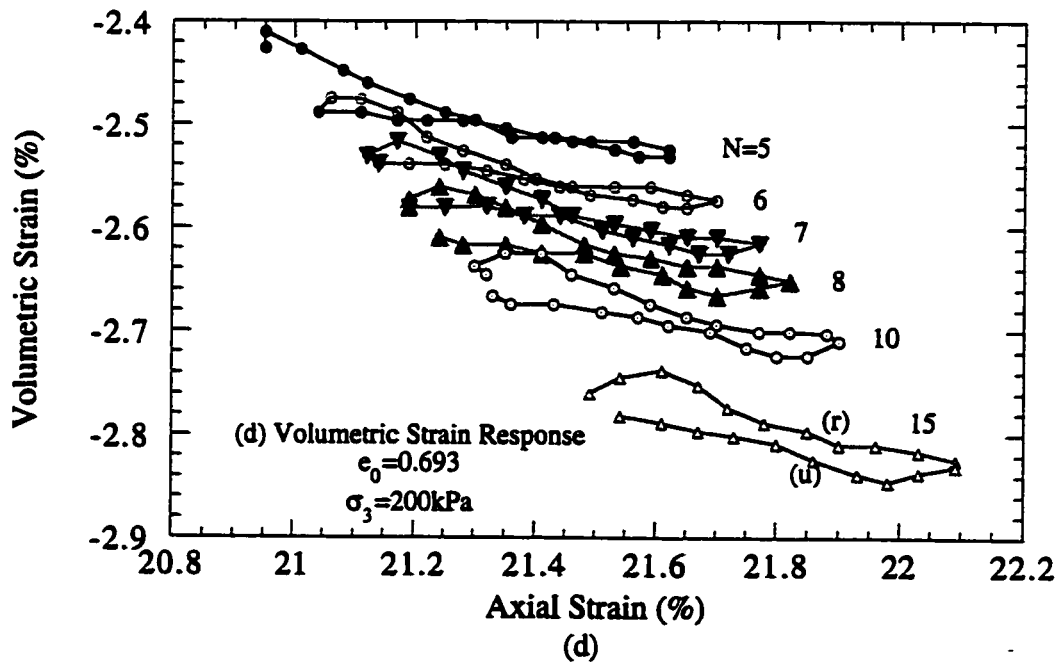

(d)

Figure 7.9 Behaviour of Dense Ottawa Sand in the Cyclic Loading Regime (strain position #4); σ_3 = 200kPa

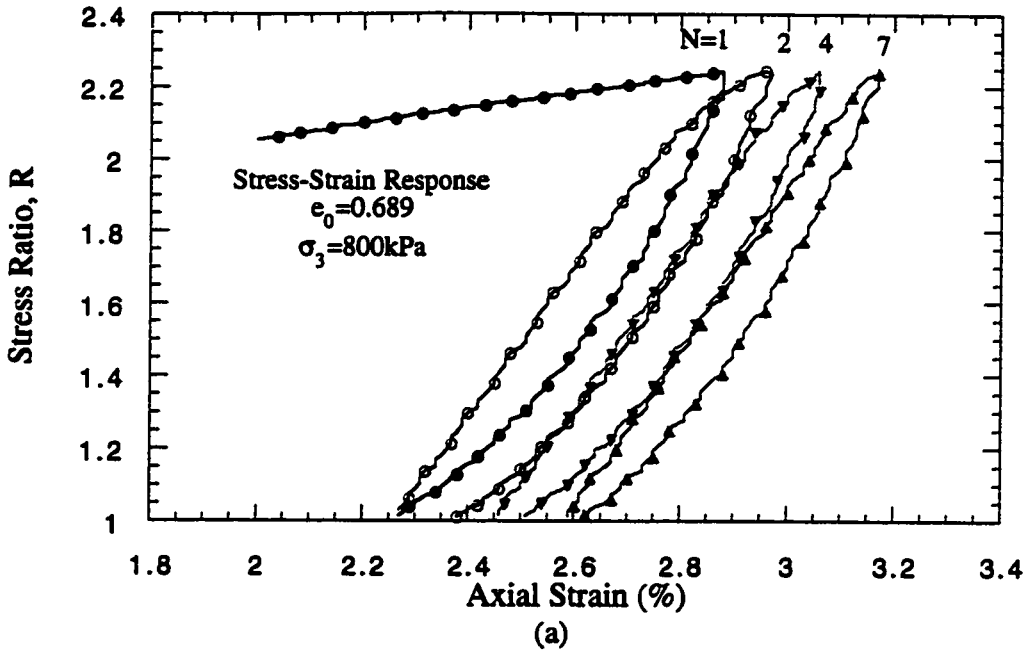

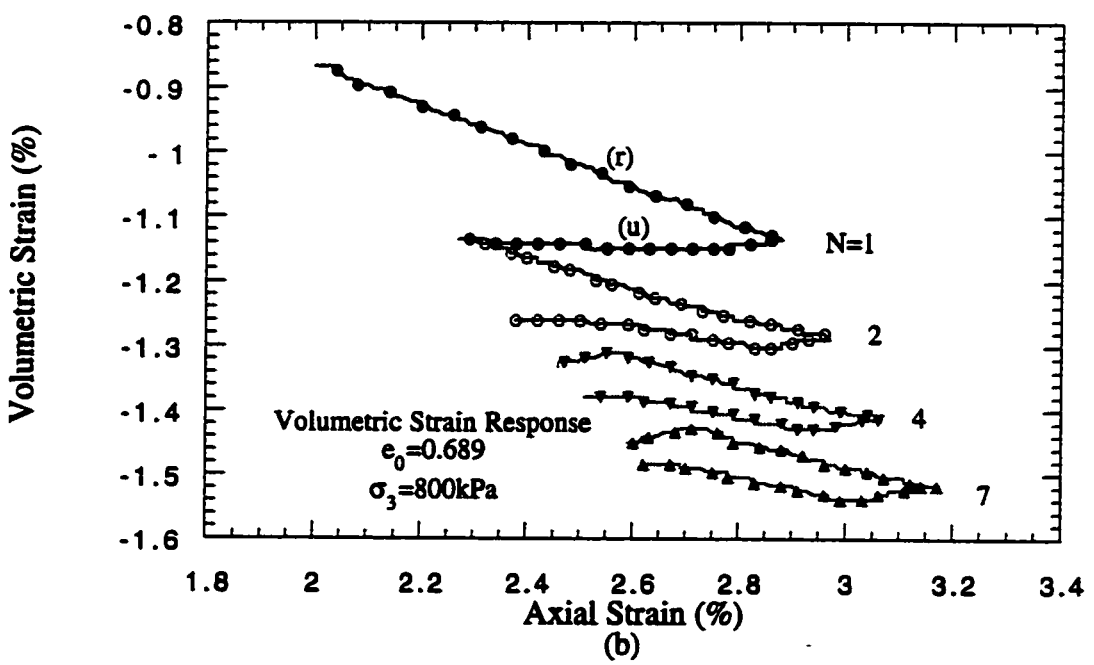

Figure 7.10 Behaviour of Dense Ottawa Sand in the Cyclic Loading Regime (strain position #1); σ_3 = 800kPa

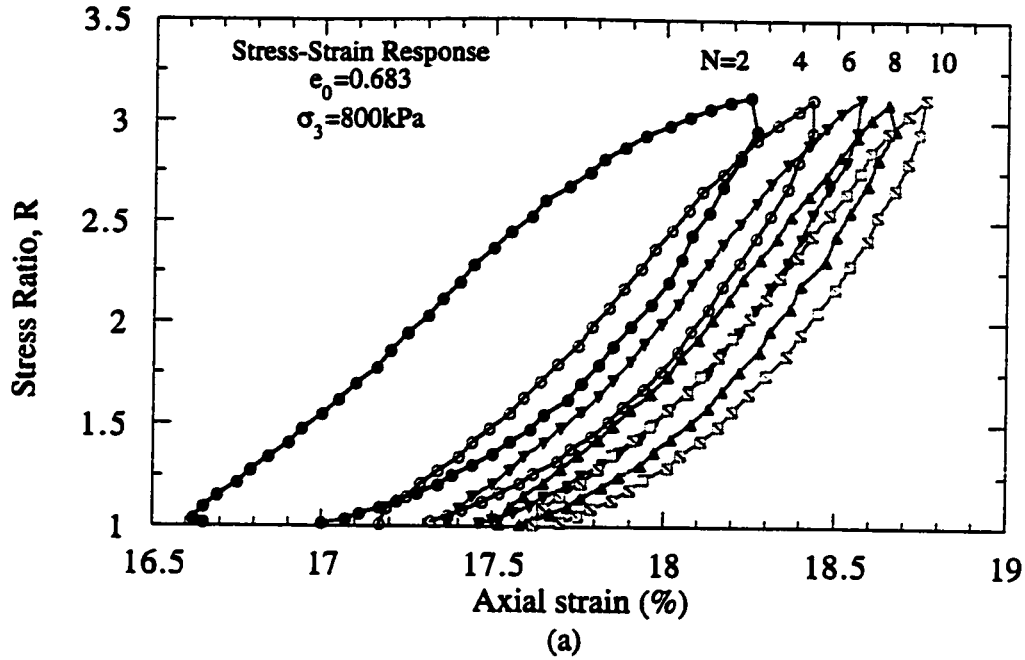

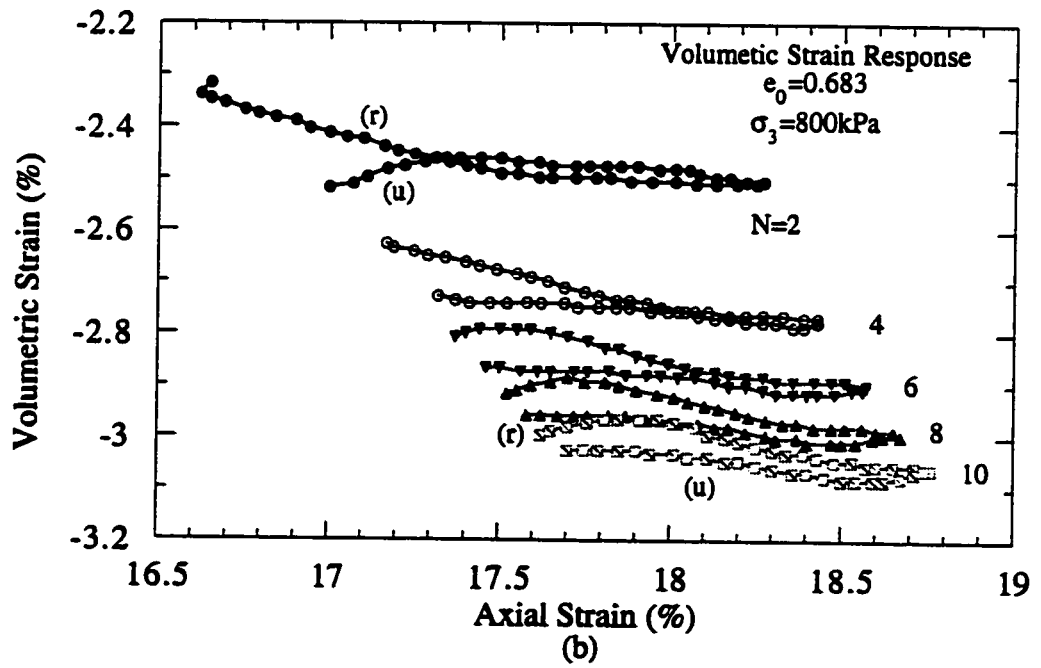

Figure 7.11 Behaviour of Dense Ottawa Sand in the Cyclic Loading Regime (strain position #4); σ_3 = 800kPa

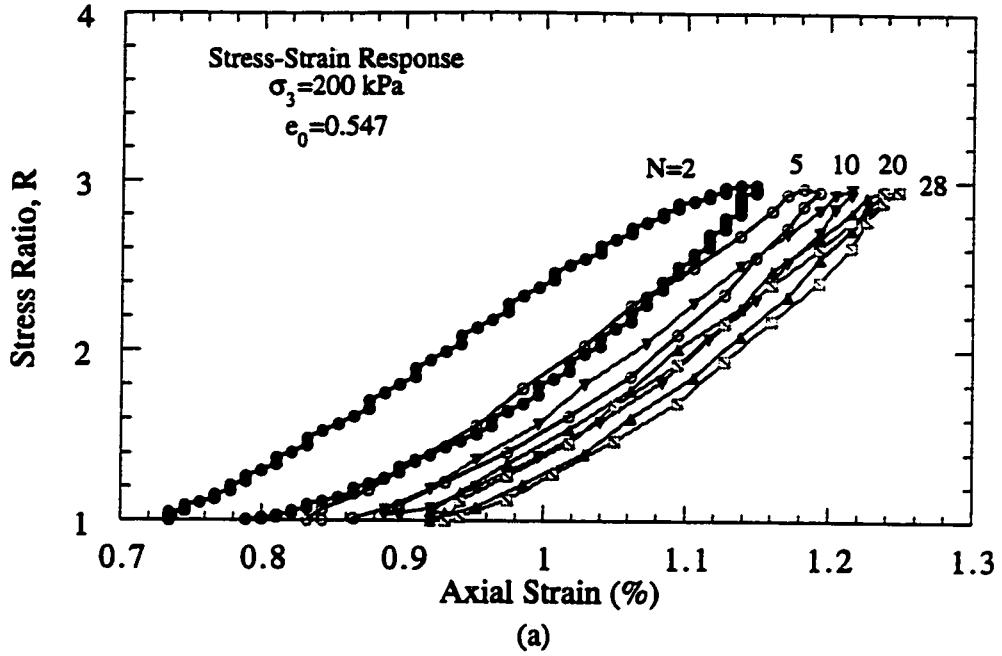

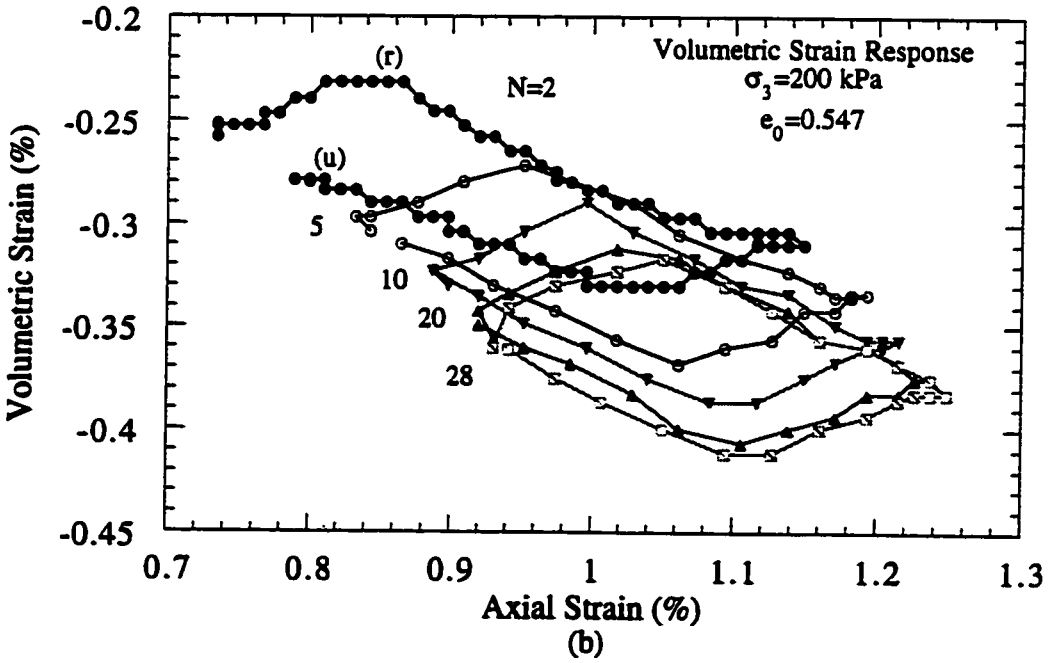

Figure 7.12 Behaviour of Dense Ottawa Sand in the Cyclic Loading Regime (strain position #1); σ_3 = 200kPa

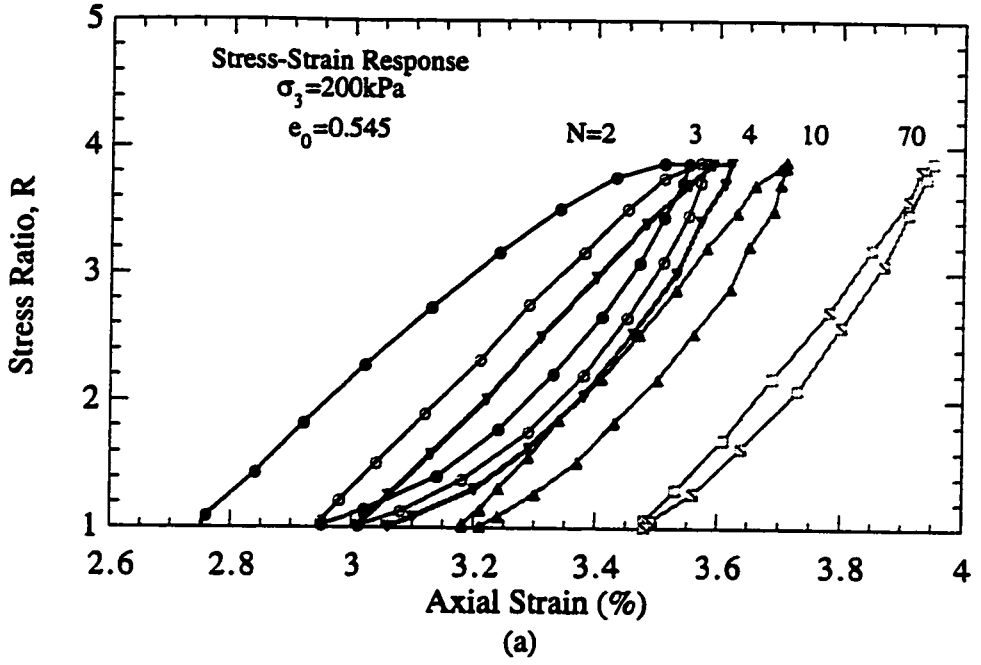

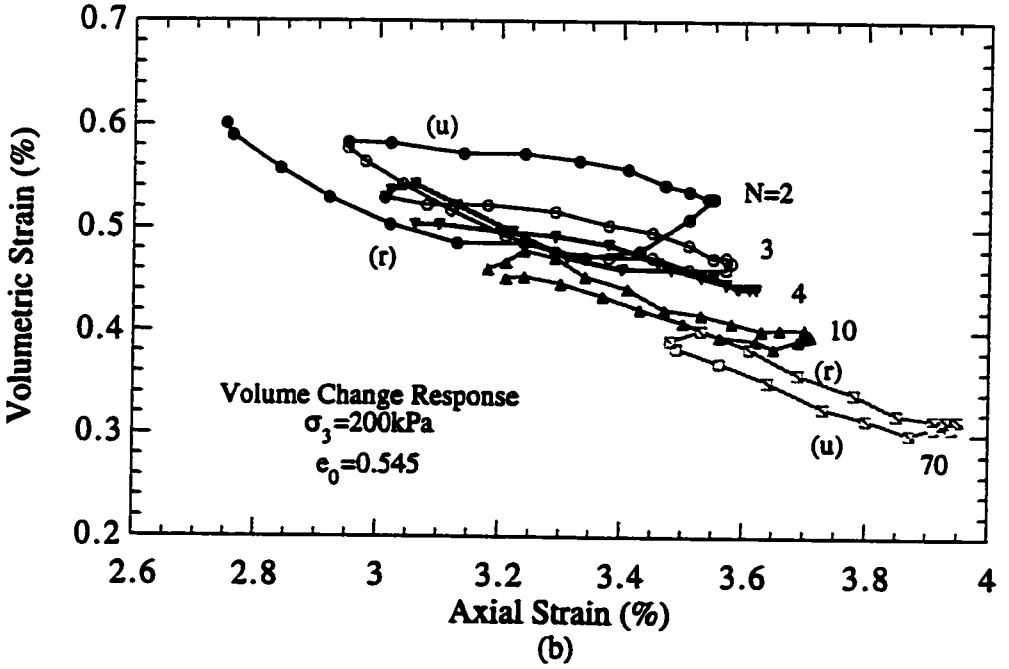

Figure 7.13 Behaviour of Dense Ottawa Sand in the Cyclic Loading Regime (strain position #2); σ_3 = 200kPa

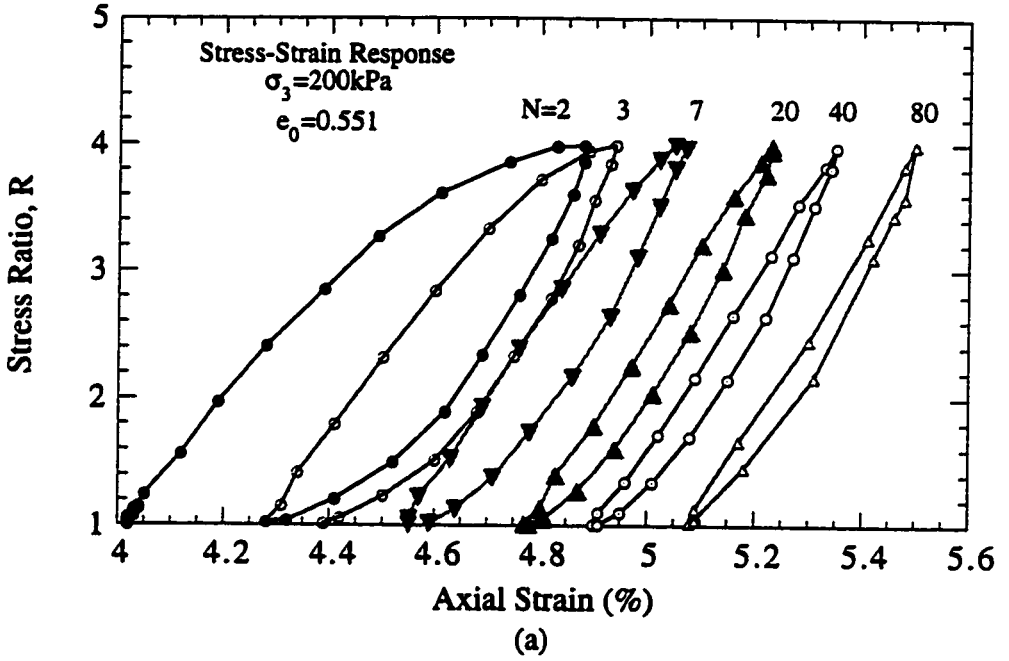

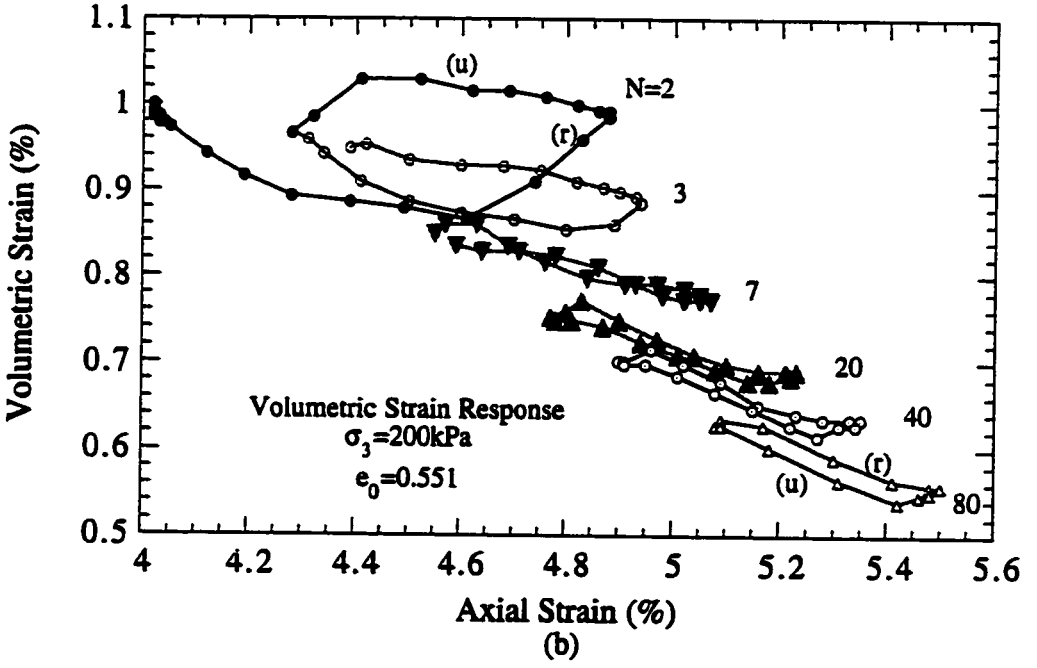

Figure 7.14 Behaviour of Dense Ottawa Sand in the Cyclic Loading Regime (strain position #3); σ_3 = 200kPa

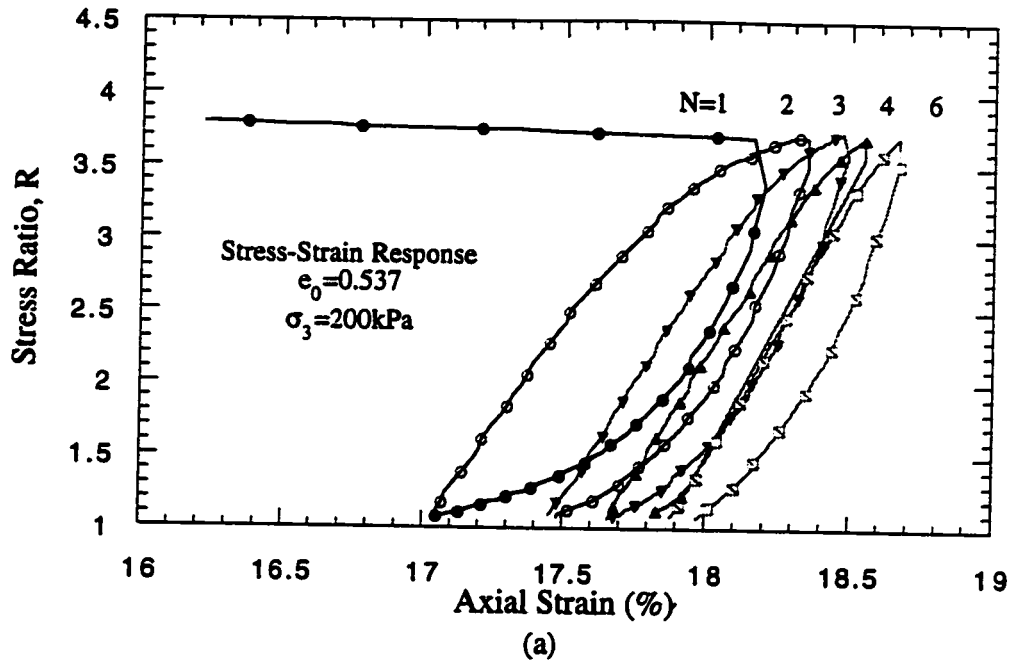

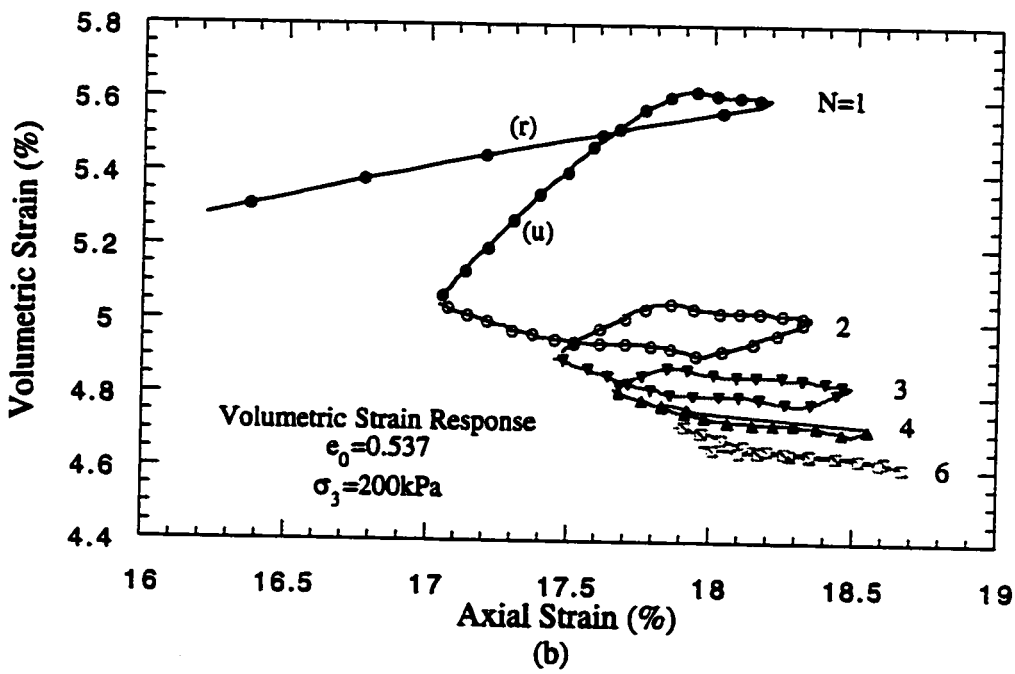

Figure 7.15 Behaviour of Dense Ottawa Sand in the Cyclic Loading Regime (strain position #4); σ_3 = 200kPa

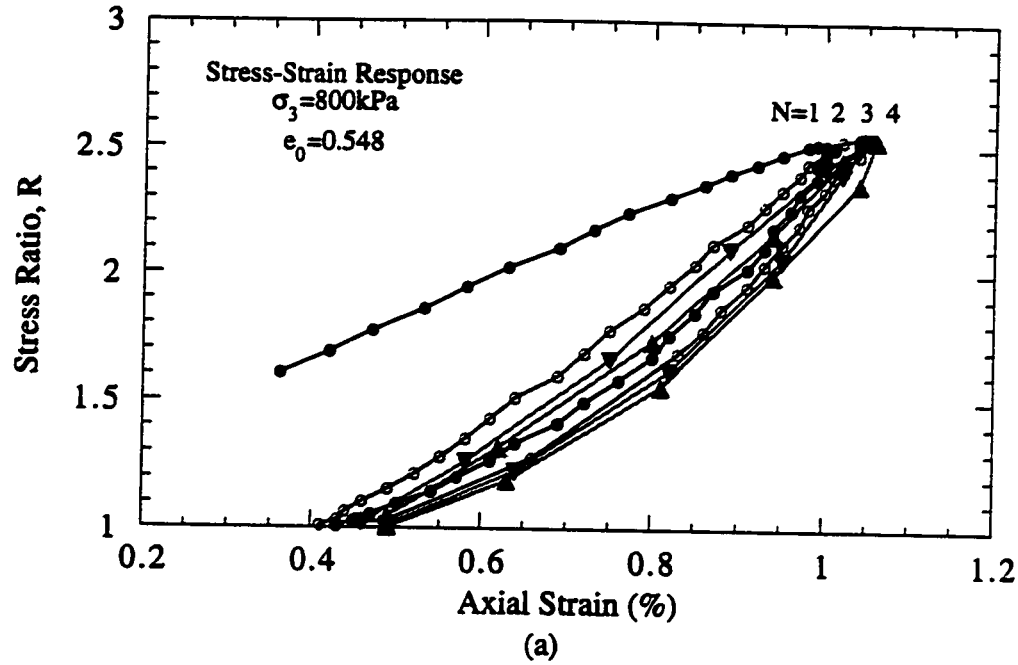

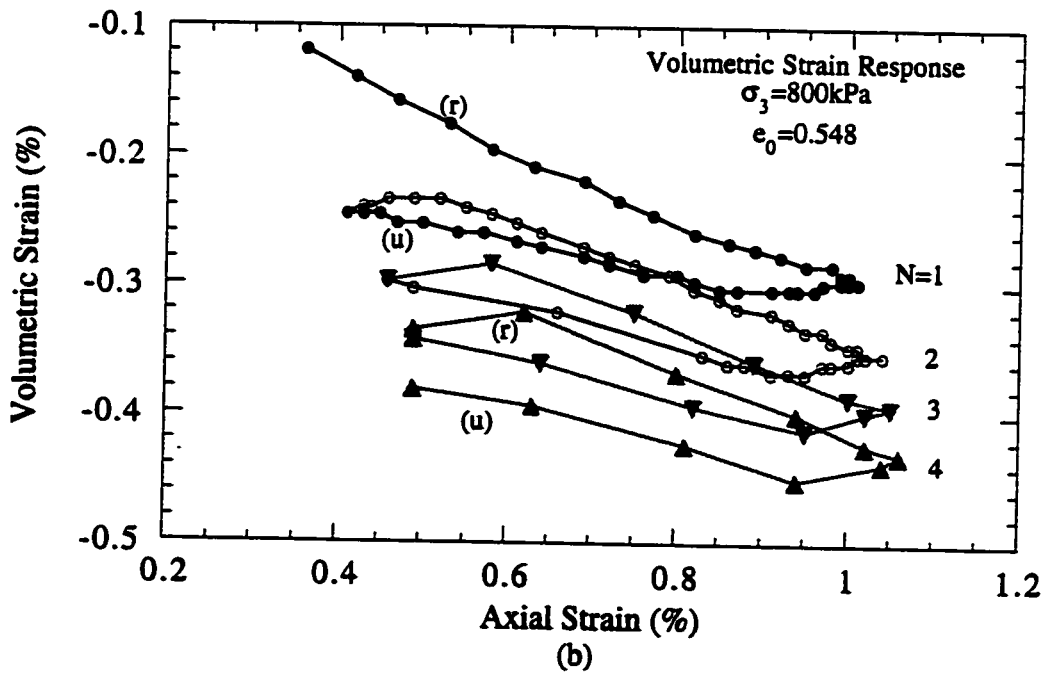

Figure 7.16 Behaviour of Dense Ottawa Sand in the Cyclic Loading Regime (strain position #1); σ_3 = 800kPa

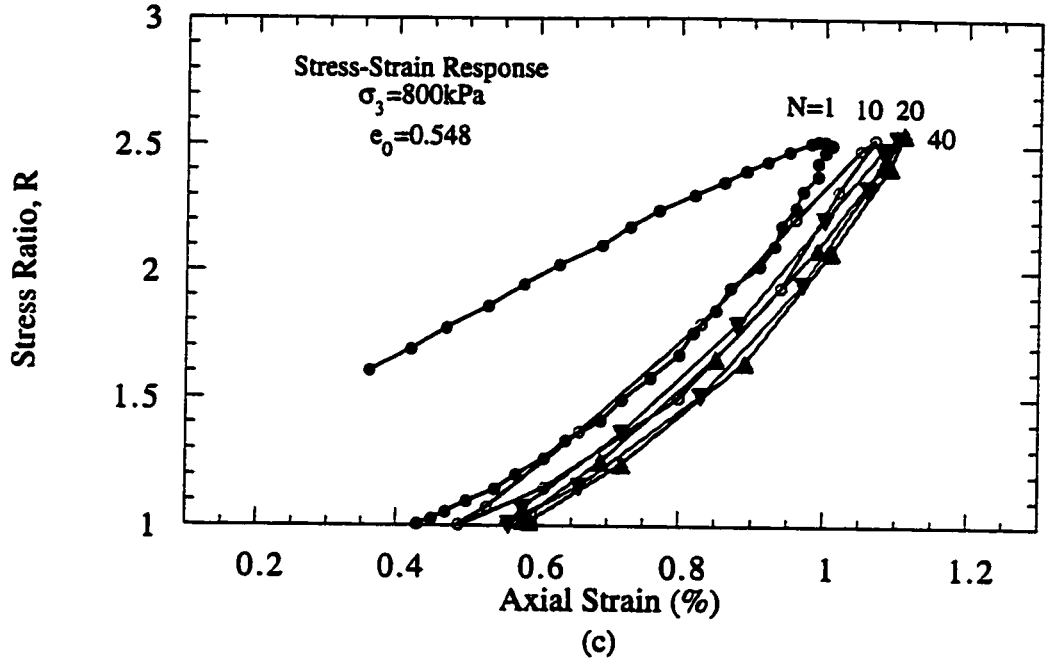

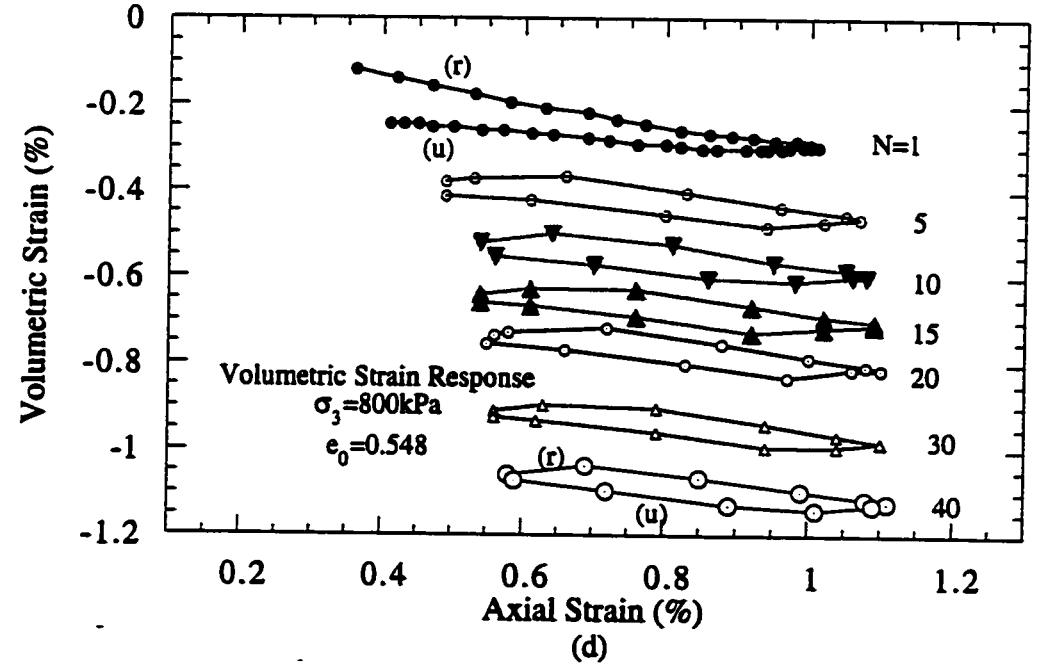

Figure 7.16 Behaviour of Dense Ottawa Sand in the Cyclic Loading Regime (strain position #1); σ_3 = 800kPa

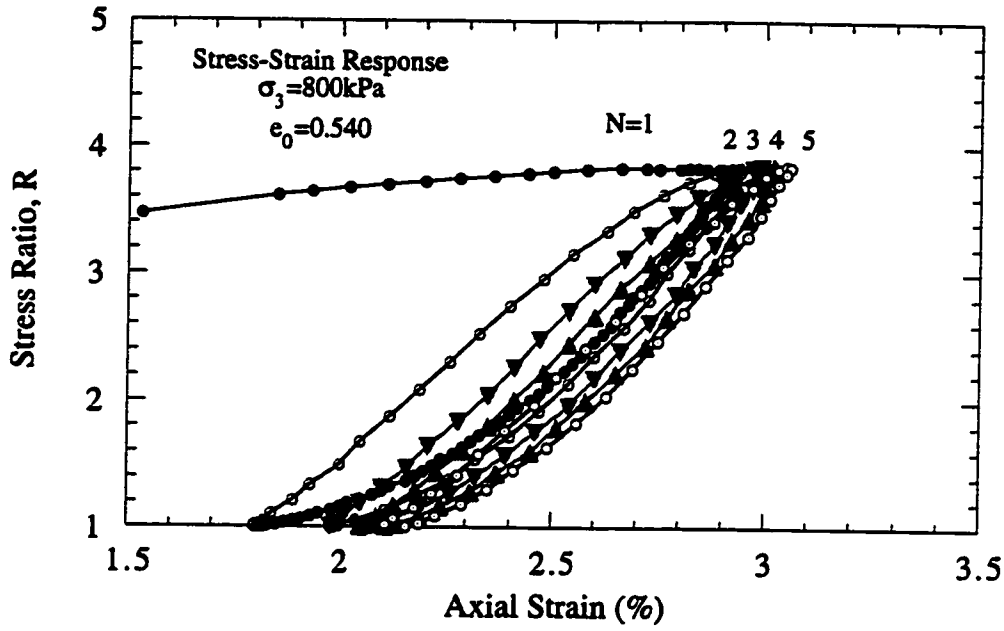

(a)

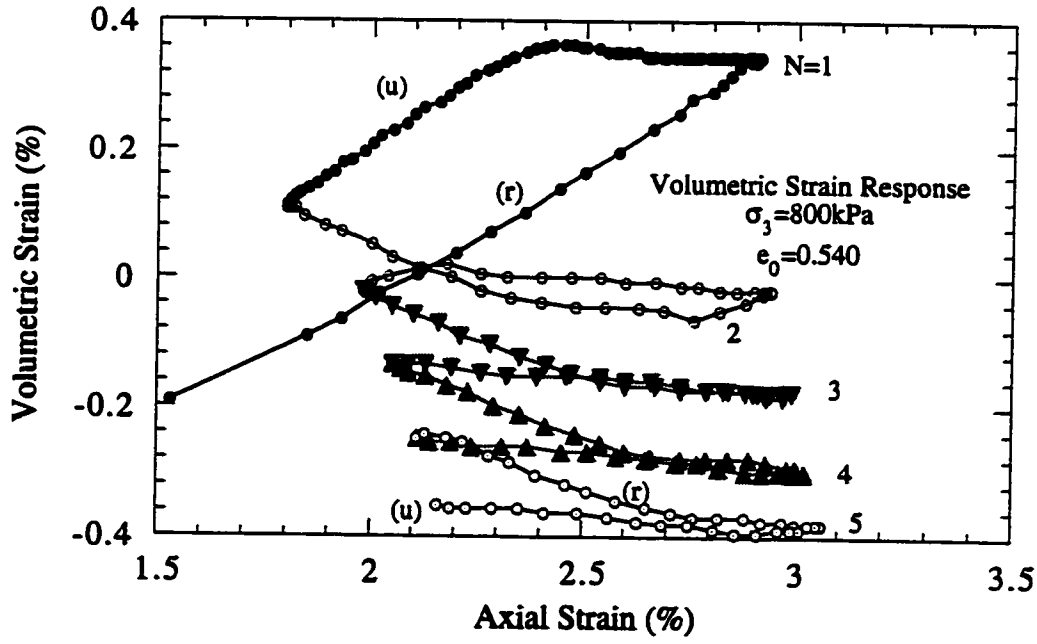

(b)

Figure 7.17 Behaviour of Dense Ottawa Sand in the Cyclic Loading Regime (strain position #2); σ_3 = 800kPa

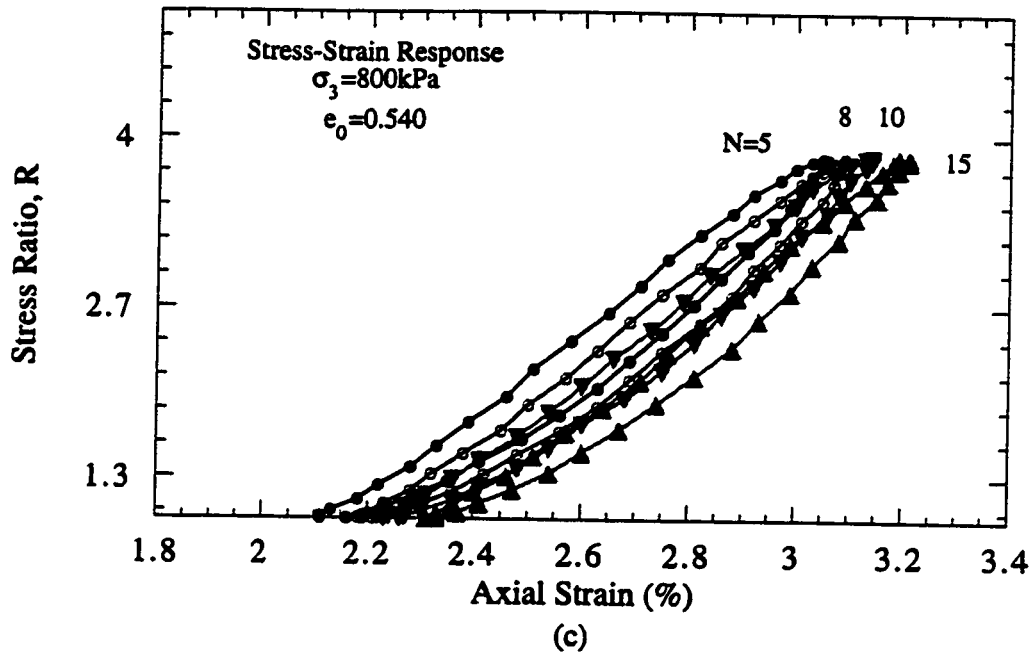

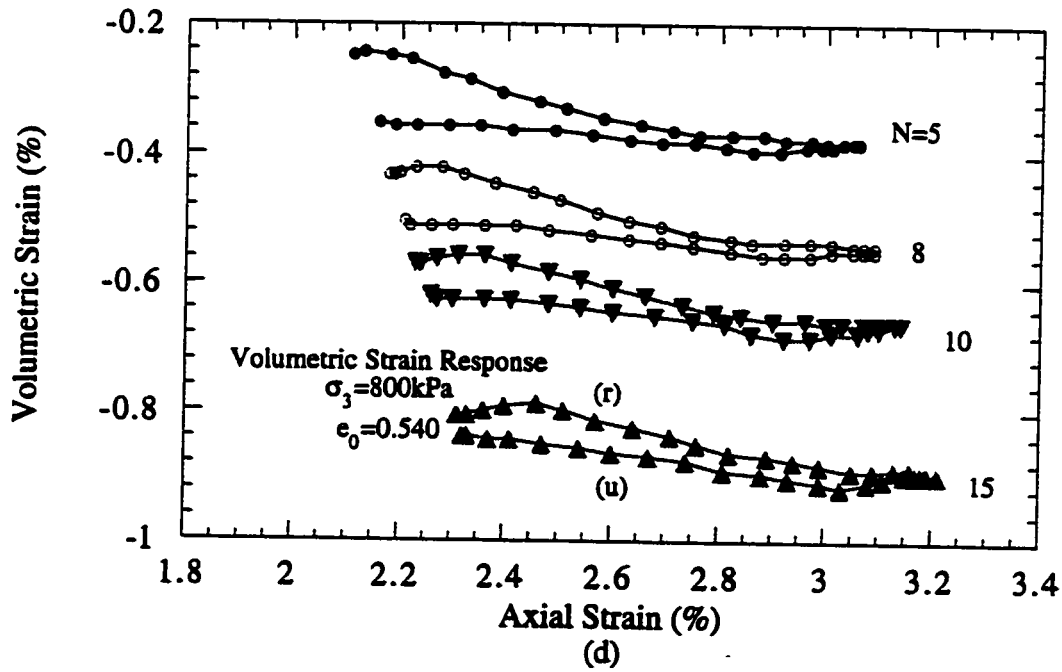

Figure 7.17 Behaviour of Dense Ottawa Sand in the Cyclic Loading Regime (strain position #2); σ_3 = 800kPa

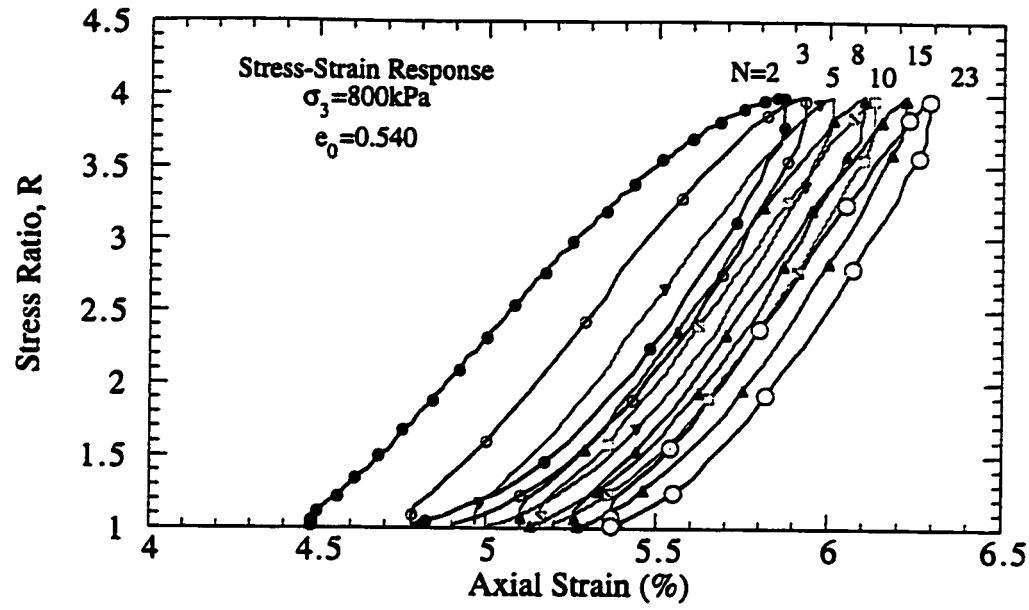

(a)

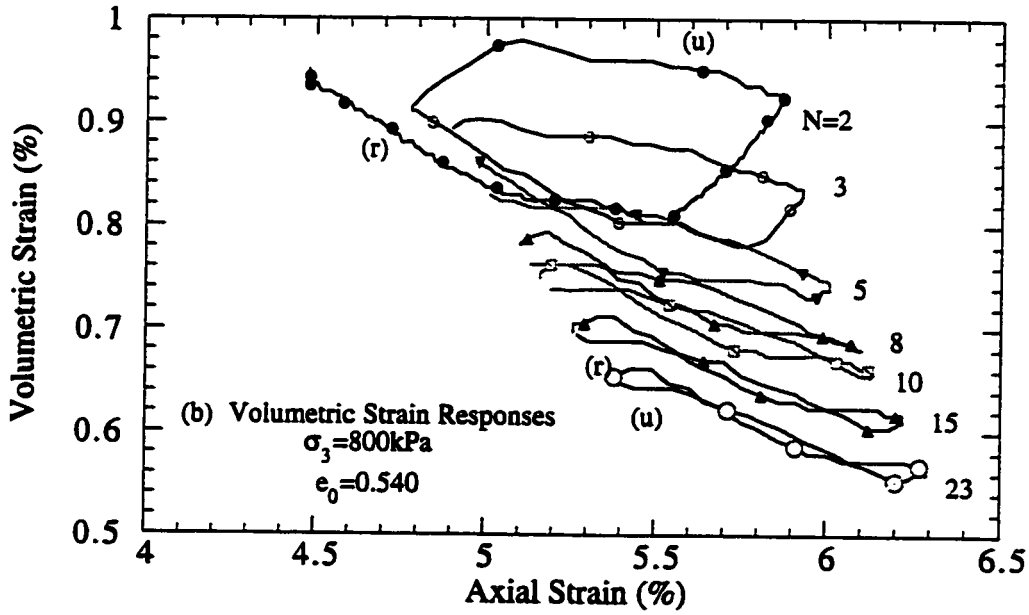

(b)

Figure 7.18 Behaviour of Dense Ottawa Sand in the Cyclic Loading Regime (strain position #3); σ_3 = 800kPa

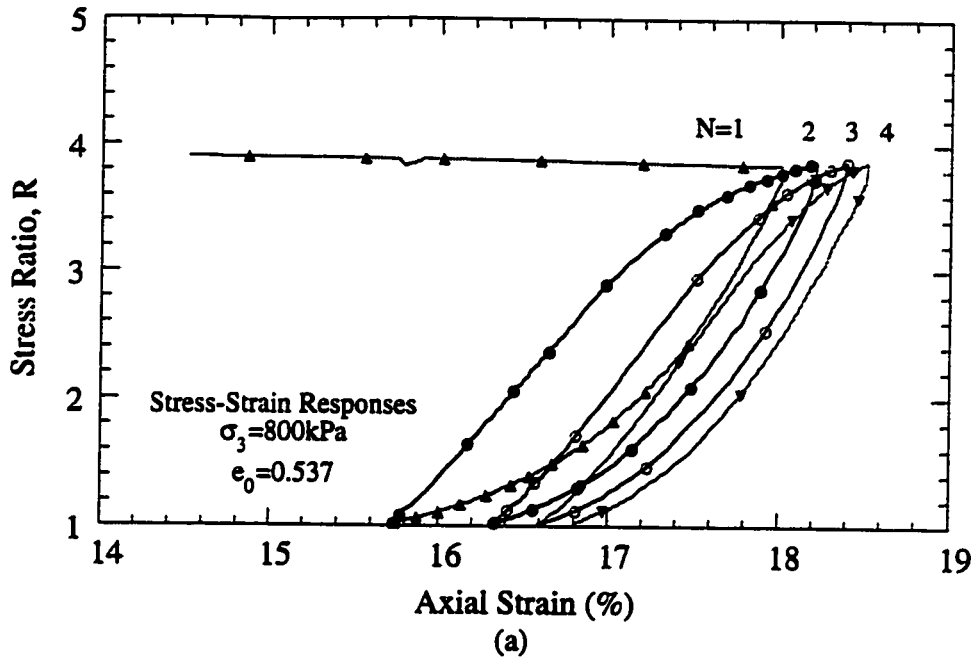

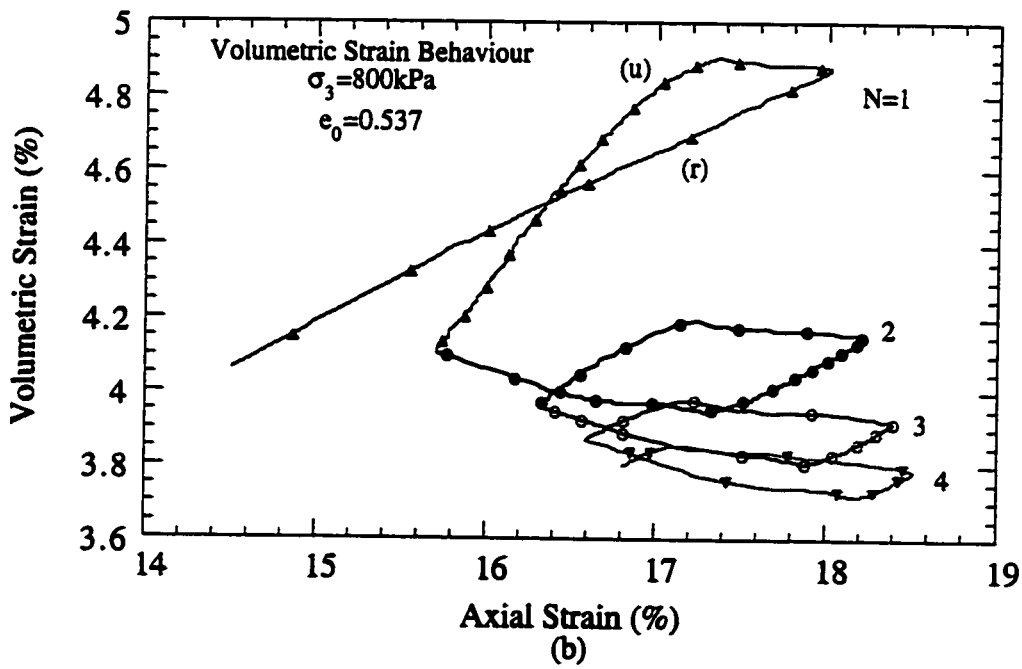

Figure 7.19 Behaviour of Dense Ottawa Sand in the Cyclic Loading Regime (strain position #4); σ_3 = 800kPa

Chapter 8

CONCLUSIONS AND RECOMMENDATIONS

8.1 Summary

This research included experimental triaxial testing on a fine Ottawa Sand with the results being utilized in the verification of a modified stress-dilatancy relationship. The reconstituted samples were prepared over a range of densities and tested through a range of confining pressures to obtain the 11 parameters necessary to validate the proposed constitutive model.

The experimental portion of this research originated with a study to determine the optimum method of sample preparation to ensure a homogeneous, reproducible reconstituted sand specimen. This method was found to be the wet tamping procedure and, with practice, essentially identical samples could be produced for use in the triaxial tests.

Three initial void ratios and as many confining pressures provided nine independent testing conditions. The results of these tests were sufficient to describe the measured density and pressure dependencies of the fine Ottawa Sand behaviour.

Cyclic triaxial testing was performed on the Ottawa Sand at an observational level. Experiments were conducted on the two extreme void ratios, 0.53 and 0.70, and confining pressures, 200 and $800kPa$. The commencement of the cyclic loading

was controlled and occurred at strategic axial strain values. A total of 12 tests were performed, with the responses graphed and discussed in Chapter seven.

Subsequent to the presentation and discussion of the experimental program, a proposed constitutive method of granular material behaviour prediction was presented. This model is unique when compared to others in that it allows density and pressure dependencies of the behaviour to effect the model predictions without involving complicated calculations and procedures. The experimental results are analyzed and the 11 required parameters are extracted for use in the model verification.

Plots of the measured and calculated curves are compared to analyze the model's ability to predict stress-strain, volumetric and dilatancy responses. A discussion of the discrepancies between theoretical and experimental results includes comments on possible experimental errors, as well as model oversights.

8.2 Conclusions

The following statements can be made about the monotonic, drained, conventional triaxial testing of fine Ottawa Sand, the proposed stress-dilatancy relationship with pressure and density dependencies, the resulting constitutive model describing granular material behaviour and the characteristics of fine Ottawa Sand subjected to low frequency, drained, cyclic loading.

1. Buildup of pore water pressures during the isotropic consolidation and shearing of the samples were observed to be greater than the recommended allowable values when using consolidation rates of one second per kPa and strain rates

of 10% per hour. These rates correspond to typical values used in triaxial testing, recalling that the drainage of granular materials in such tests is considered instantaneous. A blockage in the tubing or fixtures between the platens and the internal pressure source was most likely the cause of the internal pressure buildup, as testing done both with and without free ends showed similar results. To maintain acceptable pressure values, the rates of consolidation and shearing were slowed to two to four seconds per kPa and 3.5 to 6.5% per hour respectively.

2. The preliminary investigation into the physical material properties of Ottawa Sand encompassed the determination of particle size distribution, specific gravity and maximum and minimum void ratios. The results of this testing were typical of the material, with the exception of the maximum void ratio, which was slightly lower than previously published values. This finding is not unusual, as the methods of analyzing the maximum void ratio is non-standardized and the results are highly dependent on these methods as well as the individual performing them.

3. The use of enlarged platens provided additional area for the lateral expansion of the sample during shear. This allowed the experiments to continue to a high value of axial strain as the outward radial strain of the sample was accommodated by the excess space. This was shown to be particularly important for the dense samples as the volumetric expansion during dilatant behaviour was reflected entirely in the direction of minor principal stress.

4. Homogeneity of the sample was promoted by the implementation of free ends, a 1.2 to 1 height to diameter ratio and radial wet tamping procedure. While the preparation and testing of perfectly uniform reconstituted samples is difficult, the use of the above techniques did much to alleviate localized behaviour.

5. The flushing of the sample with CO_2 prior to saturation reduces the time required to flush water through the sample as well as the back pressure needed to achieve complete saturation.

6. The use of push-to-connect fittings in the triaxial cell base and top platen instead of the typical o-ring seal allowed a tight connection in the internal cell pressure tubing. The pressure differential between cell and sample stresses was easily maintained throughout the research.

7. Filter paper was required at the soil-platen interface, as the sand grains were small enough to penetrate the porous stone and enter the drainage outlets. This caused undesirable changes in soil mass during the drained testing and created difficulties in the connections of the system.

8. The use of a free end design without the circular drainage cutout was observed to visibly reduce bulging behaviour of the sample at high axial strains. Drainage for this new design was provided by four small notches cut into the free end. Strips of filter paper were placed around the notches to allow water movement from the sample to the porous stone.

9. Comparative triaxial tests performed on loose and dense samples exhibited the effects of free ends on experimental results. The loose sample response was essentially identical regardless of the chosen end conditions. However, dense samples tested with frictionless ends showed lower peak strengths, less strain-softening and greater contractive and dilatant responses when compared to those tested with rough ends. This behaviour is expected as the volumetric strain of a specimen of low density shows contraction throughout the deviatoric load application, while the that of a dense material is predominantly dilatant. The radial expansion exhibited during contraction is quite small, muting the effects of the soil-platen interaction. Conversely, relatively greater radial strains are experienced during dilatant behaviour, amplifying the influence of the frictional stresses that the platen distributes to the soil surface.

10. Results of the monotonic triaxial testing experiments showed typical granular material behaviour for the loose, medium dense and dense samples. The dense plots all exhibit peak and residual behaviour with volume change curves showing initial contraction followed by expansion. The medium dense curves also demonstrate these characteristics, although to a lesser extent. Loose sample responses show no evidence of strain softening or dilation within the range of applied confining pressures.

11. Within the capabilities of triaxial apparatus used in this research, constant volume conditions are witnessed in only the plots of the loose material. The axial loading was stopped prior to this condition for both the dense and medium

dense material, as the radial expansion of the dense sand reached the edges of the platen and the axial strain of the medium dense sand exceeded 30% before volume changes ceased.

12. The influence of confining pressure was typical. Increases in the hydrostatic stresses lower the peak stress and strain softening response. Greater contractive behaviour is also demonstrated, as loose samples will densify to a greater extent and dense samples will exhibit less dilation.

13. The determination of the initial shear modulus parameter, G_0, from experimental results was underestimated due to the insensitive small strain measurements of the initial portions of the stress-strain curves. However, when using the initial slope of the unloading curves from the cyclic portion of the research, a much higher value of is G_0 obtained. This larger value, was much more successful when used in the model predictions.

14. The parameters used in the mobilized friction angle equation, a and β, were found to be overestimated when calculated from the experimental data. These values were adjusted in a similar manner as the G_0 constant, resulting in a more accurate correlation between model and experimental behaviour.

15. The model proposed in this research predicts relatively accurate results of the strength and volume change characteristics of fine Ottawa Sand. The use of a modified stress-dilatancy relationship allows pressure and density dependencies of granular materials to be reflected in the model predictions. The actual measurement of dilatancy, however, is difficult to characterize due to its sensitivity

with respect to determination techniques. Laboratory values of the dilatancy factor were measured by the slope of the volumetric strain curves. While there are definite similarities between the model and experimental values of volume change, the slopes of the curves are not as similar, leading to discrepancies in the comparisons of the stress-dilatancy plots.

16. Model predictions seemed to better describe the experimental results of triaxial testing when the mobilized friction angle constant, a, was made a function of void ratio. To maintain the simplicity of the model, however, this relationship was not utilized in the research.

17. The use of the model to describe the behaviour of Ottawa Sand under conditions not explored in the experimental portion of this research, such as extreme densities and confining pressures, demonstrates the ability of the modified stress-dilatancy relationship to characterize material behaviour over a wide range of conditions. The impact of the above variables is also seen to have a prominent effect on the strength and volume change behaviour of granular soils.

18. The use of the MTS load frame for cyclic triaxial testing of the Ottawa Sand created difficulties in that it did not allow both stress-controlled and strain-controlled loading to occur in the same test. This limited its use in the cyclic loading that commenced after the onset of strain-softening behaviour as this required the ability to monotonically load the material to a given strain and then provide the stress limits of the cyclic regime. The large load capacity of the MTS also caused difficulties in the testing, as the lack of sensitivity at the

required shear stress of the sand reduced the accuracy of stress application.

19. Unstable (runaway) behaviour was not observed, as expected, for the sands subjected to cyclic loading during post-peak conditions. Instead these tests displayed shakedown conditions similar to all other cyclic experiments. This could be due to the use of ELE load frame, which was employed instead of the MTS system in these cases, as this machine is capable only of strain controlled loading. Other system errors, such as drainage capabilities, could also be responsible for the uniform behaviour of the soil samples independent of pressure, density and stress ratio in the cyclic testing

20. The stress-strain responses of cyclic testing show a consistent decrease in strain limits as the number of cycles increase. These limits eventually become constant as the expansion and contraction segments of strain become equal and further cycles no longer cause net axial strain.

21. The volume change characteristics of cyclic testing do not correspond to the axial deformations. Emphasized after a number of cycles, the unloading and reloading curves show segments of both contractive and dilatant behaviour. This suggests that a change in axial stress direction will not be immediately reflected in the volume change of the sample as the internal structure undergoes momentary locking before any deformation takes place.

22. Loose samples subjected to cyclic loading require more cycles than dense samples to exhibit dilatant behaviour in the initial portion of the reloading curve and contractive behaviour in the initial portion of the unloading curve. This is

because the loose sand is gradually densifying with cycles, eventually behaving a dense material.

23. Increasing confining pressure tends to hinder the extent of contraction and expansion in the individual cycles and promotes the overall contraction of the sand throughout the test.

24. The influence of the amount of strain prior to cyclic loading on the volume change results is primarily due to the density of the material. A large portion of monotonic shearing prior to the cyclic loading will cause an initially loose sample to densify and an initially dense sample to become less dense. If the cyclic loading is initialized at very large axial strains, constant volume conditions should control the behaviour of the sand, irrespective of the initial void ratio.

8.3 Further Research

While an extensive list of conclusions incorporating the monotonic and cyclic testing regimes, the parameter determination methods and the capabilities of the proposed stress-dilatancy model were drawn in the previous section, these topics have not yet been exhaustively researched. Future studies are needed in the development of an effective means of characterizing granular material behaviour and the experimental knowledge to support these theories.

The methods used in this testing program were generally those accepted in the

field of geotechnical engineering. However, specific requirements of the model parameter determination create the necessity to further delve into the means of sample preparation and soil testing. Suggestions for further research in the triaxial testing of granular materials are offered below, accompanied by possible modifications to the proposed model and the cyclic loading investigation.

1. The reduction of localized behaviour was visibly observed when using free ends without centre drainage holes, however, no test results were extracted from the experimental program as this was outside the scope of the research. The reduction of the platen soil stress interface should be examined to determine whether the use of the proposed free ends are influential to the behaviour of the sample.

2. A measurement of the homogeneity of the samples was not undertaken in this testing program. This type of experiment would be necessary to determine whether the given material parameters are valid as the model assumes a homogeneous soil.

3. The use of end platens with a diameter $13mm$ greater than the sample was necessary to reduce resistance at the specimen ends. While functioning favourably for the loose and medium dense samples, the cross-sectional area of the dense samples, which experienced relatively large amounts of dilation during shear, expanded past the edge of the platens prior to reaching the desired constant volume conditions. Larger end platens should be used in triaxial testing of dense materials when undertaken for the purposes of constant volume research.

4. Time dependent behaviour is assumed not to affect the testing of granular materials, however, the fine Ottawa Sand sample did not experience instantaneous drainage. This was likely due to a blockage in the drainage system. Difficulties with the fluctuating pore water pressures were alleviated only by reducing the axial strain rates. Further work could be done to determine the exact cause of the pore pressure buildup and methods to ensure its prevention in future triaxial testing.

5. The need to determine the stress-strain behaviour of the sand at very small strains stems from the model parameter requirement of the small shear strain constant, G_o. The measurements of this value are required at axial strains of up to approximately 0.05%. Unfortunately, the capabilities of the axial strain measurement must also extend to values over 30% to capture the constant volume behaviour of the soil. The external linear displacement transducer used in this research was adequate for the latter readings, but did not provide the accuracy needed for the former strain values. The improvement of the method of axial strain measurement is essential in the use of the proposed stress-dilatancy model because of its dependency on the shear modulus.

6. Difficulties were encountered with the model's ability to characterize the mobilized frictional angle curves when incorporating the constant values of a and β. Subsequent observation of the model parameters showed that a better correlation could be attained when varying the a value with current void ratio. Although this was not implemented in the current study, it may be valuable

in future research.

7. The parameters used in the validation of the stress-dilatancy model were determined by using all of the triaxial data in the monotonic loading regime. This model was then compared to the same triaxial data. Further comparisons should be undertaken using the parameters determined in this research and data independent of the research.

8. Ottawa Sand was the only material tested in the determination of the model's validity. Additional comparisons to the experimental measurements of other granular materials are required to both strengthen the verification of the stress-dilatancy model and provide insight towards necessary model modifications.

9. The cyclic testing regime undertaken in this research did not achieve results of great accuracy as the equipment used was not particularly suitable for the testing of soils under relatively low confining pressures. More advanced equipment is necessary before undertaking a testing program which is capable of measuring accurate and reliable triaxial testing results.

10. The consistant results of the cyclic experiments over wide ranges of density, confining pressure and stress ratio suggest the domination of system responses over soil behaviour measurements. Tests performed using a dummy sample could show the extent of these system influences.

11. The modified stress-dilatancy relationship [7] has done much to improve the ability to predict the behaviour of granular materials by expanding accepted

theories to incorporate pressure and density dependencies. Further work is needed, however, to expand this model once again, accounting for factors such as stress path influence, stress induced anisotropy and low frequency cyclic loading. For example, the inclusion of particle slip and override considerations in the model is sufficient to describe the behaviour of the Ottawa Sand under compressive conventional triaxial conditions. If the testing involved a change in principal stress direction however, the influence of particle microstructure and rolling effects may require the modification of the model. Undrained results should also be explored as the volume change in the model can be constrained to zero. The calculation of effective stresses can then be used to determine pore pressures by subtracting these effective stress values from the total stresses applied to the sample.

Appendix A

Determination of Model Parameters

This section describes the development of the model parameters from the experimental data provided in Chapter 4 and the model relationships given in the initial pages of Chapter 5.

A.1 Critical Void Ratio

The extraction of the critical void ratio parameters, hcr and ncr, from experimental data originates from Equation 5.14

$$e_{cr} = e_{cro} \exp\left[-\left(\frac{p}{h_{cr}}\right)^{n_{cr}}\right]. \tag{A.1}$$

The expression is first normalized to

$$e_{cro}/e_{cr} = \frac{1}{\exp\left[-\left(\frac{p}{h_{cr}}\right)^{n_{cr}}\right]}.$$

The first log of the equation yields

$$\ln(e_{cro}/e_{cr}) = \ln(1) - \ln\left(\exp\left[-\left(\frac{p}{h_{cr}}\right)^{n_{cr}}\right]\right)$$

which reduces to

$$\ln(e_{cro}/e_{cr}) = \left(\frac{p}{h_{cr}}^{n_{cr}}\right).$$

Taking the second log of the equation gives the linear relationship

$$\ln(\ln(e_{cro}/e_{cr})) = n_{cr}\ln(p) - n_{cr}\ln(h_{cr})$$

where the slope of the $\ln(\ln(e_{cro}/e_{cr}))$ vs. $\ln(p)$ graph is n_{cr} and the y intercept is $-n_{cr}\ln(h_{cr})$. Figure A.1 shows this relationship for the loose Ottawa Sand, giving an n_{cr} value of 0.232 and a value $-n_{cr}\ln(h_{cr})$ of -3.45. The medium dense and dense data were not used in the determination of the critical void ratio parameters, as the specimens of these densities were not observed to reach critical conditions at the end of the triaxial testing regime. Figure A.2 displays the comparison between the model and experimental results, with excellent correlation of the two curves.

A.2 Parameter Alpha, α

The graphical determination of α is given in Figure A.3 with the double log plot of X vs. (e/e_{cr}). The value of α is equal to the slope of the graph, measuring 1.69.

A.3 Hydrostatic Compaction

The method of determination of the hydrostatic compaction parameters is essentially identical to that of the critical void ratio parameters. One exception is that the experimental data from all three initial densities are used, as it is not important whether or not the soils reached critical state. The expression

$$\ln(\ln(e_o/e)) = m\ln(p) - m\ln(h_l)$$

resulted in the linear graphical solution at the three soil densities as shown in Figure A.4. The resulting average of the y-intercept gave an $-m\ln(h_l)$ value of 5.492 and the slope showed an m of 0.43.

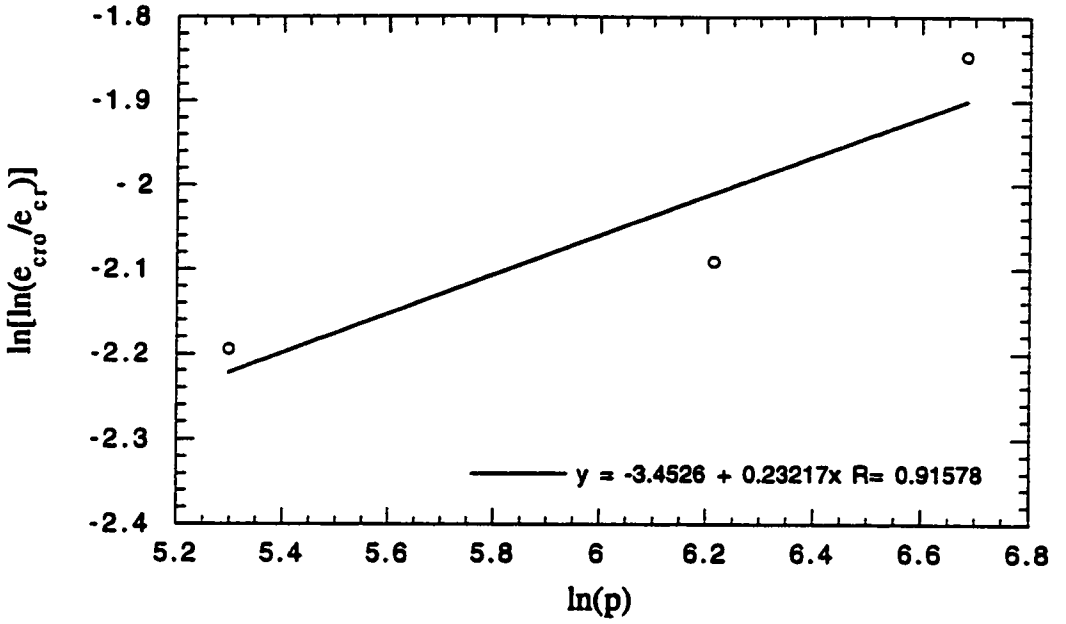

Figure A.1 Critical Void Ratio Parameter Determination

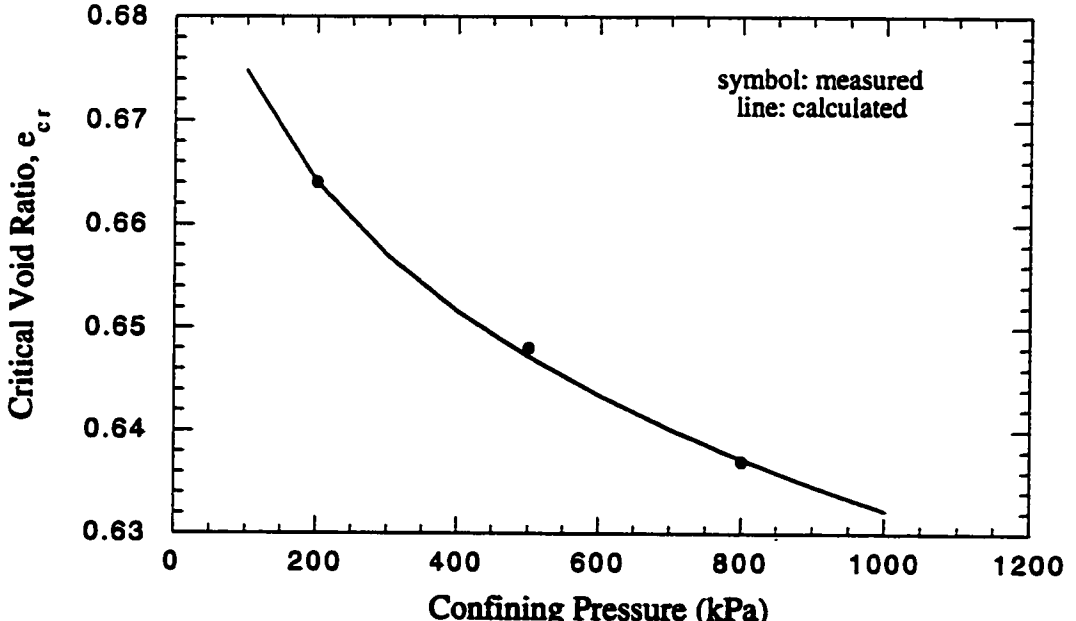

Figure A.2 Comparison of Experimental and Model Determination of Critical Void Ratio

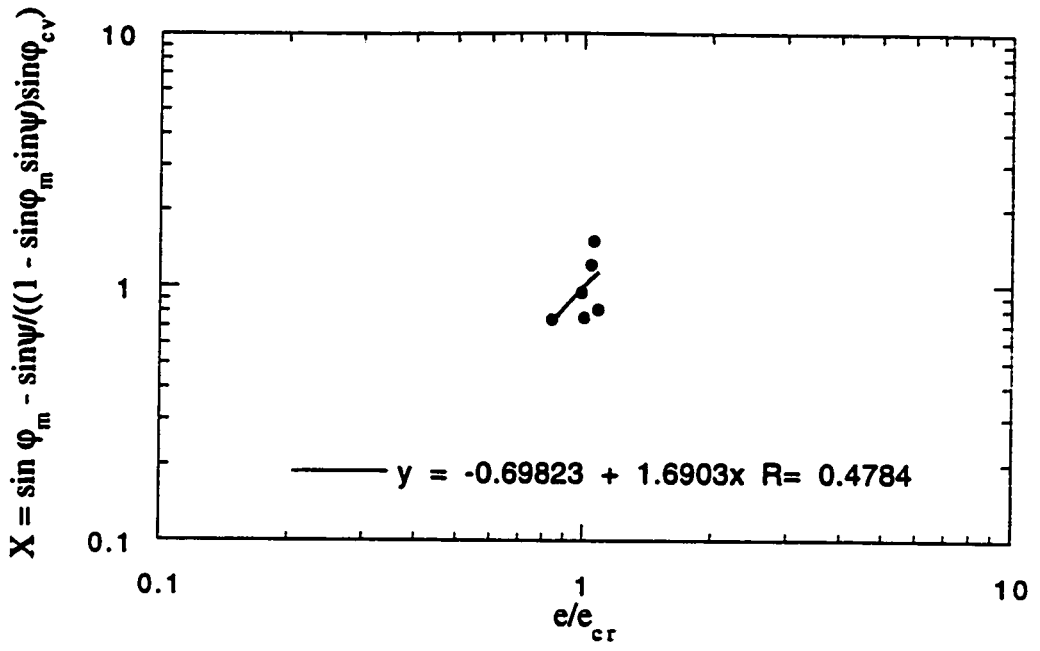

Figure A.3 Alpha Parameter Determination

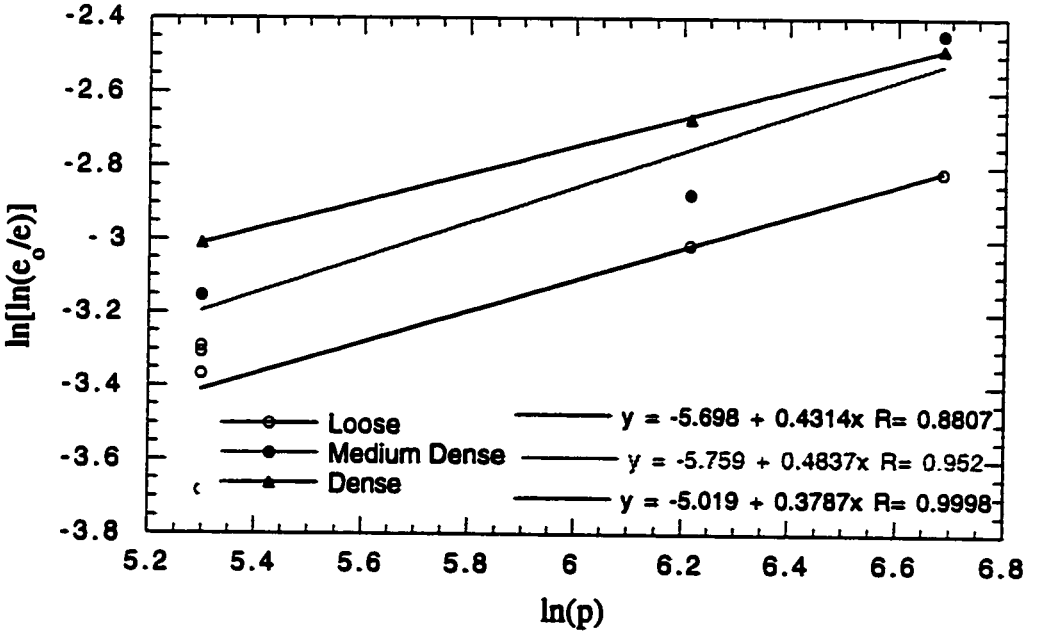

Figure A.4 Hydrostatic Compaction Parameter Determination

Bibliography

[1] Casagrande, A. (1936). "Characteristics of Cohesionless Soils Affecting the Stability of Earthfills". Journal of the Boston Society of Civil Engineering. In Contribution to Soil Mechanics 1925-1940, Oct. 1940, Boston Society of Civil Engineering, pp. 257-276.

[2] Rowe, P.W. (1962). "The Stress-Dilatancy Relation for Static Equilibrium of an Assembly of Particles in Contact". Proc. of the Royal Society of London, Vol. 269, Series A, pp. 500-527.

[3] Newland, P.L. and Allely, B.H. (1957). "Volume Change in Drained Triaxial Test on Granular Materials". Geotechnique, Vol. 7, No. 1, pp. 17-34.

[4] Nova, R and Wood, D.M. (1979). "A Constitutive Model for Sand in Triaxial Compression". International Journal of Numerical Analysis Methods in Geomechanics, Vol. 3, pp. 255–278.

[5] Bolton, M.D. (1986). "The Strength and Dilatancy of Sands". Geotechnique, Vol. 36, No. 1, pp. 65-78.

[6] Ueng, T. and Lee, C. (1990). "Deformation Behavior of Sand under Shear - Particulate Approach". Journal of Geotechnical Engineering, ASCE, Vol. 116, No. 11, pp. 1625-1640.

[7] Wand, R.G. and Guo, P.J. (1996). "A Simple Constitutive Model for Granular Soils: Modified Stress-Dilatancy Approach". Submitted to Computers and

Geotechnics, under review.

[8] Coulomb, C.A. (1776). "Essai sur une Application des Rĕgles de Maximis et Minimis a Quelques Problĕmes de Statique Rĕlatifs a l'Architecture". Mĕmoires de l'Academie Royale des Sciences 7, pp. 343-382 .

[9] Reynolds, O. (1885). "On the Dilatancy of Media Composed of Rigid Particles in Contact". Phil. Mag. Vol. 5, Series 20. pp. 469.

[10] Roscoe, K.H., Schofield, A.N. and Wroth, C.P. (1958). "On the Yielding of Soils". Geotechnique, Vol. 8, No. 1, pp. 25-53.

[11] Rowe, P.W., Barden, L. and Lee, I.K. (1964). "Energy Components During the Triaxial and Direct Shear Tests". Geotechnique, Vol. 14, No. 3, pp. 7-17.

[12] Atkinson, J. (1993). "An Introduction to the Mechanics of Soils and Foundations". McGraw-Hill International Ltd., Berkshire, England.

[13] Fellinius (1927). "Erdstatische Berechnungen". W. Ernst and Sohn, Berlin.

[14] Bishop, A.W. (1955). " The Use of the Slip Circle in the Stability Analysis of Earth Slopes". Geotechnique, Vol. 5, pp. 7-17.

[15] Janbu, N. (1973). "Slope Stability Computations". in Embankment Dam Engineering, Casagrande Memorial Volume. Hirschfield and Poulos (eds),Wiley, New York.

[16] Morgenstern, N.R. and Price, V.E. (1965). "The Analysis of the Stability of General Slip Surfaces". Geotechnique, Vol. 15, pp. 79-93.

[17] Mroz. Z. (1985). "Current Problems and New Directions in Mechanics if Geomaterials". inMechanics of Geomaterials. Bazant (ed). Wiley, New York.

[18] Kondner, R.L. (1963). "Hyperbolic Stress-Strain Response: Cohesive Soils". Journal of Soil Mechanics and Foundations Division, ASCE, Vol. 89, SM1, pp. 115-143.

[19] Duncan, J.M. and Chang, C. (1970). "Nonlinear Analysis of Stress and Strain in Soils". Journal of Soil Mechanics and Foundations Division, ASCE, Vol. 96, SM5, pp. 1625-1653.

[20] Kulhawy, F.H. and Duncan, J.M. (1972). "Stresses and Movements in Oroville Dam". Journal of Soil Mechanics and Foundations Division, ASCE, Vol. 98, SM7, pp. 653-665.

[21] Duncan, J.M., Byrne, P., Wong, Kai S. and Mabry, P. (1979). "Strength Stress-Strain and Bulk Modulus Parameters for Finite Element Analysis of Stresses and Movements in Soil Masses". Geotechnical Engineering Report, University of California, Berkeley.

[22] Vermeer, P.A. and de Borst, R. (1984). "Non-associated Plasticity for Soils, Concrete and Rock". Heron, Witteveen (ed), Vol. 29, No. 3.

[23] Drucker, D.C. and Prager, W. (1952). "Soil Mechanics and Plastic Analysis or Limit Design". Quarterly of Applied Math, Vol. 10, No. 2, pp. 157-165.

[24] Matsuoka, H. and Nakai, T. (1982). "A New Failure Criteria for Soils in Three-Dimensional Stresses". Proceedings IUTAM Conference on Deformation and

Failure of Granular Materials, Delft, Balkema, Rotterdam, pp. 253-263.

[25] Shanz, T. and Vermeer, P.A. (1996). "Angles of Friction and Dilatancy of Sand". Geotechnique, Vol. 46, No. 1, pp. 145-151.

[26] Roscoe, K.H., Schofield, A.N. and Thurairajah, A. (1963). "Yielding of Clays in States Wetter than Critical". Geotechnique, Vol. 13, No. 3, pp. 211-240.

[27] Schofield, A.N. and Wroth, C.P. (1968). "Critical State Soil Mechanics". McGraw-Hill, London.

[28] Roscoe, K.H., Schofield, A.N. and Wroth, C.P. (1958). "On the Yielding of Soils". Geotechnique, Vol. 8, No. 1, pp. 22-53.

[29] Taylor D.W. (1948). "Fundamentals of Soil Mechanics". John Wiley and Sons Inc., New York.

[30] King, G.J.W and Dickin, E.A. (1970). "Comparison of Stress-Dilatancy Theories". Journal of Soil Mechanics and Foundations Division, ASCE, Vol. 96, SM5, pp. 1697–1714.

[31] De Josselin de Jong, G. (1976). "Rowe's Stress-Dilatancy Relation Based on Friction". Geotechnique, Vol. 26, No. 3, pp. 527-534.

[32] Horne, M.R. (1965). "The Behaviour of an Assembly of Rotund, Rigid, Cohesionless Particles". Proceedings, Royal Society, A., London, Vol. 286, pp. 62-97.

[33] Tokue, T. (1979). "Deformation Behaviors of Dry Sand Under Cyclic Loading and Stress-Dilatancy Model". Soils and Foundations, Vol. 19, No. 2, pp. 63-78.

[34] Matsuoka, H. (1974). "A Microscopic Study on the Shear Mechanism of Granular Materials". Soils and Foundations, Vol. 14, No. 1, pp. 29-43.

[35] Nemat-Nasser, S. (1980). "On Behaviors of Granular Materials in Simple Shear". Soils and Foundations, Vol. 20, No. 3, pp. 59-73.

[36] Bishop, A.W. and Henkel, D.J. (1957). "The Measurement of Soil Properties in the Triaxial Test". Arnold, London.

[37] Baldi, G., Hight, D.W. and Thomas, G.E. (1988). "A Reevaluation of Conventional Triaxial Test Methods". Advanced Triaxial Testing of Soil and Rock, ASTM STP 977, R.T. Donaghe, R.C. Chaney and M.L. Silver (eds.), ASTM, Philadelphia, pp. 219-263.

[38] Das, B.M. (1992). "Soil Mechanics Laboratory Manual". 4th ed., Eng. Press Ltd.

[39] Liu and Evett. (1984). "Soil Properties". Prentice Hall Inc.

[40] Labtech Notebook (1992). "Labtech Notebook. Family of Products". Laboratory Technologies Corp., Wilmington, MA, USA.

[41] Humphrey Fluid Power Limited (1995). "Push-To-Connect Fittings and Pneumatic Tubing". Ontario, Canada.

[42] GDS Instruments Limited. "GDS 3MPa Pressure Controller". Egham, Surrey, England.

[43] ELE International Limited (1995). "Digital Tritest 50 Operating Instructions". Hertfordshire, England.

[44] Colliat-Dangus, J.L., Desrues, J.,and Foray, P. (1988). "Triaxial Testing of Granular Soil Under Elevated Cell Pressure". Advanced Triaxial Testing of Soil and Rock, ASTM STP 977, R.T. Donaghe, R.C. Chaney and M.L. Silver (eds.), ASTM, Philadelphia, pp. 290-310.

[45] Lee, K.L. and Seed, H.B. (1967). "Drained Strength Characteristics of Sands". Journal of Soil Mechanics and Foundations Division, ASCE, Vol. 93, SM6, pp. 117-141.

[46] Ueng, T. Tzou, Y. and Lee, C. (1988). "The Effect of End Restraint on Volume Change and Particle Breakage of Sands in Triaxial Tests". Advanced Triaxial Testing of Soil and Rock, ASTM STP 977, R.T. Donaghe, R.C. Chaney and M.L. Silver (eds.), ASTM, Philadelphia, pp. 679-691.

[47] Germaine J.T. and Ladd, C.C. (1988). "Triaxial Testing of Saturated Cohesive Soils". Advanced Triaxial Testing of Soil and Rock, ASTM STP 977, R.T. Donaghe, R.C. Chaney and M.L. Silver (eds.), ASTM, Philadelphia, pp. 421-459.

[48] Samieh, A.M. (1995). "Behavioural Characteristics and Constitutive Modelling of Athabasca Tar Sand at Low Effective Stresses". Ph.D. Thesis, University of Calgary.

[49] Mulilis, J.P., Seed, H.B., Chan, C.K., Mitchell, J.K. and Arulanandan, K. (1977). "Effects of Sample Preparation on Sand Liquefaction". Journal of

Geotechnical Engineering Division, ASCE, Vol. 103, No. GT2, pp. 91–108.

[50] Vaid, Y.P. and Negussey, D. (1988). "Preparation of Reconstituted Sand Specimens". Advanced Triaxial Testing of Soil and Rock, ASTM STP 977, R.T. Donaghe, R.C. Chaney and M.L. Silver (eds.), ASTM, Philadelphia, pp. 405-419.

[51] Ladd, R.S. (1974). "Specimen Preparation and Liquefaction of Sands". Journal of Geotechnical Engineering Division, ASCE, Vol. 100, No. GT10, pp. 1180–1184.

[52] Ladd (1978). "Preparing Test Specimens using Undercompaction". Geotechnical Testing Journal, Vol. 1, No. 1, pp. 16–23.

[53] Gilbert, P.A. (1984). "Investigation of Density Variation in Triaxial Test Specimens of Cohesionless Soil Subjected to Cyclic and Monotonic Loading". Department of the Army, US Army Corps of Engineers.

[54] Holtz, R.D. and Kovacs, W.D. (1981). "An Introduction to Geotechnical Engineering". Prentice-Hall Inc., Englewood Cliffs, New Jersey, USA.

[55] Black D.K. and Lee K.L. (1973). "Saturating Laboratory Samples by Back Pressure". Journal of Soil Mechanics and Foundations Division, ASCE, Vol. 99, SM1, pp. 75–93.

[56] Lacasse, S. and Berre, T. (1988). "Triaxial Testing Methods for Soils". Advanced Triaxial Testing of Soil and Rock, ASTM STP 977, R.T. Donaghe, R.C. Chaney and M.L. Silver (eds.), ASTM, Philadelphia, pp. 264-289.

[57] Linton, P.F., McVay, M.C. and Bloomquist, D. (1988). "Measurement of Deformations in the Standard Triaxial Environment with a Comparison of Local Versus Global Measurements on a Fine, Fully Drained Sand". Advanced Triaxial Testing of Soil and Rock, ASTM STP 977, R.T. Donaghe, R.C. Chaney and M.L. Silver (eds.), ASTM, Philadelphia, pp. 202-217.

[58] La Rochelle, P., Leroueil, S., Trak, B., Blais-Leroux, L. and Tavenas, F. (1988). "Observational Approach to Membrane and Area Corrections in Triaxial Tests". Advanced Triaxial Testing of Soil and Rock, ASTM STP 977, R.T. Donaghe, R.C. Chaney and M.L. Silver (eds.), ASTM, Philadelphia, pp. 715-731.

[59] Matsuoka, H. and Nakai, T. (1974). "Stress-Deformation and Strength Characteristics of Soil Under Three Different Principal Stresses". Proceedings, Japan Society of Civil Engineers, Vol. 232, pp. 59-70.

[60] Kolymbas, D. (1977). "A Rate Dependent Constitutive Equation for Soils". Mech. Res. Comm., Vol. 4, pp. 367-372.

[61] Bauer, E. and Wu, W. (1993). "A Hypoelastic Model for Granular Soils under Cyclic Loading". Proceedings of the International workshop on Modelling Approaches to Plasticity, Elsevier, pp. 247-258.

[62] Gudehus, G. (1996). "A Comprehensive Constitutive Equation for Granular Materials". Soils and Foundations, Vol. 36, No. 1, pp. 1-12.

[63] Hardin, B. O. (1978). "The Nature of Stress-Strain Behaviour of Soils". Proceedings of the ASCE Geotechnical Engineering Division Specialty Conference,

Vol. 3, p. 80.

[64] Iwasaki, T., Tatsuoka, F. and Takagi, Y. (1978). "Shear Moduli of Sands under Cyclic Torsional Shear Loading". Soils and Foundations, Vol. 18, pp. 39-56.

[65] Goddard, J.D. (1990). "Non-linear Elasticity and Pressure-Dependent Wave Speeds in Granular Media". Proc. of the Royal Society of London, Vol. 430, Series A, pp. 105-131.

[66] Cornforth, D.H. (1964). "Some Experiments on the Influence of Strain Conditions on the Strength of Sand". Geotechnique, Vol. 14, No. 2, pp. 143-167.

[67] Bishop, A.W. and Green, D.G. (1965). "The Influence of End Restraints on Compressive Strength of a Cohesionless Soil". Geotechnique, Vol. 15, pp. 243-266.

TEST TARGET (QA-3)

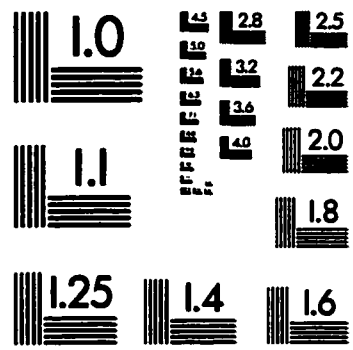

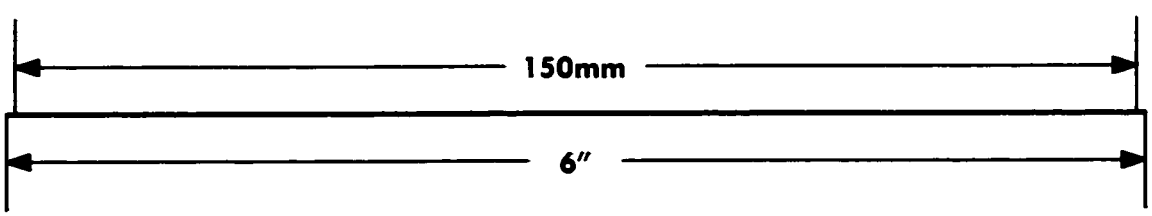

APPLIED IMAGE, Inc
1653 East Main Street
Rochester, NY 14609 USA
Phone: 716/482-0300
Fax: 716/288-5989